THE BROTHERS Q: MULTIMODE ENTANGLED PHOTONS WITH PARAMETRIC DOWN CONVERSION

Stephen Patrick Walborn

junho de 2004

THE BROTHERS Q: MULTIMODE ENTANGLED PHOTONS WITH PARAMETRIC DOWN CONVERSION

Stephen Patrick Walborn

Orientador: Prof. Carlos Henrique Monken

Tese apresentada à UNIVERSIDADE FEDERAL DE MINAS GERAIS, como requisito parcial para a obtenção do grau de DOUTOR EM CIÊNCIAS.

Acknowledgments

With the last 10 years of life spread (smeared might be a better word) over two coast lines and two continents, I look back and realize that the reason I am where I am is due to the friendship and support of countless individuals. As I look back, the quantity of people seems overwhelming. Here I go:

I cannot offer enough thanks to my advisor Carlos Henrique Monken for his guidance, advice, and friendship over the last 6 years. I am grateful also for his dedication to his students and his patience in general, and especially with my portuguese.

This work was performed with financial support from the brasilian funding agency Conselho Nacional de Desenvolvimento Científico e Tecnológico (CNPq); Thank you.

The past few years in the laboratory have been enjoyable and productive mostly thanks to fellow lab rats Wallon A. T. Nogueira and Álvaro N. de Oliveira. Thank you for always being available to discuss and distract.

I would like to thank Professors Marcelo O. Terra Cunha, Sebastião de Pádua, Paulo Henrique Souto Ribeiro and Reinaldo Viana, as well as Dilson P. Caetano for valuable conversations over the last few years. Thanks also to everyone in Sebastião's lab for discussions and frequent equipment loans.

I thank Professors Johnny Powell and Osiel Bonfim for their support and encouragement.

The past 6 years in Belo Horizonte would not have been fun (or even possible) without the many friends that I have made here. Thanks go out to:

The inhabitants of the Lama Lar (*na minha casa todo mundo é lama...*): Nathan, Cabelim, Álvarot (*...like a crazed Leati...*), Alex; also Bira, Márcio, Mário, Aline, Alexandre, Mônica, Erlinda, Erildo, Cristiano, Tatiana, Simone, Craudão, Rosângela, Terra, Ana Mara, Dona Adélia and Seu Ignácio, Catarina, Expedito, Lucas, Luciana, and everyone in the physics dept.

Thank you Marluce for the laughter and the constant supply of official letters and documents which kept me in check with the feds;

Thanks to the physics department staff, especially Seu João Batista and everyone

in the machine shop for all the work they have done over the past few years;

Thanks to all my friends (read family) in the U.S. for their friendship, the good times, and for not disowning me for my late email responses and other correspondence misdemeanors. Thank you Katie, Todd, Matt, Kevin, Eric, southern Mark, Chuck and Betsy, Doc, Sarah B, Mark, Amanda Hugenkeis, Luca James, Bret, Natasha, Seth, Brahmani, Alex, Ovide, Chad, René, Matei, my grandparents, aunts, uncles and cousins, and everyone else you know who you are.

Thank you Celeste.

Thank you dad and Kathy.

For my mother Jane and my sister Kathy,
who have always inspired

"Papa Toe! Papa Toe! Papa Toe!"
-David James Duncan, *The Brothers K*

CONTENTS

LIST OF FIGURES

LIST OF TABLES

Resumo

Esta tese é um estudo das propriedades quânticas de fótons multimodais gerados por meio da conversão paramétrica descendente espontânea, tendo por objetivo a aplicação em problemas de informação quântica, tais como medidas de estados de Bell e a geração de fótons emaranhados nos graus de liberdade espaciais transversais.

Como uma primeira investigação, realizamos um estudo teórico sobre a interferência Hong-Ou-Mandel (HOM) multimodal. Mostramos que os efeitos de interferência de quarta ordem dependem das propriedades transversais do estado do bifóton (par de fótons). Devido à transferência do espectro angular do feixe bombeador para este estado, mostrado por Monken *et al.* [Phys. Rev. A, **57** 3123 (1998)], a paridade do feixe bombeador pode ser usada como um parâmetro de controle da interferência de quarta ordem. Executamos uma experiência de interferência HOM usando feixes Hermite-Gaussianos de primeira ordem como feixe bombeador. Os resultados experimentais mostram que o comportamento da interferência de quarta ordem depende da paridade do feixe bombeador, como foi previsto teoricamente.

Uma primeira aplicação da interferência HOM multimodal pode ser feita na análise de estados de Bell, que utiliza interferência de quarta ordem. As técnicas precedentes requerem detectores que sejam sensíveis ao número de fótons. Por outro lado, com interferência HOM multimodal esta análise pode ser feita usando detectores de um fóton. Para mostrar que a interferência multimodal poderia ser usada para melhorar estes métodos, realizamos uma experiência simples de discriminação dos estados de Bell usando fótons multimodais emaranhados em polarização. Três grupos de estados de Bell foram identificados na base de coincidências (com detectores de um fóton). Além disto, discutimos dois métodos similares para análise de estado de Bell utilizando estados hiperemaranhados (emaranhados em mais de um grau de liberdade). Mostramos que uma proposta precedente de Kwiat *et al.* [Phys. Rev. A **58** R2623 (1998)], que requer fótons emaranhados em mais de um grau de liberdade, funcionará melhor usando a interferência HOM multimodal. Finalmente, propomos um novo método de análise de estados de Bell de fótons hiperemaranhados que não requer

detectores sensíveis ao número de fótons e pode ser executada não-localmente.

Como um estudo adicional das propriedades multimodais de fótons produzidos pela conversão paramétrica descendente, investigamos a conservação e emaranhamento de momento angular orbital neste processo. Sabe-se bem que um campo eletromagnético pode carregar momento angular orbital na forma de uma fase azimutal no plano transversal. Desta forma, mostramos teoricamente que a geração de fótons emaranhados em momento angular orbital na conversão paramétrica descendente pode ser explicada através da transferência do espectro angular. Realizamos uma experiência multimodal simples de interferência de quarta ordem que comprovou as nossas previsões teóricas.

Finalmente, estudamos a geração de fótons emaranhados nos modos transversais Hermite-Guassianos. Usando a teoria da transferência do espectro angular, mostramos que a conversão paramétrica descendente gera pares de fótons emaranhados em modos Hermite-Gaussianos, e para quaisquer pares destes modos, calculamos a amplitude de geração. Além disto, discutimos a geração de estados maximamente e não-maximamente emaranhados usando modos de primeira ordem.

Abstract

This thesis is a study of the quantum properties of multimode entangled photons created by spontaneous parametric down-conversion. More specifically, we attempt to utilize this multimode character in quantum information tasks such as Bell-state measurement and the generation of photons entangled in transverse spatial degrees of freedom.

As a first investigation, a theoretical study of multimode Hong-Ou-Mandel interference was conducted. It is shown that the fourth-order interference effects depend upon the transverse spatial properties of the biphoton. Due to the transfer of the angular spectrum of the pump beam to the biphoton state shown by Monken *et al.* [Phys. Rev. A **57** 3123 (1998)], the parity of the pump beam can be used as a control parameter of fourth-order interference. A Hong-Ou-Mandel interference experiment was performed using first-order Hermite-Gaussian pump beams. The experimental results show that the observed fourth-order interference behavior depends upon the parity of the pump beam.

A first application of multimode interference in quantum information is in optical Bell-state analysis, which uses fourth-order interference techniques. A technical difficulty encountered with previous methods of Bell-state analysis is the requirement that the detectors be sensitive to photon number. However, using multimode interference, Bell-state analysis can be performed using single-photon detectors. To show that multimode interference could be used to improve upon these schemes, a simple Bell-state measurement experiment using multimode polarization entangled-photons was performed. Three classes of Bell-states were identified in the coincidence basis (with single photon detectors). In addition, similar methods for Bell-state analysis using hyperentangled states are discussed. Using multimode interference, we improve upon a previous proposal of Kwiat and Weinfurter [Phys. Rev. A **58** R2623 (1998)], which requires photons entangled in more than one degree of freedom. Finally, we propose a new method of Bell-state analysis of hyperentangled photons that does not require detectors sensitive to photon number and can be implemented non-locally.

As a further study of the multimode properties of down-converted photons, we investigate the conservation of orbital angular momentum in spontaneous parametric down-conversion. It is well known that a light field can carry orbital angular momentum in the form of an azimuthal phase dependence. We show theoretically that the angular spectrum transfer enables the generation of photons entangled in orbital angular momentum. A simple multimode fourth-order interference experiment was performed which confirms these theoretical predictions.

Finally, we studied the generation of photons entangled in Hermite-Gaussian modes. Using the theory of angular spectrum transfer, we show that spontaneous parametric down-conversion generates photons entangled in Hermite-Gaussian modes and calculate the probability amplitude to generate arbitrary Hermite-Gaussian modes. In addition we discuss the generation of maximally entangled Bell-states and arbitrary bipartite pure states.

Author's Note

This document was compiled with LaTeX using the hyperref package, which provides the PDF file with inter-document links for all cited references, sections, figures, tables and equations, as well as links to URLs. Text appearing in dark blue indicates a link to a reference within the document, while text appearing in red indicates a link to an internet URLs. The backref option has been used, which, for each reference in the bibliography, provides a link to the section(s) in which that reference was cited. The links should work with most PDF viewers, including Adobe Acrobat Reader and Apple Preview.

1

Introduction

1.1 Background

Just a century old, quantum theory has been the subject of serious debate among physicists and philosophers since the beginning. Perhaps the most famous debates were between Albert Einstein and Niels Bohr, which took place in a large part at the Solvay conferences in 1920's. On one hand, quantum mechanics was extremely successful in its predictions, but on the other hand it predicted controversial phenomena such as wave-like interference of "particles" like electrons. Bohr proposed that the physical properties of a quantum system may not be well defined until some type of observation (measurement) defines them, while Einstein argued that the physical properties of a quantum system must always be well-defined or real (a part of reality). In their seminal paper [1], Einstein, Podolsky and Rosen (EPR) showed that according to standard quantum theory it would be possible to create quantum systems with long-distance correlations. EPR argued that these correlations could be used to violate Bohr's complementarity principle. Another issue was that these long-distance correlations seemed to give rise to what Einstein referred to as "spooky action at a distance", which could enable faster-than-light communication, in conflict with Einstein's theory of special relativity. To address these issues EPR proposed the idea of *hidden variables* - that there was some yet undiscovered physical parameter that would give rise to a more intuitive "classical" model. "Verschränkung", translated as "Entanglement", is the name Erwin Schrödinger [2, 3] gave to these strange non-classical correlations between certain quantum systems.

In 1964, John Bell showed that entanglement can be stronger than strictly classical correlations. That is, he showed that the predictions of quantum mechanics conflict with those of any local hidden variable theory, the sort suggested by EPR. Through a simple argument, Bell derived an inequality that any local realistic probability theory must obey. Violation of Bell's inequality implies that once realism is assumed, quantum mechanics is inherently non-local. However, it has been shown that there is no danger of violating relativity, since information cannot be sent through quantum correlations alone [4] [1]. Later, Clauser, Horne, Shimony and Holt [5] reformulated Bell's inequality to fit actual experimental situations. This set the stage for a multitude of experiments testing Bell's inequality [6, 7, 8, 9, 10, 11, 12, 13, 14, 15, 16, 17, 18, 19]. Nearly all experimental results have agreed with quantum mechanics, though none has been entirely conclusive due to various technical *loopholes*. A few skeptics notwithstanding, most scientists are placing their money on quantum theory.

1.2 Quantum Information

Ironically, what was first seen as a serious flaw in quantum theory has since led to a lot of interesting new physics as well as promising technical applications. Specifically, it has been shown that it may be advantageous to use quantum systems to process and communicate information. Paul Benioff [20], David Deutsch [21, 22], Richard Feynman [23, 24] and others laid some of the first bricks in the theoretical foundations of *quantum computation*. Benioff and Deutsch developed the idea of the Quantum Turing Machine, a theoretical quantum computer, and Feynman pointed out that efficient simulation of a quantum system can only really be performed by another quantum system. Deutsch formulated the first quantum algorithm with a speed-up over its classical counterpart [22], and roughly ten years later, Peter Shor provided an algorithm that showed that a quantum computer could be used to factor large numbers faster than any known classical computer algorithm [25, 26]. This caught the attention of the non-physics community, since the difficulty of factorization plays a key role in many cryptography schemes, including the RSA protocol, which is widely used to send encrypted information such as credit card numbers for on-line internet purchases. Cryptographers and internet shoppers need not worry, however. Several cryptography

[1] In quantum teleportation, for example, classical communication is required to complete the transmission of quantum information.

protocols, such as the one-time pad for example, are known to be secure provided that two users can establish a secret random key string. In 1984, Gilles Brassard and Charles Bennett [27, 28], and later Artur Ekert [29] showed that the laws of quantum physics guarantee secure communication with *quantum key distribution*. In fact, cryptography based on quantum key distribution is the only encryption scheme that has been proven to be secure, provided the encryption scheme functions within certain thresholds. Since the early 1990's many sub-fields have developed, including quantum key distribution and quantum cryptography, quantum dense coding, quantum communication and quantum computation. All of these fields, and others, now form the field of Quantum Information [30].

1.2.1 The qubit

In contrast with the classical binary "bit", the basic unit of quantum information is known as the *qubit*. Whereas the bit can be found in the logical states `0` or `1`, the quantum bit is a two-state quantum system that can be found in the arbitrary superposition $\alpha\,|\mathtt{0}\rangle + \beta\,|\mathtt{1}\rangle$. The only restriction placed on the complex coefficients α and β is that they obey the normalization condition $|\alpha|^2 + |\beta|^2 = 1$. Many two-level quantum systems, such as photon polarization, can represent a qubit. The quantum states $|\mathtt{0}\rangle$ and $|\mathtt{1}\rangle$ correspond to the classical logic states `0` and `1`, and are known as the *computational basis*. The fact that quantum states can be superpositions of the computational basis states gives rise to a quantum parallelism that is not available in ordinary (digital) classical computation. Furthermore, quantum superposition is at the heart of quantum entanglement, which is now regarded as a physical resource to be used in computation and communication tasks. For example, to entangle two qubits all that is required is quantum superposition and a classical two-bit logic operation such as a CNOT gate [30].

As evidence of the importance (or at least the recent popularity) of the qubit, I give you:

> **quantum bit** *n.* The smallest unit of information in a computer designed to manipulate or store information through effects predicted by quantum physics. Unlike bits in classical systems, a quantum bit has more than two possible states: a state labeled 0, a state labeled 1, and a combination of the two states that obeys the superposition principle.
> **qubit** (kyōobĭt′) *n.* A quantum bit.

> *-The American Heritage ® Dictionary of the English Language, Fourth Edition Copyright © 2000 by Houghton Mifflin Company.*

As to the history and appropriateness of the word itself:

> "Qubit seems to have been used first in print by Benjamin Schumacher, 'Quantum coding,' Phys. Rev. A **51**, 2738-2747 (1995). A brief history of the term can be found in the Acknowledgments of this paper. Although qubit honors the English rule that q should be followed by u, it ignores the equally powerful requirement that qu should be followed by a vowel. My guess is that it has gained acceptance because it visually resembles an ancient English unit of distance, the homonymic cubit. To see its ungainliness with fresh eyes, imagine that Dirac had written qunumber instead of q-number, or that one erased transparencies and cleaned ones ears with Qutips."
>
> -N. David Mermin, "From Cbits to Qbits: Teaching computer scientists quantum mechanics", American Journal of Physics, **71** 23 (2003), footnote 3.

1.3 Motivation

Evidently, the ability to produce and control entangled quantum systems has tremendous advantages. In addition to the possible technological applications, the experimental study of entanglement has shed much light on the foundations of quantum mechanics. There are several physical systems that have played a large role in recent investigations, including Nuclear Magnetic Resonance, Cavity QED, Solid-State devices, and optical systems.

Given the relative ease with which one can create and send entangled photons from one place to another, optical systems are the leading contenders for implemetations of quantum cryptography and long-distance quantum communication. Quantum cryptographic systems are well within the limits of contemporary technology. Plug and play quantum cryptography devices using fiber optics have been developed, and recent experiments have been performed using laser beams propagating in free space during daylight hours [31].

In addition to quantum communication systems, optical systems may play a role in quantum computation. It has been shown that single-qubit gates along with certain controlled logic operations such as the two-qubit *controlled-not* (CNOT) gate is universal [32], meaning that any quantum computation can be performed using only these gates. For the photon, single-qubit gates can be easily implemented using linear optical

elements such as wave plates, beam splitters and phase shifters. However, controlled gates acting on multiple photons remain difficult due to the nonlinear interaction required. Recently, Knill, Laflamme and Milburn have shown that scalable quantum optical computation is possible using only linear optical elements [33]. Several quantum optical controlled logical gates have been proposed [33, 34, 35, 36], which rely on two-photon interference at a beam splitter, with photodetection and post-selection providing the non-linearity [33]. Andrew White's group has recently built [37] the linear-optical CNOT gate proposed in [35]. A current drawback to these gates is the low reliability and low efficiency, mostly due to detector inefficiency [38].

There is also the possibility of encoding information in more than one degree of freedom of the photon, resulting in 2 or more qubits per photon. Logic gates and quantum algorithms have been performed using polarization and spatial modes of the same photon [39]. Our group has developed a universal quantum CNOT gate, which acts on the polarization and the first-order Hermite-Gaussian transverse spatial mode of the same photon [40, 41]. Recently and independently, Fiorentino and Wong have built an improved device and demonstrated it's operation at the single photon level [42].

1.3.1 Spontaneous Parametric Down-conversion

One of the most important resources in testing the foundations of quantum mechanics as well as quantum information protocols are entangled photons produced using spontaneous parametric down-conversion (SPDC). SPDC was first studied theoretically by Klyshko [43] in 1969 and experimentally by Burnham and Weinberg [44] in 1970. Since then, there have been many studies investigating the various non-classical properties exhibited by the down-converted "twin" photons.

In SPDC, a pump photon excites a nonlinear crystal, creating two daughter photons. There are several physical constraints that can give rise to entanglement: energy conservation, momentum conservation and phase matching. These constraints will be discussed in more detail in section 2.1. Taking advantage of these constraints, physicists have been able to generate photons that are entangled in polarization [13, 16], linear momentum [10], energy [11] and orbital angular momentum [45, 46, 19]. Many experiments have been performed using SPDC, including:

- Bell's inequalities experiments [8, 9, 10, 11, 12, 14, 13, 16, 15, 17, 18, 19]

- quantum erasers [47, 48, 49, 50, 51]
- quantum dense coding [52]
- quantum key distribution [53, 54, 55]
- quantum teleportation [56, 57, 58]
- entanglement swapping [59]
- quantum "cloning" [60, 61]
- quantum logic gates [36, 37]
- entanglement distillation/concentration/purification [62, 63]
- two-photon interference effects [64, 65, 66, 67, 68]
- spatial antibunching [69, 70]

and others. A terrific reference for theoretical and experimental work is Adán Cabello's *Bibliographic guide to the foundations of quantum mechanics and quantum information*, (quant-ph/0012089) avalaible on the Los Alamos eprint server (http://arxiv.org), which is updated several times a year.

In the past years, many studies have been made investigating the non-classical nature of the two-photon state generated by SPDC [71, 72, 73, 74, 75, 76, 77, 78, 65, 66, 67, 68, 79, 69, 80, 81, 70]. In 1998, Monken, Ribeiro and Pádua [77] showed that, in the SPDC process, the angular spectrum of the pump beam is transferred to the two-photon state, or *biphoton*. This important and useful result is responsible for many of the nonlocal and non-classical phenomena that have been observed using the biphoton [46, 65, 69]. The angular spectrum transfer enables the experimenter to control the angular spectrum of the biphoton by manipulating the pump beam. The majority of the works completed since 1998 in both our group at UFMG as well as professor P. H. Souto Ribeiro's group at UFRJ have used these results in a variety of applications and studies.

1.4 Objectives

During this doctoral research, several experiments and theoretical investigations were conducted. The main objective and central theme was to use the theory of transfer of angular spectrum in quantum information tasks. The main topics present are multimode interference, Bell-state analysis and generation of entangled states with SPDC.

Multimode interference. We have performed several experiments investigating two-photon interference with a variety of pump beams with different transverse spatial properties. We have discovered that the transverse profile of the pump beam can be used to control two-photon interference of down-converted photon pairs. The theory and experiment are presented in chapter 3.

Optical Bell-state analysis. This additional control parameter provided by multimode interference is useful in performing a *Bell-state measurement*, that is, distinguishing between the four Bell-states. The entangled Bell-states and Bell-state measurement are essential to many quantum information schemes, including quantum dense coding and quantum teleportation. In chapter 4, we present experimental results for an improved Bell-state measurement scheme using multimode two-photon interference as well as theoretical results for hyperentangled Bell-state analysis.

Generating entangled states. Exploring the possibility of entanglement in other degrees of freedom is a potentially fruitful line of research. It has been demonstrated that orbital angular momentum is conserved in SPDC [45, 46, 82], and Bell's inequality-type experiments have been performed [19], showing that the down-converted photons are entangled in orbital angular momentum. In chapter 5 theoretical results are presented which show that the two-photon state generated by SPDC is indeed entangled in orbital angular momentum. To prove the validity of our theoretical results, we investigate the amplitude and phase characteristics of the two-photon state using multimode interference.

In chapter 6, the generation of photons in entangled Hermite-Gaussian modes is investigated. It is shown that the parity of each cartesian index is conserved. Conservation of these spatial properties is a direct result of the angular spectrum transfer. A simple proof is provided which shows that the down-converted photons are entangled

in Hermite-Gaussian modes.

1.4.1 Publications

Below is a list of journal articles that have been either published or submitted to be published during this doctorate research. Items marked with an asterisk are related to topics covered in this thesis but are not explicitly discussed.

1. S. P. Walborn, A. de Oliveira, S. Pádua and C. H. Monken, "Multimode Hong-Ou-Mandel Interference", Physical Review Letters **90**, 143601 (2003).

2. S. P. Walborn, W. A. T. Nogueira, S. Pádua and C. H. Monken, "Optical Bell-state analysis in the coincidence basis", Europhysics Letters **62**, 161-167 (2003).

3. S. P. Walborn, S. Pádua and C. H. Monken, "Hyperentanglement-assisted Bell-state analysis", Physical Review A **68**, 042313 (2003).

4. * W. A. T. Nogueira, S. P. Walborn, S. Pádua and C. H. Monken, "Generation of a Two-Photon Singlet Beam", Physical Review Letters **92**, 043602 (2004). [2]

5. S. P. Walborn, R. S. Thebaldi, A. de Oliveira, S. Pádua and C. H. Monken, "Conservation and entanglement of orbital angular momentum in parametric down-conversion", Physical Review A **69**, 023811 (2004).

6. S. P. Walborn, S. Pádua and C. H. Monken, "Conservation and entanglement of Hermite-Gaussian modes in parametric down-conversion", accepted for publication in Physical Review A, (2005).

7. S. P. Walborn, W. A. T. Nogueira, A. N. de Oliveira, S. Pádua and C. H. Monken, "Multimode Hong-Ou-Mandel Interferometry", Brief Review to be published in Modern Physics Letters B, (2005).

[2] To be covered in W. A. T. Nogueira's Ph.D. Thesis.

2

Fundamentals

In this chapter, the fundamental theoretical results and experimental techniques used in this work are introduced.

2.1 Spontaneous parametric down-conversion

2.1.1 Introduction

Spontaneous parametric down-conversion (SPDC) [43, 44] is a nonlinear optical process in which a pump beam photon with wave vector $\mathbf{k}_p$ and frequency ω_p propagating inside a nonlinear optical medium is spontaneously converted into two photons, with wavevectors $\mathbf{k}_s$, $\mathbf{k}_i$ and frequencies ω_s, ω_i, respectively. Here p stands for "pump" and s and i refer to the down-converted fields[1]. Under most circumstances, the quantum state of the two down-converted photons is non-separable, meaning that it cannot be written as a product of two one-photon states. Thus the two-photon, or *biphoton* state must be regarded as a single entity, which results in a plethora of interesting quantum phenomena. This non-separability arises from the various constraints and conservation laws present in the SPDC process.

As we will see in the next section, energy is nearly conserved in SPDC, so that

$$\omega_p = \omega_s + \omega_i. \tag{2.1}$$

[1] Called "signal" and "idler" for historical reasons.

If the nonlinear crystal is thin (on the order of a few millimeters), the transverse component of momentum is nearly conserved, giving

$$\mathbf{q}_p = \mathbf{q}_s + \mathbf{q}_i. \tag{2.2}$$

In order to satisfy the conservation of momentum inside the uniaxial birefringent crystal, there are certain *phase-matching conditions* [83] to be satisfied. In a uniaxial crystal, there are two ways of satisfying the phase matching condition, known as type I and type II. In type I phase matching, a pump photon polarized in the extraordinary (e) direction creates two ordinarily (o) polarized photons:

$$\mathtt{e} \longrightarrow \mathtt{oo} \qquad \text{type} - \text{I} \tag{2.3}$$

whereas in type-II, the down-converted photons are orthogonal:

$$\mathtt{e} \longrightarrow \mathtt{eo} \quad \text{or} \quad \mathtt{o} \longrightarrow \mathtt{eo} \qquad \text{type} - \text{II} \tag{2.4}$$

The down-converted light is emitted in a solid cone or cones (depending on the type of phase matching) with its point(s) in the center of the crystal. For type-I, light of a given wavelength is emitted around the rim of a single cone. The cones corresponding to different wavelengths are all coaxial. Photon pairs are emitted on opposite sides of the cones.

The situation is slightly more complicated for type-II, in which there are two cones for each wavelength, as shown in figure 2.1. Down-converted light that is extraordinarily polarized is emitted on one cone, while ordinarily polarized light is emitted on the other cone. The extraordinary cones corresponding to different wavelengths are coaxial, as are the ordinary cones.

2.2 Quantum theory of SPDC

There have been many theoretical treatments of SPDC, beginning with the early work of Klyshko [43] and later Hong and Mandel [84]. A detailed account of these calculations is out of the scope of this thesis. A detailed calculation can be found in the PhD. thesis of L. Wang, University of Rochester [85], as well as several theses in the UFMG physics department [45, 86]. In this section, I present the highlights of the detailed calculation, taken from the PhD. thesis of L. Wang [85].

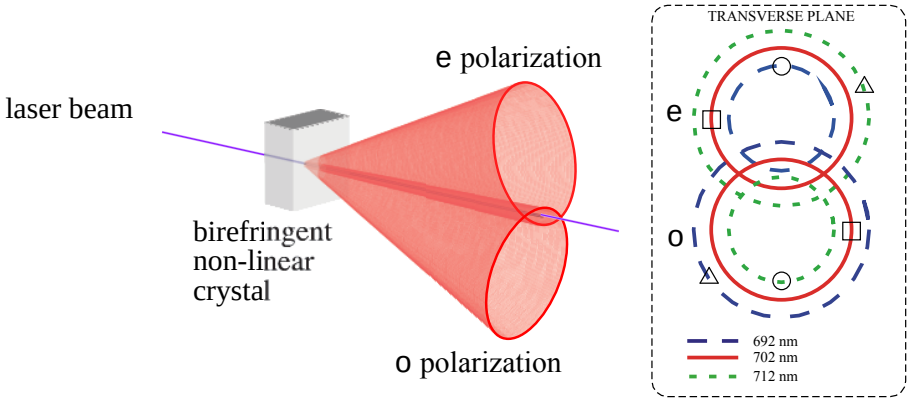

Figure 2.1: *Type-II spontaneous parametric down-conversion. The inset shows the arrangement of the cones of light in the transverse plane for 3 different wavelengths in a negative uniaxial crystal. Note that, due to the phase matching conditions, larger (smaller) wavelengths result in a larger cone for extraordinary (ordinary) polarization. The triangles, circles and squares give examples of regions where photon pairs can be found.*

2.2.1 Quantum theory of SPDC

When a sufficiently weak electric field $\boldsymbol{E}$ propagates through a second-order nonlinear optical medium, the electrical polarization of the medium is given by [87, 88]

$$\begin{aligned}\boldsymbol{P}(\mathbf{r},t) = &\epsilon_0 \int_0^\infty \chi^{(1)}(t')\boldsymbol{E}(\mathbf{r},t-t')dt' \\ &+ \int_0^\infty \int_0^\infty \chi^{(2)}(t',t'')\boldsymbol{E}(\mathbf{r},t-t')\boldsymbol{E}(\mathbf{r},t-t'')dt'dt''. \end{aligned} \tag{2.5}$$

We begin by defining a Hamiltonian

$$\mathcal{H} = \mathcal{H}_0 + \mathcal{H}_I, \tag{2.6}$$

where $\mathcal{H}_0$ is the linear component given by

$$\mathcal{H}_0 = \frac{1}{2}\int_V (\boldsymbol{D}\cdot\boldsymbol{E} + \boldsymbol{B}\cdot\boldsymbol{H}), \tag{2.7}$$

and the "perturbation" $\mathcal{H}_I$ is the nonlinear component, given by

$$\begin{aligned}\mathcal{H}_I =& \frac{1}{2}\int_{\mathrm{V}} \boldsymbol{E}\cdot\boldsymbol{P}_{\mathrm{nl}} \\ =& \frac{1}{2}\int_{\mathrm{V}}\int_{0}^{\infty}\int_{0}^{\infty}\chi^{(2)}_{ijk}(t',t'')E_i(\mathbf{r},t)E_j(\mathbf{r},t-t')E_k(\mathbf{r},t-t'')d\mathbf{r}dt'dt'', \end{aligned} \tag{2.8}$$

where $\boldsymbol{P}_{\mathrm{nl}}$ is the nonlinear component of the polarization. From this point on we concern ourselves only with this nonlinear portion.

The electric field can be expanded in terms of plane waves:

$$\boldsymbol{E}(\mathbf{r},t) = \boldsymbol{E}^{+}(\mathbf{r},t) + \boldsymbol{E}^{-}(\mathbf{r},t), \tag{2.9}$$

with

$$\boldsymbol{E}^{+}(\mathbf{r},t) = \frac{1}{\sqrt{\mathrm{V}}}\sum_{\mathbf{k},\mathtt{s}} \mathbf{e}_{\mathbf{k},\mathtt{s}}\varepsilon_{\mathbf{k}}\alpha_{\mathbf{k},\mathtt{s}}e^{i(\mathbf{k}\cdot\mathbf{r}-\omega t)} = \left[\boldsymbol{E}^{-}(\mathbf{r},t)\right]^{*} \tag{2.10}$$

and $\varepsilon_{\mathbf{k}} = \sqrt{\hbar\omega(\mathbf{k},\mathtt{s})/2\epsilon\mathrm{V}}$, where

- $\epsilon_0 \equiv$ free space permittivity
- $\mathrm{V} \equiv$ crystal volume
- $\mathbf{k} \equiv$ wavevector inside crystal
- $\mathtt{s} \equiv$ polarization
- $\mathbf{e}_{\mathbf{k},\mathtt{s}} \equiv$ two-dimensional polarization vector
- $\omega \equiv$ frequency.

We adopt the usual method of quantization of the electric field, letting $\alpha_{\mathbf{k},\mathtt{s}} \longrightarrow \mathbf{a}_{\mathbf{k},\mathtt{s}}$, where $\mathbf{a}_{\mathbf{k},\mathtt{s}}$ is the photon destruction operator. Then, the electric field becomes a field operator, given by

$$\boldsymbol{E}^{+}(\mathbf{r},t) \longrightarrow \mathbf{E}^{+}(\mathbf{r},t) = \frac{1}{\sqrt{\mathrm{V}}}\sum_{\mathbf{k},\mathtt{s}} \mathbf{e}_{\mathbf{k},\mathtt{s}}\varepsilon_{\mathbf{k}}\mathbf{a}_{\mathbf{k},\mathtt{s}}e^{i(\mathbf{k}\cdot\mathbf{r}-\omega t)} = \left[\mathbf{E}^{-}(\mathbf{r},t)\right]^{\dagger}. \tag{2.11}$$

Substituting expression (2.11) into the classical Hamiltonian (2.8) we have a quantum Hamiltonian operator

$$\begin{aligned}\mathbf{H}_I =& \frac{1}{2\mathrm{V}^{3/2}} \sum_{\mathbf{k}_s,\mathbf{s}_s} \sum_{\mathbf{k}_i,\mathbf{s}_i} \sum_{\mathbf{k}_p,\mathbf{s}_p} f^*(\omega_s) f^*(\omega_i) f(\omega_p) \mathbf{a}^\dagger_{\mathbf{k}_s,\mathbf{s}_s} \mathbf{a}^\dagger_{\mathbf{k}_i,\mathbf{s}_i} \mathbf{a}_{\mathbf{k}_p,\mathbf{s}_p} \times \\ & e^{i(\omega_s+\omega_i-\omega_p)t} [\chi_{ijk} (\mathbf{e}_{\mathbf{k}_s,\mathbf{s}_s})^*_i (\mathbf{e}_{\mathbf{k}_i,\mathbf{s}_i})^*_j (\mathbf{e}_{\mathbf{k}_p,\mathbf{s}_p})_k] \int_{\mathrm{V}} e^{-i(\mathbf{k}_s+\mathbf{k}_i-\mathbf{k}_p)\cdot\mathbf{r}} d\mathbf{r} \\ & + \text{H.C.}, \end{aligned} \tag{2.12}$$

where

$$f(\omega_j) = i \sqrt{\frac{\hbar\omega(\mathbf{k}_j, \mathbf{s}_j)}{2\epsilon_o n(\mathbf{k}_j, \mathbf{s}_j)^2}}. \tag{2.13}$$

Here $n(\mathbf{k}_j, \mathbf{s}_j)$ is the index of refraction of the nonlinear medium. We have also eliminated all terms which do not conserve energy and have defined

$$\chi_{ijk} \equiv \chi^{(2)}_{ijk}(w_p = \omega_s + \omega_i) + \chi^{(2)}_{ijk}(w_2 = \omega_s + \omega_p) + \chi^{(2)}_{ijk}(w_s = \omega_i + \omega_p) \tag{2.14}$$

with

$$\chi^{(2)}_{ijk}(\omega = \omega' + \omega'') = \int_0^\infty \int_0^\infty \chi^{(2)}_{ijk}(t', t'') e^{-i(\omega' t' + \omega'' t'')} d\mathbf{r} dt' dt''. \tag{2.15}$$

Here H.C. denotes the Hermitian conjugate. To find the quantum state at a given time t, we assume that the nonlinear interaction is turned on at time $t - t_1$ when the system is in the initial state $|\psi(t - t_1)\rangle$. When the interaction time t_1 is much longer than the coherence times of the down-converted fields and the pump field, a steady state is reached[2]:

$$|\psi(t)\rangle = \mathbf{U}(t, t - t_1) |\psi(t - t_1)\rangle \tag{2.16}$$

where

$$\mathbf{U}(t, t - t_1) = \exp\left(\frac{1}{i\hbar} \int_{t-t_1}^{t} d\tau \mathbf{H}_I(\tau) \right). \tag{2.17}$$

If the pump field is sufficiently weak, such that the interaction time is small compared to the average time between down-conversions, then we can Taylor expand and keep only the two-photon term:

$$\mathbf{U}(t, t - t_1) = 1 + \left(\frac{1}{i\hbar} \int_{t-t_1}^{t} d\tau \mathbf{H}_I(\tau) \right) + \cdots. \tag{2.18}$$

[2]For a cw laser, the interaction time t_1 is the time that the laser is operating.

It is straighforward to show that

$$\begin{aligned}\int_{t-t_1}^{t} \mathbf{H}_I(\tau)d\tau =& \frac{1}{2\mathrm{V}^{3/2}} \sum_{\mathbf{k}_s,\mathtt{s}_s} \sum_{\mathbf{k}_i,\mathtt{s}_i} \sum_{\mathbf{k}_p,\mathtt{s}_p} f^*(\omega_s) f^*(\omega_i) f(\omega_p) \mathbf{a}^\dagger_{\mathbf{k}_s,\mathtt{s}_s} \mathbf{a}^\dagger_{\mathbf{k}_i,\mathtt{s}_i} \mathbf{a}_{\mathbf{k}_p,\mathtt{s}_p} \times \\ & e^{i(\omega_s+\omega_i-\omega_p)(t-t_1/2)} [\chi_{ijk} (\mathbf{e}_{\mathbf{k}_s,\mathtt{s}_s})^*_i (\mathbf{e}_{\mathbf{k}_i,\mathtt{s}_i})^*_j (\mathbf{e}_{\mathbf{k}_p,\mathtt{s}_p})_k] \times \\ & \mathrm{sinc}((\omega_s+\omega_i-\omega_p)t_1/2) \int_{\mathrm{V}} e^{-i(\mathbf{k}_s+\mathbf{k}_i-\mathbf{k}_p)\cdot\mathbf{r}} d\mathbf{r} \\ & + \text{H.C.} \end{aligned} \tag{2.19}$$

The conservation of energy restriction is contained in the sinc $\equiv (\sin x)/x$ function. For sufficiently large t_1, only terms with $\omega_s + \omega_i \approx \omega_p$ will contribute substantially, and we can approximate the sinc function by a delta function. Integration in $\mathbf{r}$ leads to a similar sinc function involving the wavevectors, which provides the conservation of momentum condition.

In calculating the two-photon state of the down-converted photons, there are two basic approximations that can be made: the *monomode* approximation and the *monochromatic* approximation. These approximations facilitate not only the calculations but also the recognition of any interesting physics that may be present. The monomode approximation considers the fact that experiments are usually performed using narrow detection apertures which define the propagation direction of the down-converted photons. The monochromatic approximation recognizes that most experiments are realized using narrow interference filters, determining the magnitude of the wave vectors. Most treatments use at least one of these approximations.

Utilized in the majority of the work of the quantum optics group at UFMG [77, 89], the quantum theory of SPDC under the monochromatic approximation enables one to consider multimode (multi-directional) situations. This enables the study of transverse spatial characteristics of the biphoton. Our calculation of the quantum state of the biphoton will use the following assumptions and/or approximations:

1. The monochromatic approximation is valid for the down-converted photons, which are detected using narrow band interference filters.

2. The pump beam is a monochromatic continuous laser beam, linearly polarized in the extraordinary $\mathtt{e}$ direction, that passes through the entire length of the nonlinear crystal in the $+z$ direction along the z axis.

3. Photons in the pump beam can be accurately represented by a coherent state.

4. We will work in the paraxial approximation around different axes z_p, z_s and z_i for the pump and down converted photons, respectively.

2.2.2 The Fresnel and paraxial approximations

Let us assume that an optical field is propagating along the z direction. Here we are considering only monochromatic waves with $k = |\mathbf{k}|$ constant, such that for each wave vector $\mathbf{k} = (\mathbf{q}, k_z)$ with $k^2 = q^2 + k_z^2$, we can solve for the k_z component:

$$k_z = \sqrt{k^2 - q^2} \approx k\left(1 - \frac{q^2}{2k^2}\right), \qquad \text{if } q^2 \ll k^2. \tag{2.20}$$

The above approximation, known as the Fresnel approximation, is obtained by simple Taylor expansion and is valid when $q^2 \ll k^2$. To see the robust validity of the Fresnel (paraxial) approximation, let us set $q = k/2$ and perform the simple calculation:

$$k\left(1 - \frac{q^2}{2k^2}\right) = \frac{7}{8}k,$$

while the exact form gives:

$$\sqrt{k^2 - q^2} = \frac{\sqrt{3}}{2}k \approx \frac{6.928}{8}k.$$

Even for a huge value of q, the Fresnel (paraxial) approximation gives an error of only about 0.01. In the experiments considered in this thesis $q \sim k/100$, which corresponds to an error less than 0.00001.

The Fresnel approximation is essentially a particular application of the more general paraxial approximation. In geometric optics, where light is represented by rays, paraxial rays are those that lie at small angles to the optical axis of the optical system under consideration. If we were to draw rays from the origin to points $\mathbf{k}$ in k-space satisfying the approximation in expression (2.20), they would be paraxial rays. In this respect the paraxial approximation and the Fresnel approximation are essentially the same. Throughout this thesis we will make use of both the Fresnel and paraxial approximations, though starting in the next section we will refer to both as the paraxial approximation.

A thorough account of the paraxial approximation can be found in most classical optics textbooks [90, 91]. Here we will present only the bare essentials. The paraxial approximation can be extended to wave optics if one considers only waves whose

wavefront normals are paraxial rays. In wave optics an optical wave $E(\mathbf{r},t)$ satisfies the wave equation:

$$\nabla^2 E(\mathbf{r},t) - \frac{1}{c^2}\frac{\partial^2}{\partial t^2}E(\mathbf{r},t) = 0.$$

If one considers that the optical wave is monochromatic with harmonic time dependence, so that $E(\mathbf{r},t) = \mathcal{E}(\mathbf{r})\exp(i\omega t)$, where ω is the angular frequency, one arrives at the Helmholtz equation:

$$\nabla^2 \mathcal{E}(\mathbf{r}) + k^2 \mathcal{E}(\mathbf{r}) = 0.$$

If we now consider only paraxial waves propagating near the z axis, we can write $\mathcal{E}(\mathbf{r}) = \mathcal{U}(\mathbf{r})\exp(ikz)$, where $\mathcal{U}(\mathbf{r})$ is a slowly varying function of $\mathbf{r}$ such that $\mathcal{E}(\mathbf{r})$ maintains a plane wave structure for distances within that of a wavelength. Using this form of $\mathcal{E}(\mathbf{r})$ in the Helmholtz equation, one arrives at the paraxial Helmholtz equation.

$$\left(\frac{\partial^2}{\partial x^2} + \frac{\partial^2}{\partial y^2}\right)\mathcal{U}(\mathbf{r}) + 2ik^2\mathcal{U}(\mathbf{r}) = 0. \tag{2.21}$$

In arriving at (2.21), we have used the fact that the term $\partial^2\mathcal{U}(\mathbf{r})/\partial z^2$ is very small within distances of a wavelength. The paraxial Helmholtz equation admits several well known solutions, including the Hermite-Gaussian and Laguerre-Gaussian beams introduced in section 2.4. It has been shown by several authors that the paraxial Helmholtz equation is analogous to the Schrödinger equation in quantum mechanics [92]. In reference [92] an alternative derivation of equation (2.21) is provided which requires that the optical wave is only nearly monochromatic.

2.2.3 The angular spectrum

In this thesis we will make use of several techniques from Fourier Optics, in particular the propagation of the angular spectrum. Fourier Optics [91, 93] provides a useful method of calculating the propagation of an optical field through a given optical system. Here we consider a monochromatic scalar field satisfying the Helmholtz equation (2.21), which can be represented as [93]

$$\mathcal{E}(\boldsymbol{\rho},z) = \frac{1}{2\pi^2}\iint v(\mathbf{q},z)e^{i\mathbf{q}\cdot\boldsymbol{\rho}}d\mathbf{q}, \tag{2.22}$$

where we assume that the field is propagating along the z direction and have defined $\boldsymbol{\rho}$ and $\mathbf{q}$ as the transverse components of $\mathbf{r}$ and $\mathbf{k}$, respectively. The angular spectrum

$v(\mathbf{q}, z)$ is the inverse Fourier transform of the field:

$$v(\mathbf{q}, z) = \frac{1}{2\pi^2} \iint \mathcal{E}(\boldsymbol{\rho}, z) e^{-i\mathbf{q}\cdot\boldsymbol{\rho}} d\boldsymbol{\rho}. \tag{2.23}$$

One can also understand the angular spectrum by recognizing equation (2.22) as an expansion of $\mathcal{E}(\boldsymbol{\rho}, z)$ in terms of plane waves $\exp(i\mathbf{q}\cdot\boldsymbol{\rho})$, in which the angular spectrum $v(\mathbf{q}, z)$ acts as a weighting function.

2.2.4 The biphoton state

If the nonlinear crystal is thin enough, under the approximations mentioned above the two-photon quantum state created by SPDC is accurately given by [77, 89]

$$|\psi\rangle_{SPDC} = C_1 |\text{VAC}\rangle + C_2 |\psi\rangle , \tag{2.24}$$

where

$$|\psi\rangle = \sum_{\mathbf{s}_s, \mathbf{s}_i} C_{\mathbf{s}_s, \mathbf{s}_i} \iint_D d\mathbf{q}_s d\mathbf{q}_i \; \Phi(\mathbf{q}_s, \mathbf{q}_i) \, |\mathbf{q}_s, \mathbf{s}_s\rangle_s \, |\mathbf{q}_i, \mathbf{s}_i\rangle_i , \tag{2.25}$$

and $|\text{VAC}\rangle$ represents the zero-photon vacuum state in modes s and i. The coefficients C_1 and C_2 are such that $|C_2| \ll |C_1|$. C_2 depends on the crystal length, the nonlinearity coefficient and the magnitude of the pump field, among other factors. The kets $|\mathbf{q}_j, \mathbf{s}_j\rangle$ represent Fock states labeled by the transverse component $\mathbf{q}_j$ of the wave vector $\mathbf{k}_j$ and by the polarization $\mathbf{s}_j$ of the mode $j = s$ or i. The polarization state of the down-converted photon pair is defined by the coefficients $C_{\mathbf{s}_s, \mathbf{s}_i}$. When the crystal output angles of s and i are small, the function $\Phi(\mathbf{q}_s, \mathbf{q}_i)$, which can be regarded as the normalized angular spectrum of the two-photon field [77], is given by

$$\Phi(\mathbf{q}_s, \mathbf{q}_i) = \frac{1}{\pi} \sqrt{\frac{2L}{K}} \; v(\mathbf{q}_s + \mathbf{q}_i) \; \text{sinc}\left(\frac{L|\mathbf{q}_s - \mathbf{q}_i|^2}{4K} \right), \tag{2.26}$$

where $v(\mathbf{q})$ is the normalized angular spectrum of the pump beam, L is the length of the nonlinear crystal in the z-direction, and K is the magnitude of the pump field wave vector defined above. The integration domain D is defined by the paraxial approximation. However, in most experimental conditions, the region in which $\Phi(\mathbf{q}_s, \mathbf{q}_i)$ is appreciable is much smaller than D. Note that the angular spectrum of the pump beam is transferred to the fourth-order spatial correlation properties of the two-photon state [77]. $v(\mathbf{q}_s + \mathbf{q}_i)$ is not a separable function of $\mathbf{q}_s$, and $\mathbf{q}_i$, meaning that $v(\mathbf{q}_s + \mathbf{q}_i)$ cannot be written

as a product of a function $F_s(\mathbf{q}_s)$ with a function $F_i(\mathbf{q}_i)$: $v(\mathbf{q}_s + \mathbf{q}_i) \neq F_s(\mathbf{q}_s)F_i(\mathbf{q}_i)$. This non-separability is responsible for many of the nonlocal and non-classical effects observed with the state (2.25).

Eqs. (2.25) and (2.26) include the wave vectors inside the nonlinear birefringent crystal, which, upon propagation through the crystal, may suffer transverse and longitudinal walk-off effects, as well as refraction at the exit surface. In a type-II crystal, the photons are orthogonally polarized, and these effects, which can be considerable, may decrease the quality of the entanglement between the photons. There are several ways to remedy this problem. Walk-off effects can be corrected by additional birefringent crystals, as discussed in section 2.3.1. For the degenerate case, where $\lambda_s = \lambda_i = 2\lambda_p$, Snell's law gives equal exit angles for extraordinary and ordinary polarized photons. We use narrow interference filters in our experiments (centered at $2\lambda_p$) which guarantee that we work near this regime.

If the crystal is thin enough (on the order of a few millimeters), the sinc function in (2.26) can be considered to be equal to unity [77]. Almost all calculations in this work will begin with the state (2.24).

2.2.5 The biphoton wavefunction

The two-photon detection probability is defined as

$$\mathcal{P}(\mathbf{r}_1, \mathbf{r}_2) = |\mathbf{\Psi}(\mathbf{r}_1, \mathbf{r}_2)|^2 \tag{2.27}$$

where $\mathbf{r}_1 = (x_1, y_1, z_1)$ and $\mathbf{r}_2 = (x_2, y_2, z_2)$ are the positions of the photon detectors. Here we have used the orthonormality and completeness of the Fock states to define the two-photon detection probability amplitude

$$\mathbf{\Psi}(\mathbf{r}_1, \mathbf{r}_2) = \langle \text{VAC} | \, \mathbf{E}^{(+)}(\mathbf{r}_1) \otimes \mathbf{E}^{(+)}(\mathbf{r}_2) \, | \psi \rangle \, , \tag{2.28}$$

which, in the monochromatic approximation, can be thought of as the biphoton wavefunction [74]. The $\mathbf{E}^{(+)}(\mathbf{r})$ are the field operators in the paraxial approximation, which are

$$\mathbf{E}^{(+)}(\mathbf{r}) = \text{V}\mathcal{E}_0 \frac{e^{i(kz-\omega t)}}{(2\pi)^3} \sum_\sigma \sigma \int d\mathbf{q} \, \mathbf{a}(\mathbf{q}, \sigma) e^{i\left(\mathbf{q}\cdot\boldsymbol{\rho} - \frac{q^2}{2k} z\right)} \tag{2.29}$$

where k is the magnitude of the wave vector $\mathbf{k}$ and $\boldsymbol{\rho} = x\hat{\mathbf{x}} + y\hat{\mathbf{y}}$ is the transverse component of the position vector $\mathbf{r}$. The operator $\mathbf{a}(\mathbf{q}, \sigma)$ annihilates a photon with transverse wave vector $\mathbf{q}$ and polarization σ. Here $\mathcal{E}_0$ is a frequency dependent constant.

2.2.6 The coincidence count rate

The calculations performed up until now have been done considering two point-like detectors located at positions $\mathbf{r}_1$ and $\mathbf{r}_2$. However, in the laboratory the detectors have an active detection area which we represent by the iris function $\mathcal{I}(\boldsymbol{\rho})$, which defines an opening of area A centered at $\boldsymbol{\rho}$. The function $\mathcal{I}(\boldsymbol{\rho})$ is equal to one inside A and zero outside. We then calculate the coincidence-count rate by

$$\mathrm{C} = \int d\boldsymbol{\rho}_1 \int d\boldsymbol{\rho}_2 \mathcal{I}(\boldsymbol{\rho}_1)\mathcal{I}(\boldsymbol{\rho}_2)\mathcal{P}(\mathbf{r}_1, \mathbf{r}_2), \tag{2.30}$$

that is, we integrate the detection probability over the area of the detection irises.

The coincidence count rate is included here merely for the sake of completeness. In the experiments presented in the following chapters, we will be able to analyze the theoretical predictions and experimental results by examining $\mathcal{P}(\mathbf{r}_1, \mathbf{r}_2)$ or $\mathbf{\Psi}(\mathbf{r}_1, \mathbf{r}_2)$ alone, that is, without calculating C.

2.3 Engineering entanglement

The simplest example of entangled states are the so-called Bell-states:

$$\left|\psi^{\pm}\right\rangle = \frac{1}{\sqrt{2}} \left(|h\rangle_1 |v\rangle_2 \pm |v\rangle_1 |h\rangle_2\right), \tag{2.31a}$$

$$\left|\phi^{\pm}\right\rangle = \frac{1}{\sqrt{2}} \left(|h\rangle_1 |h\rangle_2 \pm |v\rangle_1 |v\rangle_2\right), \tag{2.31b}$$

where $|\psi^-\rangle$ is the antisymmetric singlet state and $|\psi^+\rangle$,$|\phi^{\pm}\rangle$ are the symmetric triplet states. In this work we use mostly polarization Bell-states, so h and v stand for horizontal and vertical polarization and 1 and 2 represent different spatial modes, though h and v could represent any binary set of orthogonal states, such as different paths in an interferometer, spin $\uparrow$ and $\downarrow$ of electrons, energy levels in a two-state atomic system, etc. The Bell states are an invaluable resource in tests of quantum mechanics against local realism as well as in quantum information protocols.

The Bell states (2.31) are maximally entangled two-qubit states. More generally, we can define non-maximally entangled states of the form

$$|\psi(\epsilon, \phi)\rangle = \frac{1}{\sqrt{1+\epsilon^2}} \left(|h\rangle_1 |v\rangle_2 + \epsilon\, e^{i\phi} |v\rangle_1 |h\rangle_2\right), \tag{2.32a}$$

$$|\phi(\epsilon, \phi)\rangle = \frac{1}{\sqrt{1+\epsilon^2}} \left(|h\rangle_1 |h\rangle_2 + \epsilon\, e^{i\phi} |v\rangle_1 |v\rangle_2\right), \tag{2.32b}$$

where ϵ is known as the *degree of entanglement*.

The role of the photon in quantum information is promising due to the relative ease that entangled photons can be created and transported. Furthermore, the photon provides us with several degrees of freedom in which quantum information can be encoded and manipulated. For example, encoding a qubit in the polarization of a photon, all single qubit rotations can be achieved using only half- and quarter-wave plates. Beam splitters and phase plates serve the same function for the momentum degree of freedom. The difficult task then is to implement a universal two-qubit gate such as the CNOT gate, which remains a difficult task due to the nonlinear interaction required.

To date, physicists have used SPDC to generate photons that are entangled in polarization [13, 16], linear momentum [10], energy [11] and orbital angular momentum [45, 46, 19]. Several sources of entangled photons are discussed below.

2.3.1 Polarization entanglement with SPDC

To date, a number of experimental arrangements have been used to create polarization entangled photons. The two most common sources are the two type-I crystal source [16] and the type-II "crossed cone" source [13].

In chapter 3, we utilize polarization-entangled photons created using the crossed cone source [13] shown in "SOURCE " in fig. 2.2. This source was the first demonstration of Bell-states (in polarization space) that did not require post-selection [8, 9]. A type-II nonlinear crystal of thickness L generates orthogonally polarized photon pairs. The crystal is aligned so that the `e` cone and `o` cone cross at two points, as shown in figure 2.2. The quantum state detected at these two intersection regions is a Bell state. Since the down-converted photons are orthogonally polarized, they suffer transverse and longitudinal walk-off effects due to the birefringence of the crystal. The walk-off effects create a small amount of distinguishability, that is, we could use the walk-off effects to discriminate between the two photons. This distinguishability degrades the quality of the polarization entanglement of the two-photon state. To correct for this, a half-wave plate is placed after the first crystal (The mirror is used to reflect away the UV laser beam). The plate rotates the polarization 90° so that when the photons pass through a second crystal (width $L/2$), their roles are reversed: an `o` photon is now an `e` photon and vice versa. In this way, on average both photons suffer the same amount of

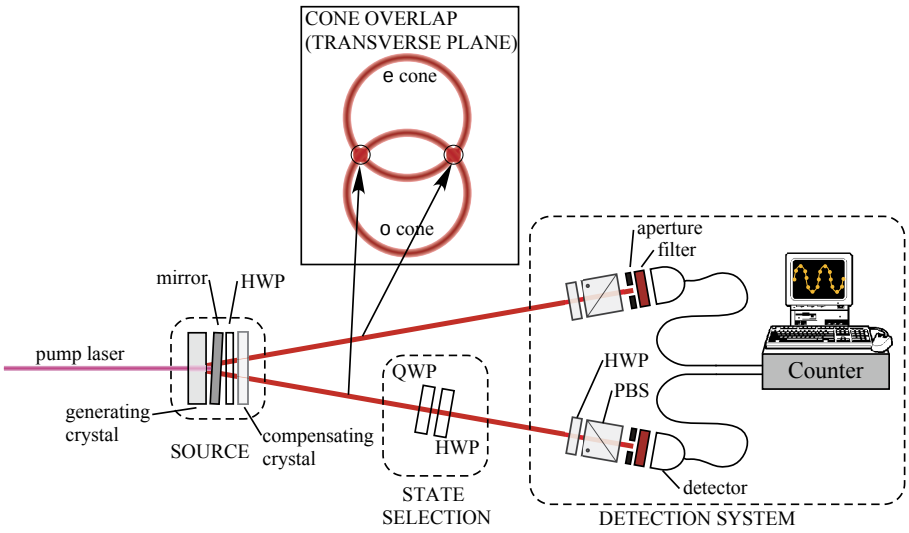

Figure 2.2: *Typical experimental setup for generation and testing of Bell-states. The source is the type-II "crossed cone" source discussed in the text. QWP and HWP are quarter- and half-wave plates used to select between the four Bell-states. Our detection system consists of computer controlled polarization analyzers (a rotatable half-wave plate (HWP) and polarizing beam splitter (PBS)), small detection apertures (typically about* 3 *mm diameter), narrow band interference filters (1 nm FWHM) and EG&G SPCM 200 photodetectors. Coincidence and single-photon counts are registered using a personal computer. The process is fully automated using LabVIEW software.*

walk-off, and the distinguishability is erased. Additional half- and quarter-wave plates are placed in the path of one of the photons ("STATE SELECTION", fig. 2.2). The half-wave plate can be orientated to switch the polarization of one of the photons and the quarter-wave plate to adjust the phase. By adjusting the angles of the wave plates, one can switch between all four Bell states.

Figure 2.2 shows a typical experimental setup for generating and testing Bell-states. To test the quality of the Bell-states, an abridged form of a Bell's inequality-type experiment is performed. Polarization analyzers are placed before each detector. One polarizer is fixed at 45° while the other is rotated, giving a sinusoidal oscillation in the two-photon detections, or *coincidence* counts. Figure 2.3 shows results for all four Bell-states obtained in our laboratory. The high visibility of these curves ($\mathcal{V} \sim 0.94 - 0.97$) is characteristic of high-quality entanglement.

2.3.2 Discriminating polarization-entangled Bell-states

Several quantum information protocols, including quantum teleportation [94] and dense coding [95] require the discrimination of the four Bell-states (2.31), as illustrated by the cartoon in figure 2.4. The ideal analyzer projects a given two-photon input state onto one of the four states in the Bell-basis (2.31). Since it has been shown that one can use quantum teleportation to implement quantum repeaters [96] as well as quantum logic operations [33, 97], it is important that there exist experimental techniques of Bell-state discrimination.

Bell-state analysis of polarization-entangled photons can be performed incompletely by using two-photon interference at a beam splitter and additional polarization analyzers [98, 52], as shown in figure 2.5. As will be discussed in detail in chapters 3 and 4, due to the overall bosonic symmetry of the photon state [99], photons in the $|\psi^-\rangle$ end up at diferent output ports of the beam splitter. The polarizing beam splitters are then used to separate the $|\psi^+\rangle$ state from the $|\phi^\pm\rangle$ states. With this experimental setup one can separate the Bell-states into 3 groups, as was shown experimentally by Mattle *et al.* [52]. Unfortunately, it has been shown that complete discrimination of all four Bell states is impossible using only linear optics [100, 101, 102, 103]. In chapter 4 we will discuss several methods to improve upon Bell-state analysis by creating hyperentangled photons (entangled in multiple degrees of freedom).

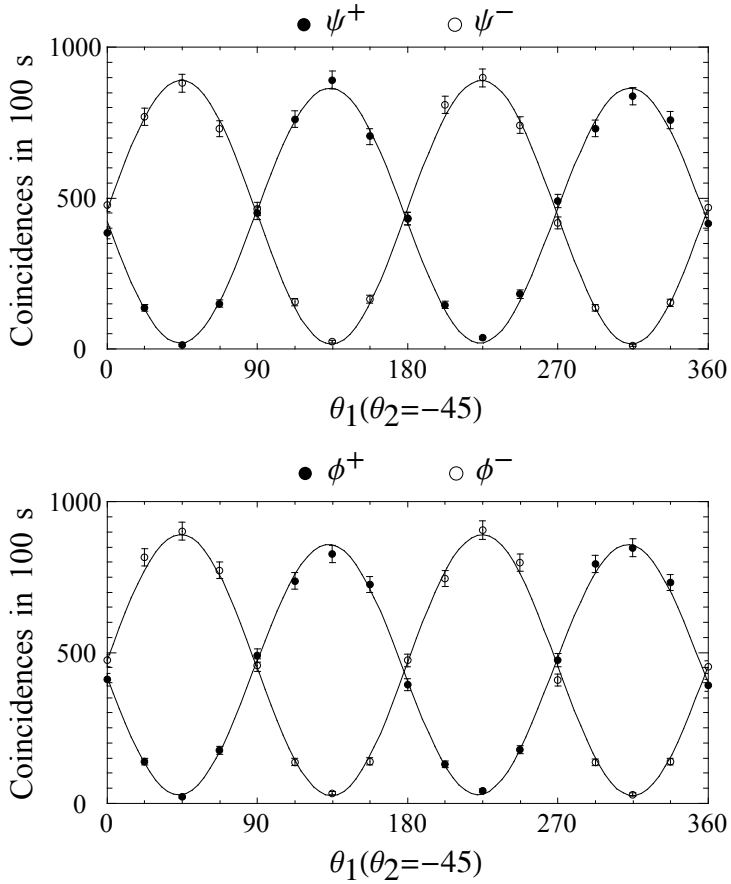

Figure 2.3: *Results of polarization analysis of Bell-states generated in our laboratory. The sinusoidal curves have visibilities of* $\mathcal{V} \sim 0.94 - 0.97$*, indicating high-quality entanglement.*

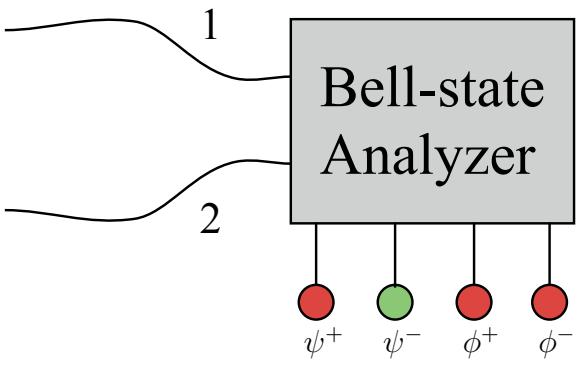

Figure 2.4: *Cartoon of an ideal Bell-state analyzer.*

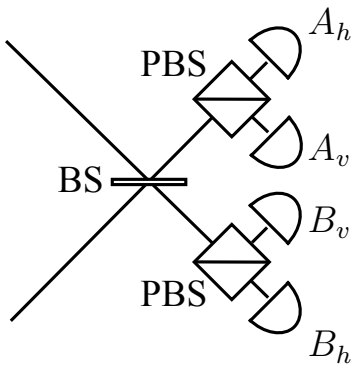

Figure 2.5: *Optical Bell-state analyzer. BS is a 50/50 non-polarizing beam splitter and PBS are polarizing beam splitters in the h/v basis.*

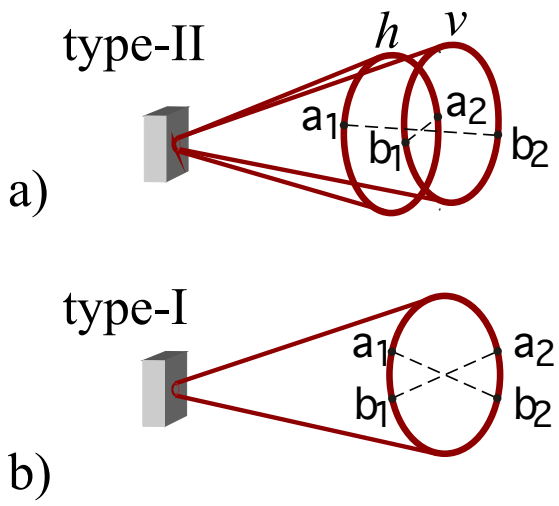

Figure 2.6: *Sources of momentum-entangled photons. a) Type-II SPDC source. b) Type-I SPDC source.*

2.3.3 Momentum entanglement with SPDC

Entanglement in the linear momentum (also called spatial mode) degree of freedom was first demonstrated experimentally in the form of a Bell's inequality experiment by Rarity and Tapster [10]. Several quantum information protocols, including Bell-state measurements [104, 105], have been performed using momentum-entangled states. Figure 2.6 shows two possible methods of generating momentum entangled pairs. Both sources require post-selection in the form of tiny apertures placed in the cone of down-converted light. With this post-selection, each photon (1 and 2) can be emitted from 2 possible positions (a and b). In this type of entanglement source, each photon field is approximated by a plane wave. Assuming that each aperture is the same size, the entangled state is of the form

$$|\psi\rangle = \frac{1}{\sqrt{2}}(|a\rangle_1 |b\rangle_2 + e^{i\varphi} |b\rangle_1 |a\rangle_2) \tag{2.33}$$

We note here that a combination of the sources producing momentum-entangled (figure 2.6) and polarization-entangled (Figure 2.2) photons can be used to generated "hyper-entangled" photons: photons entangled in more than one degree of freedom. We will discuss this type of polarization-momentum hyperentanglement in section 4.4.3.

2.3.4 Transverse mode entanglement with SPDC

The generation of down-converted fields entangled in higher-order Gaussian modes is a central topic of this thesis. Transverse modes, such as the Hermite-Gaussian and Laguerre-Gaussian modes will be introduced in section 2.4. Through SPDC it is possible to generate fields entangled in these modes. Several theoretical [82, 106, 107, 108, 109] and experimental [19, 46, 110, 109] works have shown the entanglement of orbital angular momentum (Laguerre-Gaussian modes). In particular, Anton Zeilinger's group has shown experimental evidence that the down-converted photons are entangled in orbital angular momentum [46] and have performed Bell-type inequalities [19]. In chapter 5, our theoretical and experimental results showing the conservation and entanglement of orbital angular momentum with SPDC are presented.

Recent experimental work by Andrew White's group has shown that down-converted fields can also be entangled in Hermite-Gaussian modes [110]. These modes are of particular interest since the first-order Hermite-Gaussian and Laguerre-Gaussian modes obey an algegra that is analogous to polarization of the electromagnetic field, and can thus be used to represent a qubit. The generation of entangled Hermite-Gaussian modes will be discussed in chapter 6.

2.4 Transverse modes

2.4.1 Hermite-Gaussian modes

Like the well known Gaussian beam, the Hermite-Gaussian and Laguerre-Gaussian beams are also solutions to the paraxial Helmholtz equation [90]. The Hermite-Gaussian modes are given by the complex field amplitude

$$\begin{aligned}\mathrm{HG}_{nm}(x,y,z) =& C_{nm}\frac{1}{w(z)}H_n\left(\frac{\sqrt{2}x}{w(z)}\right)H_m\left(\frac{\sqrt{2}y}{w(z)}\right)\exp\left(-\frac{x^2+y^2}{w(z)^2}\right)\\ &\exp\left\{-i\left[\frac{k(x^2+y^2)}{2R(z)}-(n+m+1)\varepsilon(z)\right]\right\},\end{aligned} \tag{2.34}$$

where the coefficients C_{nm} are given by

$$C_{nm}=\sqrt{\frac{2}{2^{(n+m)}\pi n!m!}}. \tag{2.35}$$

$H_n(x)$ is the n^{th}-order Hermite polynomial, which is an even or odd function of x if n is even or odd, respectively. The parameters $R(z)$, $w(z)$ and $\varepsilon(z)$ are defined below:

$$w(z) = w_0\sqrt{1 + \frac{z^2}{z_R^2}}, \tag{2.36}$$

is known as the beam radius at the point z,

$$R(z) = z\left(1 + \frac{z^2}{z_R^2}\right), \tag{2.37}$$

is the wavefront radius of curvature at the point z, and

$$\varepsilon(z) = \tan^{-1}\frac{z}{z_R}, \tag{2.38}$$

is the phase retardation or *Gouy phase*. The parameter z_R is known as the *Rayleigh range*. The *order* $\mathcal{N}$ of the beam is the sum of the indices: $\mathcal{N} = m + n$. Note that the usual Gaussian beam is the zeroth-order HG_{00} beam.

2.4.2 Modifying the laser cavity

Following the method outlined in references [111, 112], we can "hot rod" the argon laser to generate Hermite-Gaussian modes HG_{nm} by inserting thin wire(s) in the cavity of the laser. The wires, placed in the position of the nodes of the desired output mode, break the cylindrical symmetry of the laser cavity, which forces the laser to operate in the higher order modes. Using *only one* wire (25 μm or 50 μm diameter), we were able to generate modes HG_{01}, HG_{10}, HG_{02} and HG_{20} as well as the diagonal modes DHG_{10}, DHG_{01} (explained below) with a laser power of about 30 mW. The wire is mounted on a translation and rotation stage, allowing for fine tuning of the position and orientation of the wire. The first-order modes are created by placing the wire in the center of the beam. Placing the wire slightly off-center generates the second order modes. Placing the wire at $\pm 45°$ generates the modes DHG_{10} and DHG_{01}. However, we were not able to generate second order modes DHG_{02} or DHG_{20} with only one wire. This complication seems to arise from the geometry of optical components inside the cavity, presumably the Brewster's windows.

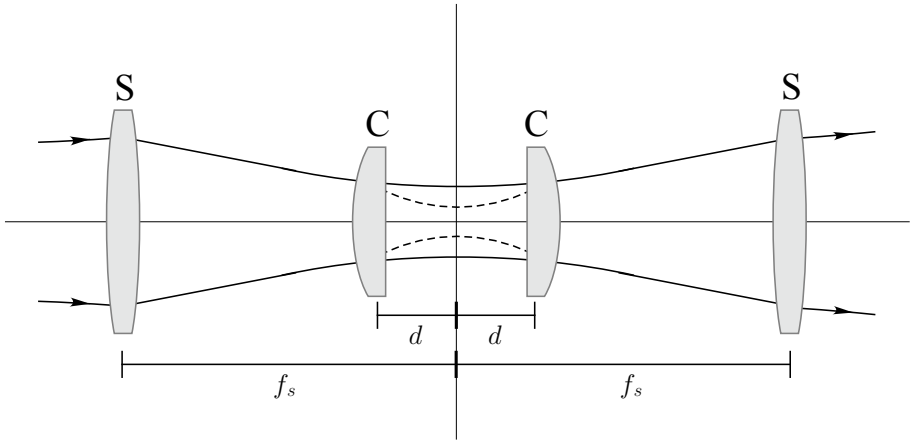

Figure 2.7: *Diagram of mode converter. The spherical lenses S have a focal length* $f = 500\,mm$*. The cylindrical lenses C (focal length* $f_c = 25.4\,mm$*, placed a distance* $d = f/\sqrt{2}$ *apart, provide a relative* $\pi/2$ *phase shift to orthogonal beam components (dashed line in center region), transforming a DHG mode into a LG mode.*

2.4.3 Laguerre-Gaussian modes

The Laguerre-Gaussian modes are given by

$$\begin{aligned} \mathrm{LG}_p^l(\rho,\phi,z) =& D_p^l \frac{1}{w(z)} \left(\frac{\sqrt{2}\rho}{w(z)}\right)^l L_p^l\left(\frac{2\rho^2}{w(z)^2}\right) \exp\left(-\frac{\rho^2}{w(z)^2}\right) \\ & \exp\left\{-i\left[\frac{k\rho^2}{2R} - (n+m+1)\varepsilon(z)\right] - (p-l)\phi\right\}, \end{aligned} \tag{2.39}$$

where (ρ,ϕ,z) are the usual cylindrical coordinates, D_p^l is a constant and L_p^l are the Laguerre polynomials. The parameters $R(z)$, $w(z)$ and $\varepsilon(z)$ are defined in eqs. (2.36) - (2.38). The order of the LG beam is $\mathcal{N} = |l| + 2p$. Note that the usual Gaussian beam is the zeroth-order LG_0^0 beam. It is well known that the Laguerre-Gaussian beams carry orbital angular momentum due to the azimuthal (ϕ) phase term [113, 114].

2.4.4 Mode-conversion

By constructing a mode converter, we can transform Hermite-Gaussian modes (HG_{mn}) into Laguerre-Gaussian (LG_p^l) modes of the same order [111, 112, 115]. HG-modes can be produced directly by a slight modification of the laser cavity, as discussed above. The following discussion quotes results found in references [111, 112].

As shown in reference [112], a first-order diagonal Hermite-Gaussian (DHG)

mode, given by $\text{DHG}_{01} \equiv \text{HG}_{01}((x+y)/\sqrt{2}, (x-y)/\sqrt{2}, z)$, is a superposition of modes HG_{01} and HG_{10}, that is

$$\text{DHG}_{01} = \frac{1}{\sqrt{2}}(\text{HG}_{01} + \text{HG}_{10}), \tag{2.40}$$

while the Laguerre Gaussian mode LG_0^1 is a superpostion of these same modes with relative phase of $\pi/2$, that is

$$\text{LG}_0^1 = \frac{1}{\sqrt{2}}(\text{HG}_{01} + i\text{HG}_{10}). \tag{2.41}$$

Thus, the diagonal mode DHG_{01} can be transformed to the LG_0^1 mode by introducing a relative $\pi/2$ phase change to the modes HG_{01} and HG_{10}, which can be introduced using a *mode converter*.

Similarly, but slightly more complicated, higher order modes satisfy the relations

$$\text{DHG}_{nm} = \sum_{j=0}^{\mathcal{N}} b(n,m,j)\text{HG}_{\mathcal{N}-j,j} \tag{2.42}$$

and

$$\text{LG}_p^l \equiv \text{LG}_{nm} = \sum_{j=0}^{\mathcal{N}} i^j b(n,m,j)\text{HG}_{\mathcal{N}-j,j}, \tag{2.43}$$

where $l = n - m$, $p = \min(n,m)$ and

$$b(n,m,j) = \left[\frac{(\mathcal{N}-j)!j!}{2^{\mathcal{N}}n!m!}\right]^{1/2} \frac{1}{j!}\frac{d^j}{dt^j}\left[(1-t)^n(1+t)^m\right]\Big|_{t=0}. \tag{2.44}$$

Using the orthogonality of the HG and LG modes, it is possible to invert (2.43) and write the HG modes in terms of the LG modes:

$$\text{HG}_{nm} = i^m \sum_{j=0}^{\mathcal{N}} b(\mathcal{N}-j, j, m)\text{LG}_{\mathcal{N}-j,j}, \tag{2.45}$$

In order to transform a DHG beam into a LG beam we can exploit the Gouy phase $\varepsilon(z)$ to provide a $\pi/2$ phase shift. The Gouy phase represents the change in phase in the beam when going through a beam waist. By creating an astigmatism along the direction of one of the HG modes (x or y) around the beam waist, a relative phase change is introduced. For an isotropic HG mode, the Gouy phase term is

$$(n+m+1)\varepsilon(z) = (n+m+1)\tan^{-1}\left(\frac{z}{z_0}\right). \tag{2.46}$$

Now consider an astigmatic HG-mode, which has different curvatures in the x and y directions. Then the amplitude must be treated separately in the two transverse directions. The contribution from the Gouy phase is then

$$\exp[-i(n+1/2)\varepsilon_x(z) + (m+1/2)\varepsilon_y(z)], \tag{2.47}$$

where

$$\varepsilon_x(z) = \tan^{-1}\left(\frac{z-z_{0x}}{z_{Rx}}\right), \tag{2.48}$$

and

$$\varepsilon_y(z) = \tan^{-1}\left(\frac{z-z_{0y}}{z_{Ry}}\right). \tag{2.49}$$

z_{0x} and z_{0y} are the positions of the beam waists and z_{Rx} and z_{Ry} are the Rayleigh ranges in each transverse direction.

We can introduce a relative phase between the x and y directions by making the beam astigmatic in a confined spatial region, which can be accomplished by placing two identical cylindrical lenses a distance $2d$ apart and properly mode-matching the input beam. Figure 2.7 illustrates the idea. The beam is made astigmatic in the region between the cylindrical lenses C and isotropic elsewhere. The transverse radii (x and y) of the beam (2.36) are equal at the positions of the cylindrical lenses ($z = \pm d$). The phase difference δ ($0 \leq \delta < \pi$) between HG modes depends on the focal length f of the cylindrical lenses and their distance d from the beam waist. Equating the beam radii at $z = \pm d$ and carrying out a simple calculation (given in detail in ref. [111]), one sees that the phase difference δ can be set to $\pi/2$ by setting $d = f/\sqrt{2}$, which requires that $z_{Ry} = (1+1/\sqrt{2})f$, which can be met using a spherical lens S at the input. The second spherical lens S is used to "collimate" the beam. Thus a mode converter consisting of a spherical lens and two cylindrical lenses can create a phase difference of $\pi/2$ between consecutive HG modes, which converts a DHG-mode into a LG mode.

Our mode-converter uses cylindrical lenses with $f = 50.2\,\text{mm}$, which required a Rayleigh range $z_R \approx 85.67\,\text{mm}$. The argon laser, operating at 351.1 nm, generates a beam with a Rayleigh range of 654.45 mm. The position of the beam waist is about 200 mm *behind* the rear mirror. Using a spherical lens with focal length $f_s = 500\,\text{mm}$, we were able to "mode match" the Rayleigh range of our laser with the required Rayleigh range when the mode converter was placed 1882 mm from the beam waist of the laser. Since we were able to generate the HG modes more easily than the DHG

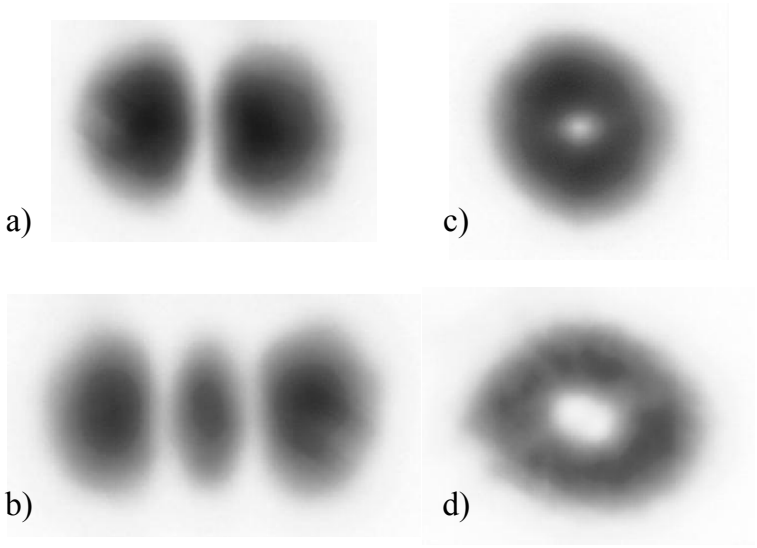

Figure 2.8: *Digital photographs of Hermite-Gaussian modes a)* HG_{01} *and b)* HG_{02}*, and Laguerre-Gaussian modes c)* LG_0^1 *and d)* LG_0^2 *generated using the* 351.1 *nm line of an* Ar^- *laser with (a and b)* $25\,\mu m$ *diameter wire aligned vertically and (c and d)* $25\,\mu m$ *wire and mode converter as discussed in the text.*

modes, we orientated the cylindrical lenses at 45°, which is just a change of basis. In this way we were able to generate first and second-order LG modes.

Figure 2.8 shows digital photographs of modes HG_{01}, HG_{02}, LG_0^1 and LG_0^2 created in our laboratory. In chapters 5 and 6 we will show that under appropriate conditions, SPDC creates photons entangled in LG and HG modes. Starting in the next chapter, we will utilize these transverse modes to study the multimode fourth-order interference properties of photons created by SPDC, and present some applications for quantum information protocols.

3

Multimode Hong-Ou-Mandel Interference

In this chapter, we consider Hong-Ou-Mandel interference [64] in a multimode setting. It is shown that the fourth-order interference depends upon the transverse parity of the pump laser beam. The theory and experimental results have been reported in Physical Review Letters, **90**, 143601 (2003).

3.1 Introduction

Two-photon interference at a beam splitter was first demonstrated by Hong, Ou and Mandel (HOM) [64]. It has since been utilized in quantum tests of local realism [12] as well as many optical implementations of quantum information protocols such as Bell-state measurements [52, 56] and may be used to construct quantum optical logic gates [35, 36]. To date, however, most experiments utilizing HOM-type interference consider an ideal monomode situation. Here multimode Hong-Ou-Mandel interference of photon pairs created by SPDC is studied for the first time. It is shown that the two-photon interference depends upon the transverse amplitude profile of the pump beam. The pump beam can then be used as a control parameter for two-photon interference.

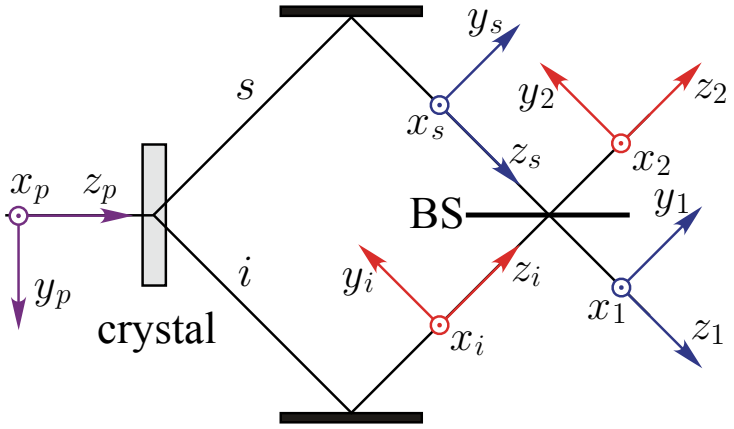

Figure 3.1: *HOM interferometer. SPDC-created photons are reflected through paths s and i onto a beam splitter (BS). The coordinate systems x_t, y_t, z_t $(t = s, i)$ are transmitted or reflected into coordinate systems x_j, y_j, z_j $(j = 1, 2)$. x_p, y_p, z_p is the coordinate system of the pump field.*

3.2 Multimode Hong-Ou-Mandel interference

Consider the Hong-Ou-Mandel (HOM) interferometer shown in Fig. 3.1, in which two photons are generated by SPDC and then reflected onto opposite sides of a beam splitter. It is well known that when the paths s and i are equal, the photons can interfere. If the path length difference is greater than the coherence length of the down-converted photons, then there is no interference and the photons leave either side of the beam splitter randomly. Here we will assume that lengths of paths s and i are equal.

The two-photon detection amplitude, given by eq. (2.28), is

$$\mathbf{\Psi}(\mathbf{r}_1, \mathbf{r}_2) = \langle \text{VAC} | \, \mathbf{E}_2^{(+)}(\mathbf{r}_2) \mathbf{E}_1^{(+)}(\mathbf{r}_1) \, | \psi \rangle \,, \tag{3.1}$$

where $\mathbf{E}_l^{(+)}(\mathbf{r}_l)$ is the field operator in the paraxial approximation given by eq. (2.29) for the mode l and $\mathbf{r}_l$ is the detection position. We assume that experimental conditions are such that the two-photon state $|\psi\rangle$ is accurately given by equation (2.24).

Using the reference frames illustrated in Fig. 3.1, the annihilation operators in exit modes 1 and 2 *after* the beam splitter can be expressed in terms of the operators

in input modes s and i:

$$\mathbf{a}_1(\mathbf{q},\sigma) = t\mathbf{a}_s(q_x,q_y,\sigma) + ir\mathbf{a}_i(q_x,-q_y,\sigma) \tag{3.2a}$$

$$\mathbf{a}_2(\mathbf{q},\sigma) = t\mathbf{a}_i(q_x,q_y,\sigma) + ir\mathbf{a}_s(q_x,-q_y,\sigma), \tag{3.2b}$$

where t and r are the transmission and reflection coefficients of the beam splitter ($t^2+r^2=1$). We have assumed that the beam splitter is symmetric. A field reflected from the beam splitter undergoes a reflection in the horizontal (y) direction, while a transmitted field does not suffer any reflection, as illustrated in Fig. 3.1. The negative sign that appears in the q_y components is due to this reflection. Until now all studies of two-photon interference at a beam splitter have considered a monomode situation, in which the sign change due to this reflection does not appear.

The two-photon wave function is split into four components, according to the four possibilities of transmission and reflection of the two photons:

$$\mathbf{\Psi} = \mathbf{\Psi}_{tr}(\mathbf{r}_1,\mathbf{r}_1') + \mathbf{\Psi}_{rt}(\mathbf{r}_2,\mathbf{r}_2') + \mathbf{\Psi}_{tt}(\mathbf{r}_1,\mathbf{r}_2) + \mathbf{\Psi}_{rr}(\mathbf{r}_1,\mathbf{r}_2), \tag{3.3}$$

where tr stands for photon s transmitted and photon i reflected, etc. It is clear that only $\mathbf{\Psi}_{tt}$ and $\mathbf{\Psi}_{rr}$ are responsible for coincidence detections at D_1 and D_2, while $\mathbf{\Psi}_{tr}$ and $\mathbf{\Psi}_{rt}$ correspond to two photons in arm 1 and two photons in arm 2, respectively. For convenience, the four components of $\mathbf{\Psi}$ are written in two different coordinate systems, $\mathbf{r}_1 = (x_1,y_1,z_1)$ and $\mathbf{r}_2 = (x_2,y_2,z_2)$, since we must work in the paraxial approximation around two different axes z_1 and z_2.

3.2.1 Two-port coincidence detection

We will first focus our attention on two-port coincidence detections, which contribute to $\mathbf{\Psi}$ through $\mathbf{\Psi}_{tt}$ and $\mathbf{\Psi}_{rr}$. Using (3.1), (3.2) and the field operators in the paraxial approximation (2.29), the probability amplitude to detect coincidences at output ports 1 and 2 is

$$\begin{aligned}\mathbf{\Psi}(\mathbf{r}_1,\mathbf{r}_2) \propto \sum_{\mathtt{s}_1,\mathtt{s}_2} \mathtt{s}_1\mathtt{s}_2 \sum_{\mathtt{s}_s,\mathtt{s}_i} C_{\mathtt{s}_s,\mathtt{s}_i} \iiiint d\mathbf{q}_1 d\mathbf{q}_2 d\mathbf{q}_s d\mathbf{q}_i e^{i\mathbf{q}_1\cdot\boldsymbol{\rho}_1} e^{i\mathbf{q}_2\cdot\boldsymbol{\rho}_2} e^{iq_1^2 z_1/2k_1} e^{iq_2^2 z_2/2k_2} \times \\ v(\mathbf{q}_s+\mathbf{q}_i) \left\langle \mathrm{VAC}\right| \left(t^2 \mathbf{a}_1(q_{sx},q_{sy},\mathtt{s}_s)\mathbf{a}_2(q_{ix},q_{iy},\mathtt{s}_i)\right. \\ \left. - r^2 \mathbf{a}_1(q_{ix},-q_{iy},\mathtt{s}_i)\mathbf{a}_2(q_{sx},-q_{sy},\mathtt{s}_s)\right| \left|\mathbf{q}_s,\mathtt{s}_s\right\rangle \left|\mathbf{q}_i,\mathtt{s}_i\right\rangle .\end{aligned} \tag{3.4}$$

Using the properties of the destruction operators, the coincidence detection amplitude is

$$\mathbf{\Psi}(\mathbf{r}_1, \mathbf{r}_2) = \mathbf{\Psi}_{tt}(\mathbf{r}_1, \mathbf{r}_2) + \mathbf{\Psi}_{rr}(\mathbf{r}_1, \mathbf{r}_2), \tag{3.5}$$

where

$$\begin{aligned}\mathbf{\Psi}_{tt}(\mathbf{r}_1, \mathbf{r}_2) \propto & t^2 \sum_{\mathtt{s}_1, \mathtt{s}_2} C_{\mathtt{s}_1, \mathtt{s}_2 \mathtt{s}_1 \mathtt{s}_2} \\ & \iint d\mathbf{q}_1 d\mathbf{q}_2 e^{i\mathbf{q}_1 \cdot \boldsymbol{\rho}_1} e^{i\mathbf{q}_2 \cdot \boldsymbol{\rho}_2} e^{iq_1^2 z_1 / 2k_1} e^{iq_2^2 z_2 / 2k_2} v(q_{1x} + q_{2x}, q_{1y} + q_{2y})\end{aligned} \tag{3.6}$$

and

$$\begin{aligned}\mathbf{\Psi}_{rr}(\mathbf{r}_1, \mathbf{r}_2) \propto & - r^2 \sum_{\mathtt{s}_2, \mathtt{s}_1} C_{\mathtt{s}_2, \mathtt{s}_1 \mathtt{s}_2 \mathtt{s}_1} \\ & \iint d\mathbf{q}_1 d\mathbf{q}_2 e^{i\mathbf{q}_1 \cdot \boldsymbol{\rho}_1} e^{i\mathbf{q}_2 \cdot \boldsymbol{\rho}_2} e^{iq_1^2 z_1 / 2k_1} e^{iq_2^2 z_2 / 2k_2} v(q_{1x} + q_{2x}, -q_{1y} - q_{2y}).\end{aligned} \tag{3.7}$$

Simplifying (3.6) is straightforward. Performing the change of variables

$$\mathbf{R} = (R_x, R_y) = \left(\frac{x_1 + x_2}{2}, \frac{y_1 + y_2}{2} \right), \tag{3.8a}$$

$$\mathbf{S} = (S_x, S_y) = (x_1 - x_2, y_1 - y_2), \tag{3.8b}$$

$$\mathbf{Q} = (Q_x, Q_y) = (q_{1x} + q_{2x}, q_{1y} + q_{2y}), \tag{3.8c}$$

and

$$\mathbf{P} = (P_x, P_y) = \left(\frac{q_{1x} - q_{2x}}{2}, \frac{q_{1y} - q_{2y}}{2} \right), \tag{3.8d}$$

so that $d\mathbf{q}_1 d\mathbf{q}_2 = d\mathbf{Q} d\mathbf{P}$ and $\mathbf{q}_1 \cdot \boldsymbol{\rho}_1 + \mathbf{q}_2 \cdot \boldsymbol{\rho}_2 = \mathbf{Q} \cdot \mathbf{R} + \mathbf{P} \cdot \mathbf{S}$, we have

$$\mathbf{\Psi}_{tt}(\mathbf{r}_1, \mathbf{r}_2) \propto t^2 \sum_{\mathtt{s}_1, \mathtt{s}_2} C_{\mathtt{s}_1, \mathtt{s}_2 \mathtt{s}_1 \mathtt{s}_2} \int d\mathbf{Q} v(\mathbf{Q}) e^{i\mathbf{Q} \cdot \mathbf{R}} e^{iQ^2 Z_{12} / 2K} \int d\mathbf{P} e^{i\mathbf{P} \cdot \mathbf{S}} e^{iP^2 Z_{12} / 2K}, \tag{3.9}$$

where Z_{12} is the biphoton focal distance [1] given by [77]

$$\frac{1}{Z_{12}} = \frac{1}{2} \left(\frac{1}{z_s} + \frac{1}{z_i} \right), \tag{3.10}$$

[1] with $k_s = k_i = 2k_p$.

and K is the magnitude of the pump photon wave vector. Integrating, we have

$$\mathbf{\Psi}_{tt}(\mathbf{r}_1, \mathbf{r}_2) \propto t^2 \mathbf{\Pi}(\mathtt{s}_1, \mathtt{s}_2) \mathcal{W}(\mathbf{R}, Z_{12}) e^{iS^2 Z_{12}/2K}, \tag{3.11}$$

where $\mathcal{W}(\mathbf{R}, Z_{12})$ is the transverse field profile of the pump beam at $z = Z_{12}$ and $\mathbf{\Pi}(\mathtt{s}_1, \mathtt{s}_2) = \sum_{\mathtt{s}_1,\mathtt{s}_2} C_{\mathtt{s}_1\mathtt{s}_2} \mathtt{s}_1\mathtt{s}_2$ is the four-dimensional polarization vector of the photon pair. For example, the singlet state in the horizontal-vertical basis is $\mathbf{\Pi}(\mathtt{s}_1, \mathtt{s}_2) = 1/\sqrt{2}(\mathtt{h}_1\mathtt{v}_2 - \mathtt{v}_1\mathtt{h}_2)$, where $\mathtt{h}_j$ and $\mathtt{v}_j$ are two-dimensional polarization vectors (for modes $j = 1, 2$) in the horizontal and vertical directions, respectively.

Similarly for the rr term (3.7) we have

$$\mathbf{\Psi}_{rr}(\mathbf{r}_1, \mathbf{r}_2) \propto r^2 \sum_{\mathtt{s}_2,\mathtt{s}_1} C_{\mathtt{s}_2,\mathtt{s}_1} \mathtt{s}_2\mathtt{s}_1 \int d\mathbf{Q} v(Q_x, -Q_y) e^{i\mathbf{Q}\cdot\mathbf{R}} e^{iQ^2 Z_{12}/2K} \int d\mathbf{P} e^{i\mathbf{P}\cdot\mathbf{S}} e^{iP^2 Z_{12}/2K}, \tag{3.12}$$

which gives

$$\mathbf{\Psi}_{rr}(\mathbf{r}_1, \mathbf{r}_2) \propto -r^2 \mathbf{\Pi}(\mathtt{s}_2, \mathtt{s}_1) \mathcal{W}(R_x, -R_y, Z_{12}) e^{iS^2 Z_{12}/2K}. \tag{3.13}$$

The coincidence detection amplitude is then

$$\mathbf{\Psi}(\mathbf{r}_1, \mathbf{r}_2) \propto t^2 \mathbf{\Pi}(\mathtt{s}_1, \mathtt{s}_2) \mathcal{W}(\mathbf{R}, Z_{12}) e^{iS^2 Z_{12}/2K} - r^2 \mathbf{\Pi}(\mathtt{s}_2, \mathtt{s}_1) \mathcal{W}(\tilde{\boldsymbol{R}}, Z_{12}) e^{iS^2 Z_{12}/2K} \tag{3.14}$$

where $\tilde{\mathbf{R}} = (R_x, -R_y)$.

3.2.2 Same-port coincidence detection

Referring to figure 3.1, the idler field is always reflected into output port 1, so the possibility of detecting both photons in output port 1 is represented by

$$\begin{aligned}\mathbf{\Psi}_{tr}(\mathbf{r}_1, \mathbf{r}_1') \propto itr \sum_{\mathtt{s}_1,\mathtt{s}_1'} \mathtt{s}_1\mathtt{s}_1' \sum_{\mathtt{s}_s,\mathtt{s}_i} C_{\mathtt{s}_s,\mathtt{s}_i} \iiiint d\mathbf{q}_1 d\mathbf{q}_1' d\mathbf{q}_s d\mathbf{q}_i e^{i\mathbf{q}_1\cdot\boldsymbol{\rho}_1} e^{i\mathbf{q}_1'\cdot\boldsymbol{\rho}_1'} e^{iq_1^2 z_1/2k_1} e^{iq_1'^2 z_1'/2k_1'} \times \\ v(\mathbf{q}_s + \mathbf{q}_i) \langle \mathrm{VAC} | (\mathbf{a}_1(q_{sx}, q_{sy}, \mathtt{s}_s)\mathbf{a}_1'(q_{ix}, -q_{iy}, \mathtt{s}_i) + \\ \mathbf{a}_1'(q_{sx}, q_{sy}, \mathtt{s}_s)\mathbf{a}_1(q_{ix}, -q_{iy}, \mathtt{s}_i) | \mathbf{q}_s, \mathtt{s}_s \rangle | \mathbf{q}_i, \mathtt{s}_i \rangle .\end{aligned} \tag{3.15}$$

which gives

$$\begin{aligned}\boldsymbol{\Psi}_{tr}(\mathbf{r}_1,\mathbf{r}_1') \propto itr\sum_{\mathtt{s}_1,\mathtt{s}_1'} C_{\mathtt{s}_1,\mathtt{s}_1'}\mathtt{s}_1\mathtt{s}_1'\times\\ \iint d\mathbf{q}_1 d\mathbf{q}_1' e^{i\mathbf{q}_1\cdot\boldsymbol{\rho}_1}e^{i\mathbf{q}_1'\cdot\boldsymbol{\rho}_1'}e^{iq_1^2 z_1/2k_1}e^{iq_1'^2 z_1'/2k_1'}v(q_{1x}+q_{1x}',q_{1x}-q_{1x}')\\ + itr\sum_{\mathtt{s}_1',\mathtt{s}_1} C_{\mathtt{s}_1',\mathtt{s}_1}\mathtt{s}_1'\mathtt{s}_1\times\\ \iint d\mathbf{q}_1' d\mathbf{q}_1 e^{i\mathbf{q}_1\cdot\boldsymbol{\rho}_1}e^{i\mathbf{q}_1'\cdot\boldsymbol{\rho}_1'}e^{iq_1^2 z_1/2k_1}e^{iq_1'^2 z_1'/2k_1'}v(q_{1x}+q_{1x}',-q_{1x}+q_{1x}')\end{aligned} \tag{3.16}$$

We will use the same change of variables as (3.8) but with $(x_2,y_2)\longrightarrow(x_1',y_1')$. To avoid confusion, let us denote this new change of variables as $\mathbf{R}_1$,$\mathbf{S}_1$,$\mathbf{Q}_1$ and $\mathbf{P}_1$, where the subscript "1" stands for output port 1. Then for equation (3.16) we have

$$\begin{aligned}\boldsymbol{\Psi}_{tr}(\mathbf{r}_1,\mathbf{r}_1') \propto itr\sum_{\mathtt{s}_1,\mathtt{s}_1'} C_{\mathtt{s}_1,\mathtt{s}_1'}\mathtt{s}_1\mathtt{s}_1'\iint d\mathbf{Q}_1 d\mathbf{P}_1 v(Q_{1x},P_{1y})e^{i(\mathbf{Q}_1\cdot\mathbf{R}_1+\mathbf{P}_1\cdot\mathbf{S}_1)}e^{i(Q_1^2+P_1^2)Z_{12}/2K}\\ + itr\sum_{\mathtt{s}_1',\mathtt{s}_1} C_{\mathtt{s}_1',\mathtt{s}_1}\mathtt{s}_1'\mathtt{s}_1\iint d\mathbf{Q}_1 d\mathbf{P}_1 v(Q_{1x},-P_{1y})e^{i(\mathbf{Q}_1\cdot\mathbf{R}_1+\mathbf{P}_1\cdot\mathbf{S}_1)}e^{i(Q_1^2+P_1^2)Z_{12}/2K},\end{aligned} \tag{3.17}$$

where again Z_{12} is the biphoton focal distance given by (3.10) and K is the magnitude of the pump photon wave vector. Integrating, we have

$$\begin{aligned}\boldsymbol{\Psi}_{tr}(\mathbf{r}_1,\mathbf{r}_1') \propto itre^{i(S_{1x}^2+R_{1y}^2)Z_{12}/2K}\times\\ \left[\boldsymbol{\Pi}(\mathtt{s}_1,\mathtt{s}_1')\mathcal{W}(R_{1x},S_{1y},Z_{12})+\boldsymbol{\Pi}(\mathtt{s}_1',\mathtt{s}_1)\mathcal{W}(R_{1x},-S_{1y},Z_{12})\right],\end{aligned} \tag{3.18}$$

where $\mathcal{W}(\mathbf{R},Z_{12})$ is the transverse field profile of the pump beam at $z=Z_{12}$. Similarly, the amplitude to find both photons in output port 2 is given by

$$\begin{aligned}\boldsymbol{\Psi}_{rt}(\mathbf{r}_2,\mathbf{r}_2') \propto itre^{i(S_{2x}^2+R_{2y}^2)Z_{12}/2K}\times\\ \left[\boldsymbol{\Pi}(\mathtt{s}_2,\mathtt{s}_2')\mathcal{W}(R_{2x},S_{2y},Z_{12})+\boldsymbol{\Pi}(\mathtt{s}_2',\mathtt{s}_2)\mathcal{W}(R_{2x},-S_{2y},Z_{12})\right].\end{aligned} \tag{3.19}$$

3.2.3 Analysis

How do $\mathcal{W}$ and $\boldsymbol{\Pi}$ affect the two-photon interference behavior? To simplify things, let us assume that $t=r=1/\sqrt{2}$ and let $z_1=z_2=Z$ so that $Z_{12}=Z$. It is illustrative to

write out all four components of the total wave function (3.3):

$$\begin{aligned}\mathbf{\Psi}_{tr}(\mathbf{r}_1,\mathbf{r}_1') =& i\exp\left\{\frac{iK}{2Z}\left[(x_1-x_1')^2+(y_1+y_1')^2\right]\right\}\times \\ &\left[\mathcal{W}\left(\frac{x_1+x_1'}{2},\frac{-y_1+y_1'}{2},Z\right)\mathbf{\Pi}(\mathtt{s}_1,\mathtt{s}_1')\right. \\ &\left.+\,\mathcal{W}\left(\frac{x_1+x_1'}{2},\frac{y_1-y_1'}{2},Z\right)\mathbf{\Pi}(\mathtt{s}_1',\mathtt{s}_1)\right], \end{aligned} \tag{3.20}$$

$$\begin{aligned}\mathbf{\Psi}_{rt}(\mathbf{r}_2,\mathbf{r}_2') =& i\exp\left\{\frac{iK}{2Z}\left[(x_2-x_2')^2+(y_2+y_2')^2\right]\right\}\times \\ &\left[\mathcal{W}\left(\frac{x_2+x_2'}{2},\frac{-y_2+y_2'}{2},Z\right)\ \mathbf{\Pi}(\mathtt{s}_2,\mathtt{s}_2')+\right. \\ &\left.\mathcal{W}\left(\frac{x_2+x_2'}{2},\frac{y_2-y_2'}{2},Z\right)\ \mathbf{\Pi}(\mathtt{s}_2',\mathtt{s}_2)\right], \end{aligned} \tag{3.21}$$

$$\begin{aligned}\mathbf{\Psi}_{tt}(\mathbf{r}_1,\mathbf{r}_2) =& \exp\left\{\frac{iK}{2Z}\left[(x_1-x_2)^2+(y_1-y_2)^2\right]\right\}\times \\ &\mathcal{W}\left(\frac{x_1+x_2}{2},\frac{y_1+y_2}{2},Z\right)\ \mathbf{\Pi}(\mathtt{s}_1,\mathtt{s}_2), \end{aligned} \tag{3.22}$$

$$\begin{aligned}\mathbf{\Psi}_{rr}(\mathbf{r}_1,\mathbf{r}_2) =& -\exp\left\{\frac{iK}{2Z}\left[(x_1-x_2)^2+(y_1-y_2)^2\right]\right\}\times \\ &\mathcal{W}\left(\frac{x_1+x_2}{2},\frac{-y_1-y_2}{2},Z\right)\ \mathbf{\Pi}(\mathtt{s}_2,\mathtt{s}_1). \end{aligned} \tag{3.23}$$

Now suppose that the photon pair is prepared in a symmetric polarization state: $\mathbf{\Pi}(\mathtt{s}_1,\mathtt{s}_2)=\mathbf{\Pi}(\mathtt{s}_2,\mathtt{s}_1)$. If $\mathcal{W}(x,y,Z)$ is an even function with respect to the y-coordinate such that all the spatial components of $\mathbf{\Psi}$ are symmetric, then Eqs. (3.22) and (3.23) cancel out and there can be no coincidence detections, as is well known [64]. However, if $\mathcal{W}(x,y,Z)$ is an odd function of the y-coordinate, direct examination of (3.20) through (3.23) shows that (3.20) and (3.21) are zero, while (3.22) and (3.23) add constructively, resulting in an increase in coincidence counts. Now suppose that the photon pair is prepared in an antisymmetric polarization state: $\mathbf{\Pi}(\mathtt{s}_1,\mathtt{s}_2)=-\mathbf{\Pi}(\mathtt{s}_2,\mathtt{s}_1)$. Then for a $\mathcal{W}(x,y,Z)$ that is an even function of y, clearly Eqs. (3.20) and (3.21) are zero, while (3.22) and (3.23) add constructively, giving a maximum in the coincidence counts.

pump beam profile	polarization state	two-photon interference
even	symmetric	destructive: $\mathbf{\Psi}_{tt} = -\mathbf{\Psi}_{rr}$
even	antisymmetric	constructive: $\mathbf{\Psi}_{tt} = \mathbf{\Psi}_{rr}$
odd	symmetric	constructive: $\mathbf{\Psi}_{tt} = \mathbf{\Psi}_{rr}$
odd	antisymmetric	destructive: $\mathbf{\Psi}_{tt} = -\mathbf{\Psi}_{rr}$

Table 3.1: *Summary of two-photon interference dependence in coincidence detections at* 1 *and* 2.

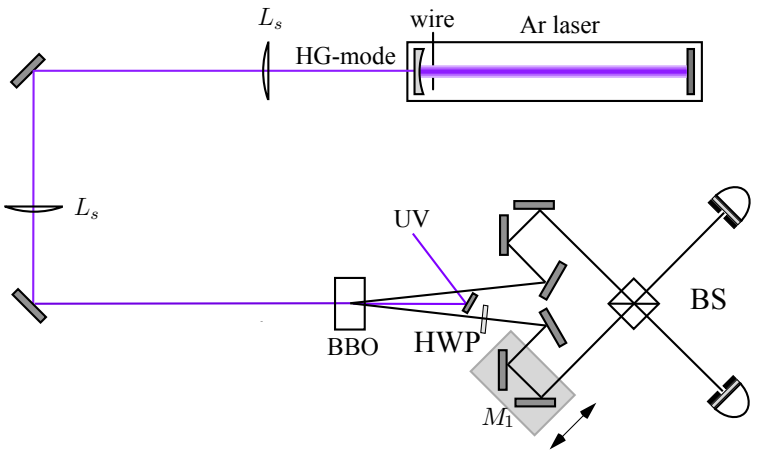

Figure 3.2: *Experimental setup for multimode HOM interference.*

For a $\mathcal{W}(x, y, Z)$ that is an odd function of y, (3.22) and (3.23) cancel, eliminating coincidence detections. A summary of these results is shown in table 3.1.

The behavior of the HOM interferometer for any combination of symmetric and antisymmetric spatial and polarization components of $\mathbf{\Psi}$ can be inferred from the bosonic character of photons, that is, $\mathbf{\Psi}$ must be symmetric.

All HOM-type experiments performed up until now have used a pump beam that is described by an even function of y. In order to demonstrate experimentally the possibilities of controlling the HOM interferometer with space and polarization variables, we performed a series of experiments in which coincidence counts were registered, combining symmetric and antisymmetric components of $\mathbf{\Psi}$.

3.3 Experiment and results

A set of beams with well defined cartesian parity are the Hermite-Gaussian (HG) beams, given by eq. (2.34). Pumping the nonlinear crystal with different HG pump beams, we can control the behavior of the down-converted photons at the beam splitter. The experimental setup is a typical HOM interferometer [64], shown in Fig. 3.2. The Argon laser is used to pump a BBO (β-BaB_2O_4) crystal cut for degenerate type-II phase matching, generating noncollinear entangled photons by spontaneous parametric down-conversion (SPDC). The L_s are spherical lenses ($f = 500\,\text{mm}$) used to focus the pump beam in the plane of the detectors to increase the coincidence detection efficiency [116]. UV is an ultra-violet mirror used to block the laser beam. The down-converted photons are reflected through a system of mirrors and incident on a $50-50$ beam splitter BS ($t = r \approx \sqrt{1/2}$). A computer-controlled stepper motor is used to control the path length difference by scanning mirror assembly M_1. HWP is a half-wave plate used to transform the polarization state. The detectors D_1 and D_2 are free space EG&G SPCM 200 photodetectors, equipped with interference filters (1 nm FWHM centered at 702 nm) and 2 mm $\varnothing$ circular collection apertures. Coincidence and single counts were registered using a personal computer. To generate HG modes we placed a 25 μm $\varnothing$ wire inside the laser cavity, forcing the laser to operate in one of the HG modes with a nodal line at the position of the wire as discussed in section 2.4.2. Symmetric and antisymmetric polarization states were used. The symmetric state chosen was $\left|\Pi^S\right\rangle = |h\rangle_1 |h\rangle_2$ and the antisymmetric state was $\left|\Pi^A\right\rangle = |\psi^-\rangle = \frac{1}{\sqrt{2}}(|h\rangle_1 |v\rangle_2 - |v\rangle_1 |h\rangle_2)$, where h and v stand for horizontal and vertical linear polarization, respectively. The state $\left|\Pi^S\right\rangle$ was obtained from type II SPDC, by collecting one photon from the ordinary (h-polarized) light cone and the other photon from the extraordinary (v-polarized) light cone followed by a half-wave plate (HWP), which rotates its polarization to h. Realigning the crystal, the antisymmetric state $\left|\Pi^A\right\rangle$ was obtained from the crossing of the ordinary and extraordinary light cones, followed by a compensating crystal, as described in section 2.3.1.

Experimental results are sumarized in Figs. 3.3, 3.4 and 3.5. Coincidence counts were registered as a function of the path length difference. When the path lengths are the same, an interference maximum or minimum is observed. The error bars represent statistical errors due to photon counting [74]. Fig. 3.3 shows the results for the symmetric polarization state $\left|\Pi^S\right\rangle$ when the crystal is pumped by first-order HG

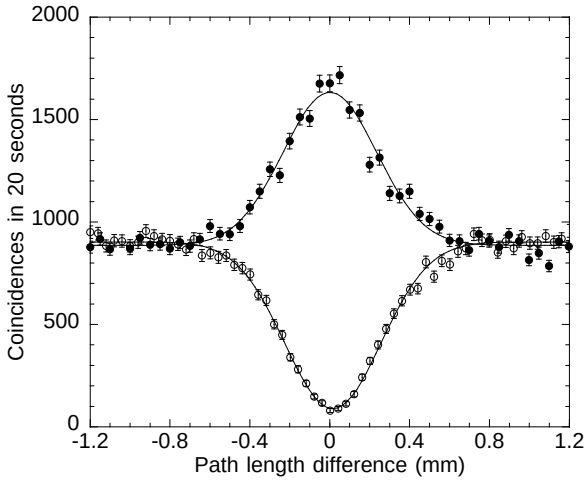

Figure 3.3: *Coincidence counts when the polarization state is symmetric and the pump beam is a first-order Hermite-Gaussian beam. Open circles (○) correspond to* HG_{10} *and solid circles (●) correspond to* HG_{01}.

beams HG_{10} and HG_{01}. HG_{10}, as an even function in y, results in $\mathbf{\Psi}_{rr} = -\mathbf{\Psi}_{tt}$, leading to an interference minimum. HG_{01}, as an odd function in y, results in $\mathbf{\Psi}_{rt} = \mathbf{\Psi}_{tr} = 0$ and $\mathbf{\Psi}_{rr} = \mathbf{\Psi}_{tt}$, leading to an interference maximum. The curves have visibilities of 0.90 ± 0.01 (HG_{10}) and 0.85 ± 0.01 (HG_{01}). Fig. 3.4 shows the results for the antisymmetric polarization state $\left|\Pi^A\right\rangle$ under the same pump beam conditions. Now, the behavior of the interference is the opposite, that is, pumping with HG_{10} produces an interference maximum, whereas pumping with HG_{01} produces a minimum. The solid lines are curve fits of the function

$$A\left(1 - \mathcal{V}\exp\frac{-|x - x_0|^2}{2\sigma^2}\right), \tag{3.24}$$

where $\mathcal{V}$ is the visibility. Visibilities of 0.70 ± 0.01 (HG_{10}) and 0.77 ± 0.01 (HG_{01}) were achieved. Differences in the visibilites were due to the alignment of the interferometer as well as the wire in the laser cavity. We can create an equally weighted superposition of the modes HG_{01} and HG_{10} by placing the wire in the cavity at a 45° angle [111]. Such a superposition is neither symmetric nor antisymmetric. As to be expected, the coincidence count rate is constant, as shown in Fig. 3.5 for the symmetric polarization state.

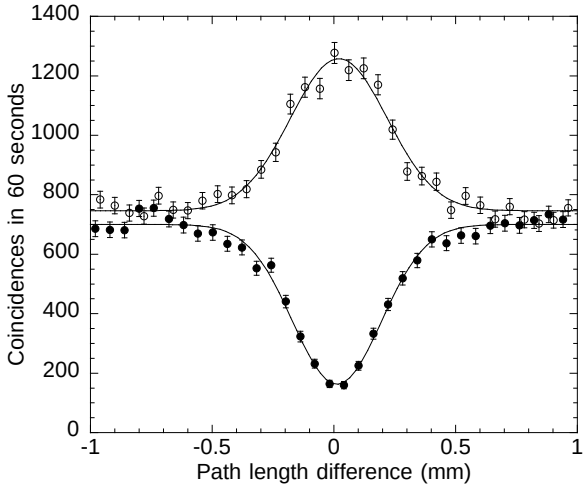

Figure 3.4: *Coincidence counts when the polarization state is antisymmetric and the pump beam is a first-order Hermite-Gaussian beam. Open circles (○) correspond to* HG_{10} *and solid circles (●) correspond to* HG_{01}.

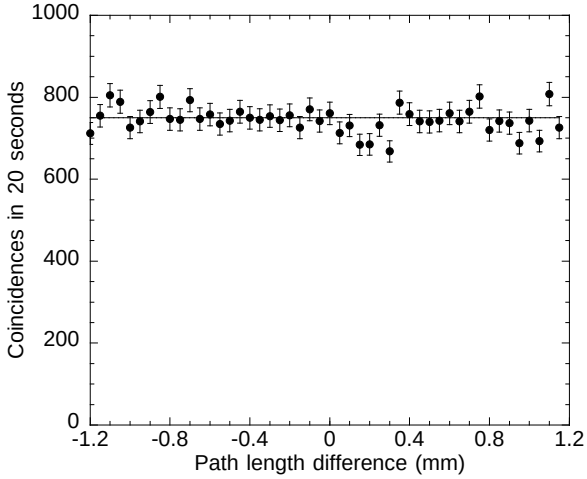

Figure 3.5: *Coincidence counts when the polarization state is symmetric and the pump beam is an equal superposition of Hermite-Gaussian modes* HG_{01} *and* HG_{10}.

3.4 Conclusion

Multimode HOM interference using photons generated by SPDC has been studied both theoretically and experimentally. The resulting interference pattern is shown to depend upon both the transverse amplitude profile of the pump laser and the polarization state of the photon pair. First-order Hermite-Gaussian beams were used to demonstrate that the two-photon interference can be controlled by manipulating the pump beam. To our knowledge, this is the first time that two-photon HOM interference has been studied using a spatially antisymmetric wave function.

A possible application of these results is Bell-state analysis without the need for detectors sensitive to photon number [117], as will be discussed in chapter 4. We expect these interference effects to be important in the construction of quantum-optical logic gates [33, 35, 36], as well as the codification of information in the transverse spatial properties of the photon [118]. In chapter 5 we use multimode interference to investigate the transverse phase structure of the biphoton. In addition, there is the possibility of using these results to create non-classical states of light with spatial properties that could be useful for quantum imaging. Recently, we used these techniques to generate a nonclassical state of light that is more robust to types of noise and exhibits spatial antibunching of photons [70] [2].

[2] This work is part of W. A. T. Nogueira's PhD thesis, Quantum Optics, UFMG.

4

Optical Bell-state Analysis

Multimode Hong-Ou-Mandel interference is used to improve upon previous optical Bell-state measurement techniques. To demonstrate the viability of these techniques, a simple Bell-state measurement experiment is performed. The theoretical and experimental limitations are discussed. The results of the experiment, which are reported in section 4.1, along with the complete Bell-state measurement scheme described in section 4.3 have been published in Europhysics Letters, **62**, 161-167 (2003). In addition, it is shown that simple hyperentangled states allow for the complete discrimination of all four Bell-states. The theoretical and experimental limitations of such an implementation are discussed. These results, described in section 4.4.3, have been published in Physical Review A, **68**, 042313 (2003).

4.1 Optical Bell-state analysis

Bell-state measurement (BSM) - distinguishing between the four maximally entangled Bell states (2.31) - is required in many quantum information schemes, including quantum dense coding [52, 95], quantum teleportation [56, 94, 119] and entanglement

swapping [59, 94, 120]. However, it has been proven that a complete BSM (distinguishing between the four states with 100% efficiency) is impossible using only linear operations and classical communication [100, 101, 102, 103]. In fact, Ghosh *et. al.* [103] have proven that, if only a single copy is provided, the best one can do is discriminate between two Bell states. Similarly, Calsamiglia and Lütkenhaus [102] have shown that the maximum efficiency for a linear Bell-state analyzer is 50%.

A favorable characteristic of the photon as a carrier of quantum information is the relative ease with which entangled photons can be created and transported. Two-photon Bell states are easily generated using spontaneous parametric down-conversion (SPDC) in one of several degrees of freedom [10, 11, 13, 16] as discussed in section 2.3. There are several methods for optical Bell-state measurement that allow one to distinguish two [52, 98, 104, 105] of the four Bell-states (resulting in 3 classes of states). All of these methods use local or non-local two-photon interference effects at beam splitters. For example, Mattle *et. al.* [52] have performed an experimental demonstration of dense coding, in which the Bell-states were created in the polarization degrees of freedom of the two photons. When the photons meet at a common beam splitter, the overall bosonic symmetry of the two-photon state requires that photons in the antisymmetric singlet state exit in different output ports, while the symmetric triplet states end up in the same output port [99]. Polarization analyzers are then used to further discriminate among the triplet states. Weinfurter has proposed a BSM method using momentum-entangled photons that allows one to distinguish all four Bell-states with 25% efficiency [104]. It is possible to distinguish among the four Bell states using nonlinear optical processes [57, 121]. However, with present technology these methods suffer from low efficiency. There have also been several proposals using two-photon absorption [122, 123].

In recent years, some attention has been paid to Bell-state analysis using hyper-entangled states [124]. Utilizing entanglement in additional auxiliary degrees of freedom, it is possible to perform a complete BSM. Due to the enlarged Hilbert space, this type of complete BSM is not restricted to the efficiency limits presented in references [100, 101, 102, 103]. Kwiat and Weinfurter [124] have proposed a scheme using photons entangled in polarization and momentum (spatial mode). Their method, which relies on linear optics and two-photon interference effects, requires detectors that distinguish between one- and two-photon detection events.

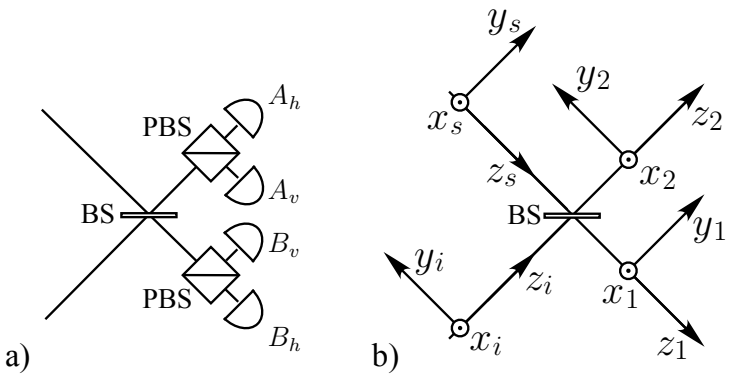

Figure 4.1: *a) Incomplete Bell-state analyzer. PBS are polarizing beam splitters at* 0°. *b) Two-photon interference at a beam splitter (BS). Photons s and i pass through the BS into modes* 1 *and* 2.

In sections 4.2 and 4.3 we will show that this requirement on the detectors could be removed if the hyperentangled photons were created by SPDC using a Hermite-Gaussian pump beam. The Hermite-Gaussian beam used is an odd function of the horizontal transverse spatial coordinate, which inverts the two-photon interference behavior (see chapter 3 or [125]), allowing for identification of all four Bell-states in coincidence detections, that is, each photon triggering a different detector. We use polarization-entanglement due to the ease with which one can generate and manipulate polarization-entangled photon pairs. In section 4.2 a Bell-state measurement experiment is reported in which 3 classes of Bell-states were identified in the coincidence basis. In section 4.3, multimode interference is further applied to improve upon the previous results of Kwiat and Weinfurter [124]. Finally in section 4.4, we outline a scheme for complete Bell-state measurement of photons using hyperentangled states. In addition to hyperentanglement, our scheme requires only linear optics and single photon detectors, and is realizable with current technology. At the cost of additional classical communication, our Bell-state measurement can be implemented non-locally. We will also discuss the possible application of these results to quantum dense coding and quantum teleportation.

4.2 Bell-state analysis using multimode HOM interference

4.2.1 Theory

Most optical BSM's [52, 98] of polarization-entangled photons rely on Hong-Ou-Mandel type two-photon interference at a 50-50 beam splitter [64]. Consider the Bell-state analyzer (BSA) shown in figure 4.1 a), such as the one used in the experimental demonstration of dense coding [52]. This BSA is capable of separating the four Bell states into 3 classes, resulting in a "trit" (≈ 1.58 bits) of transmitted information. A 50-50 beam splitter is used to separate $|\psi^-\rangle$ from $|\psi^+\rangle$, $|\phi^\pm\rangle$: bosonic symmetry requires that photons in $|\psi^-\rangle$ end up in different outputs while photons in $|\psi^+\rangle$, $|\phi^\pm\rangle$ end up in the same output [99]. With the polarizing beam splitters (PBS) separating h and v polarizations, coincidences at A_hB_v or A_vB_h are the signature of $|\psi^-\rangle$. The PBS separate $|\psi^+\rangle$ from $|\phi^\pm\rangle$: coincidences at A_hA_v or B_hB_v are characteristic of $|\psi^+\rangle$. For $|\phi^\pm\rangle$, we have two photons at A_hA_h, A_vA_v, B_hB_h or B_vB_v. Thus, detection of $|\psi^-\rangle$, $|\psi^+\rangle$ and $|\phi^\pm\rangle$ requires detectors capable of distinguishing between one and two photons. Although such detectors are presently available, they suffer from low efficiencies and/or high dark counts [126, 127, 128]. As mentioned in refs. [52, 105], this problem can be partially solved by replacing each detector with two detectors and an additional 50-50 beam splitter. This enables one to detect only half of the two-photon occurrences and increases the complexity of the detection system, since an eight detector system is necessary.

We could avoid this requirement on the detectors if we could invert the interference behavior: photons in the triplet (singlet) states go to different (the same) detectors and can then be further discriminated by the PBS. This can be achieved by generating polarization-entangled photons using an antisymmetric pump beam, such as the first-order Hermite-Gaussian beam HG_{01}, as we will show below. Then, pumping with HG_{01}, $|\psi^-\rangle$ results in two photons in either output port. Since the two photons are orthogonally polarized, coincidences at detectors A_hA_v or B_hB_v are the signature of $|\psi^-\rangle$. The states $|\psi^+\rangle$ and $|\phi^\pm\rangle$ give one photon in each output port. Since the photon pairs of $|\psi^+\rangle$ are orthogonally polarized, $|\psi^+\rangle$ gives coincidence counts at detectors A_hB_v or B_hA_v. $|\phi^\pm\rangle$ results in coincidence counts at A_hB_h or A_vB_v. All detector combinations identifying the three cases $|\psi^+\rangle$, $|\psi^-\rangle$ and $|\phi^\pm\rangle$ correspond to coincidences at different detectors. Table 4.1 summarizes these results.

A two-mode Bell-state, as given by Eq. (2.31), incident on a beam splitter as

Bell state	detector signature (even pump beam)	detector signature (odd pump beam)
$\|\psi^+\rangle$	A_hB_v or A_vB_h	A_hA_v or B_hB_v
$\|\psi^-\rangle$	A_hA_v or B_hB_v	A_hB_v or B_hA_v
$\|\phi^\pm\rangle$	A_hA_h or A_vA_v or B_hB_h or B_vB_v	A_hB_h or A_vB_v

Table 4.1: *Summary of detector signatures for Bell state analysis.*

shown in figure 4.1 b), must preserve its overall bosonic character. Thus if the polarization component of the state is symmetric (antisymmetric), then the spatial component must also be symmetric (antisymmetric) [99]. However, if we consider multimode fields, we must also take into account the transverse spatial properties of the two-photon state as additional degrees of freedom. The combined transverse-spatial and polarization symmetry of the two-photon wave packet determines whether the fields will interfere constructively or destructively. Using equations (3.22) and (3.23), it can be shown that the multimode coincidence-detection amplitudes of the polarization Bell-states in the two outputs of a balanced HOM interferometer are given by

$$\begin{aligned}\mathbf{\Psi}^{\pm}(\mathbf{r}_1,\mathbf{r}_2) = &\exp\left\{\frac{iK}{2Z}\left[(x_1-x_2)^2+(y_1-y_2)^2\right]\right\}\times \\ &\left[\mathcal{W}\left(\frac{x_1+x_2}{2},\frac{y_1+y_2}{2},Z\right)\mp\mathcal{W}\left(\frac{x_1+x_2}{2},\frac{-y_1-y_2}{2},Z\right)\right](\mathbf{hv}\pm\mathbf{vh}),\end{aligned} \tag{4.1}$$

$$\begin{aligned}\mathbf{\Phi}^{\pm}(\mathbf{r}_1,\mathbf{r}_2) = &\exp\left\{\frac{iK}{2Z}\left[(x_1-x_2)^2+(y_1-y_2)^2\right]\right\}\times \\ &\left[\mathcal{W}\left(\frac{x_1+x_2}{2},\frac{y_1+y_2}{2},Z\right)-\mathcal{W}\left(\frac{x_1+x_2}{2},\frac{-y_1-y_2}{2},Z\right)\right](\mathbf{hh}\pm\mathbf{vv}),\end{aligned} \tag{4.2}$$

where $\mathbf{\Psi}^{\pm}$ ($\mathbf{\Phi}^{\pm}$) is the coincidence-detection amplitude for $|\psi^{\pm}\rangle$ ($|\phi^{\pm}\rangle$). A quick look at (4.1) and (4.2) shows that when the pump beam profile is an even function of y, only $|\psi^-\rangle$ gives coincidence counts at the outputs of the BS (fig. 4.1 a)). If the pump beam profile is an odd function of y, then $|\phi^{\pm}\rangle$ and $|\psi^+\rangle$ give coincidence counts, while $|\psi^-\rangle$ results in two photons in the same output of the beam splitter. Thus, using a pump beam profile that is an odd function of y gives the desired interference effects for our

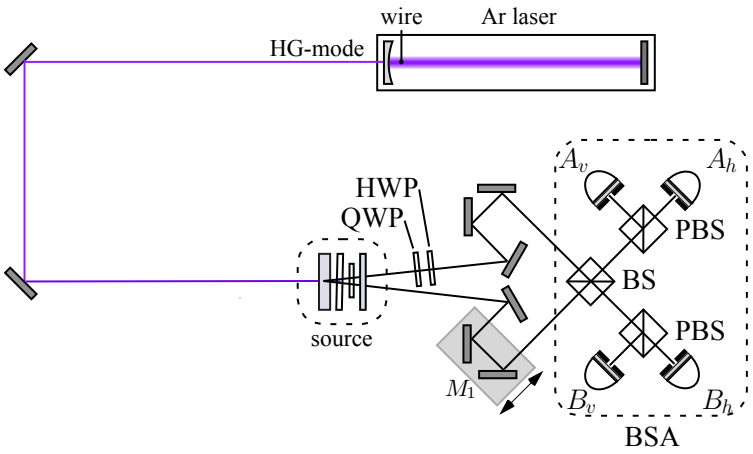

Figure 4.2: *Experimental setup for optical Bell-state analysis. The source is described in the text. BSA is the Bell-state analyzer consisting of a beam splitter (BS) and two polarizing beam splitters (PBS).*

BSM scheme mentioned above. As we saw in section 3.3, the Hermite-Gaussian HG_{01} beam has the required parity.

4.2.2 Experiment and results

The experiment is shown in figure 4.2. An argon-ion laser (351.1 nm) is used to pump a 2 mm thick BBO crystal. The crystal is cut for type-II phase matching at $\lambda_1 = \lambda_2 = 702.2\,\text{nm}$. To generate a first-order HG mode, a 25 μm diameter wire was placed inside the laser cavity, as discussed in section 2.4.2. The down-converted beams leave the crystal at angles of $\sim 3°$ and pass through a half-wave plate followed by a 1 mm thick BBO compensating crystal, as described in 2.3.1. A UV mirror is used to reflect the pump beam. A half-wave plate (HWP) and quarter-wave plate (QWP) are used to select between the four Bell states as mentioned in section 2.3.1. Trombone mirror assemblies are used to direct the down-converted beams onto a 50-50 beam splitter (BS). The relative path length is adjusted by moving mirror assembly M_1 with a motorized translation stage. The BS is mounted on a translation stage and can be moved in and out of the down-converted beams. This allows for polarization analysis of the Bell-states without the BS. The polarization analyzers (not shown) are rotatable half-wave plates followed by polarizing beam splitters. Detectors D_1 and D_2 are avalanche photodiodes equiped with 1 nm FWHM bandwidth interference filters

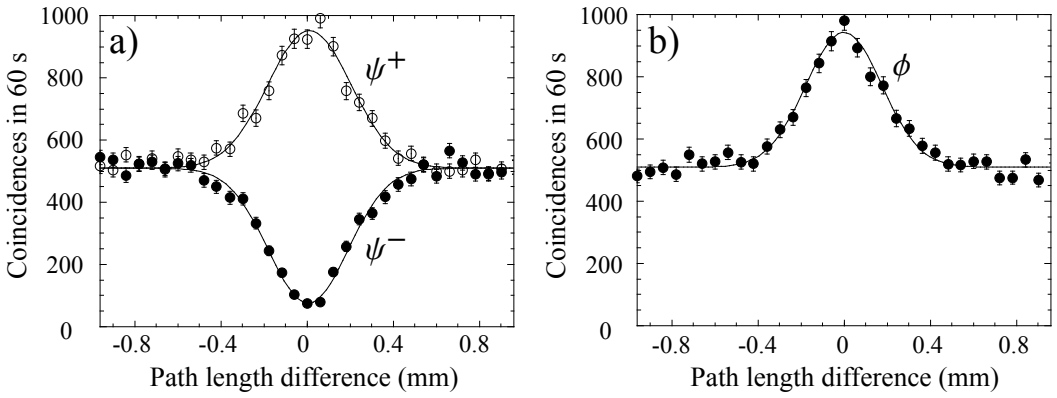

Figure 4.3: *Two-photon interference for a) $|\psi^+\rangle$ (○), $|\psi^-\rangle$ (●) and b) $|\phi\rangle$ when the pump beam is the Hermite-Gaussian mode* HG_{01}.

and 3 mm ⌀ collection apertures. Coincidence and single counts were registered by a personal computer.

Polarization analysis (BS and PBS removed) of the four Bell states generated with a HG_{01} pump beam gave interference curves (shown in figure 2.3) with visibilities $\sim 0.94 - 0.97$, which were comparable to results when a Gaussian pump beam was used. Since we are unable to distinguish between $|\phi^+\rangle$ and $|\phi^-\rangle$ with the BSA, we chose to define $|\phi^\pm\rangle \equiv |\phi\rangle$. Figure 4.3 shows the HOM interference for the states $|\psi^\pm\rangle$ and $|\phi\rangle$ when the HG_{01} beam is used and the PBS were removed. The solid curves are fits of Eq. (3.24). Visibilities of $\sim 0.85 \pm 0.02$ were achieved with the HG_{01} mode, which were slightly lower than with a Gaussian pump beam ($\sim 0.92 \pm 0.01$). This was most likely due to misalignment of the wire in the laser cavity, as well as an increased sensitivity to alignment of the interferometer with the HG_{01} pump beam. For the BSM, the mirror assembly was placed at position "0". Comparing the interference maxima and minimum at position 0 with the constant count outside the interference region, there is a $\sim 94\%$ probability that photons in $|\psi^+\rangle$ and $|\phi\rangle$ ($|\psi^-\rangle$) end up in different (the same) outputs. Figure 4.4 shows results of the incomplete BSM for the states $|\psi^-\rangle$, $|\psi^+\rangle$ and $|\phi\rangle$. States were discriminated with a success probability of $\sim 91\%$.

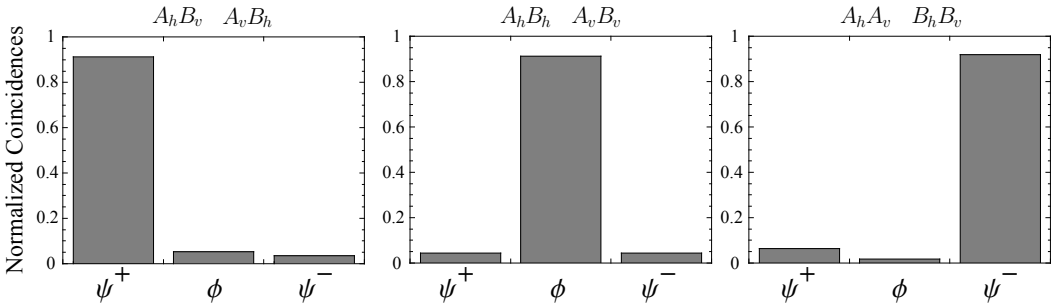

Figure 4.4: *Experimental results for incomplete Bell- state measurement (BSM) in the coincidence basis for the three input states $|\psi^+\rangle$, $|\psi^-\rangle$ and $|\phi\rangle$.*

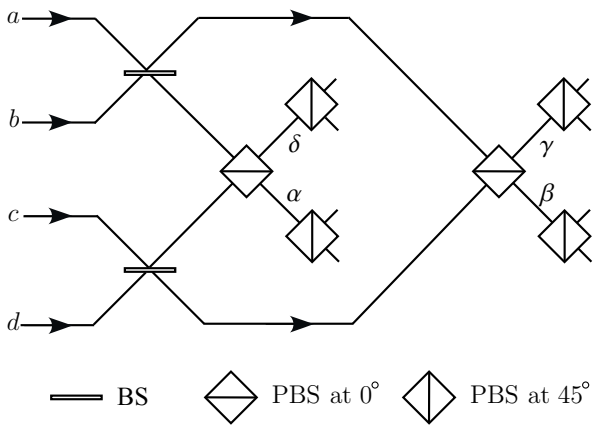

Figure 4.5: *Kwiat and Weinfurter's complete Bell-state analyzer using hyperentangled states [124]. BS and PBS are beam splitters and polarizing beam splitters, respectively.*

4.3 Complete Bell-state analysis in the coincidence basis

In ref. [124], Kwiat and Weinfurter outline a scheme for complete Bell-state analysis using hyperentanglement, shown in fig. 4.5. Working in the Heisenberg picture, using hyperentangled states of the form

$$\psi^{\pm} = \{(a_h b_v \pm a_v b_h) + (c_h d_v \pm c_v d_h)\}/2, \tag{4.3}$$
$$\phi^{\pm} = \{(a_h b_h \pm a_v b_v) + (c_h d_h \pm c_v d_v)\}/2, \tag{4.4}$$

where $a_h(a_v)$ stands for a horizontally (vertically) polarized photon in mode a, the authors show that the final states are

$$\psi^{+} = i(\alpha_{45}\delta_{45} - \alpha_{\overline{45}}\delta_{\overline{45}} + \beta_{45}\gamma_{45} - \beta_{\overline{45}}\gamma_{\overline{45}})/2, \tag{4.5}$$
$$\psi^{-} = (\alpha_{45}\gamma_{45} - \alpha_{\overline{45}}\gamma_{\overline{45}} + \beta_{45}\delta_{45} - \beta_{\overline{45}}\delta_{\overline{45}})/2, \tag{4.6}$$
$$\phi^{-} = -i(\alpha_{45}\alpha_{\overline{45}} - \beta_{45}\beta_{\overline{45}} + \gamma_{45}\gamma_{\overline{45}} - \delta_{45}\delta_{\overline{45}})/2, \tag{4.7}$$

$$\phi^{+} = i(\alpha_{45}\alpha_{45} + \alpha_{\overline{45}}\alpha_{\overline{45}} + \beta_{45}\beta_{45} + \beta_{\overline{45}}\beta_{\overline{45}} + \gamma_{45}\gamma_{45} + \gamma_{\overline{45}}\gamma_{\overline{45}} + \delta_{45}\delta_{45} + \delta_{\overline{45}}\delta_{\overline{45}})/(2\sqrt{2}), \tag{4.8}$$

where $\overline{45}$ is the polarization orthogonal to 45. Each of the four states above gives a different signature of detectors firing, however, a detector capable of distinguishing between one and two photons is required to detect ϕ^{+}.

We wish to show how the use of an antisymmetric pump beam can improve on these results. Using an antisymmetric pump beam such as the first-order Hermite Gaussian beam HG_{01}, it is easy to show that after the first set of beam splitters (BS), the states (4.3), (4.4) are

$$\psi^{+} = \{(a_h b_v + a_v b_h) + (c_h d_v + c_v d_h)\}/2, \tag{4.9}$$
$$\psi^{-} = i\{(a_h a_v - b_v b_h) + (c_h c_v - d_v d_h)\}/2, \tag{4.10}$$
$$\phi^{\pm} = \{(a_h b_h \pm a_v b_v) + (c_h d_h \pm c_v d_v)\}/2. \tag{4.11}$$

The photons are then incident on the polarizing beam splitters (PBS) at 0° and 45°. Here the 0° PBS transmits horizontally polarized light and reflect vertically polarized light, and the 45° PBS transmits light with 45° linear polarization and reflects light

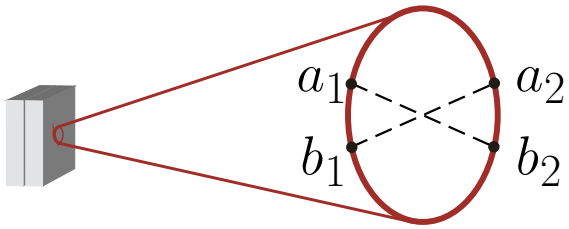

Figure 4.6: *Hyperentangled states can be generated using the type-I two-crystal source (see [16]. Selecting two sets of regions (a_1b_2 and a_2b_1) gives photon pairs entangled in momentum and polarization.*

with linear $-45°$ polarization. these states become

$$\psi^+ = (\alpha_{45}\gamma_{45} - \alpha_{\overline{45}}\gamma_{\overline{45}} + \beta_{45}\delta_{45} - \beta_{\overline{45}}\delta_{\overline{45}})/2, \tag{4.12}$$

$$\psi^- = i(\beta_{45}\gamma_{45} - \beta_{\overline{45}}\gamma_{\overline{45}} + \alpha_{45}\delta_{45} - \alpha_{\overline{45}}\delta_{\overline{45}})/2, \tag{4.13}$$

$$\phi^- = (\alpha_{45}\beta_{\overline{45}} + \alpha_{\overline{45}}\beta_{45} + \gamma_{45}\delta_{\overline{45}} + \gamma_{\overline{45}}\delta_{45})/2, \tag{4.14}$$

$$\phi^+ = (\alpha_{45}\beta_{45} + \alpha_{\overline{45}}\beta_{\overline{45}} + \gamma_{45}\delta_{45} + \gamma_{\overline{45}}\delta_{\overline{45}})/2. \tag{4.15}$$

Each of these states has its own signature of detectors firing *in coincidence*.

4.4 Hyperentanglement-assisted Bell-state analysis

4.4.1 Introduction

Here we present a new method for complete Bell-state analysis using hyperentangled states. This scheme differs from others in that it (*i*) does not rely on two-photon interference, (*ii*) does not require detectors sensitive to photon number, and (*iii*) can be implemented non-locally with 2 bits of additional classical communication. In section 4.4.2 we briefly discuss the creation of hyperentangled states. We present our hyperentangled Bell-state analyzer in section 4.4.3, and discuss the application of these results to quantum information protocol such as dense coding and teleportation.

4.4.2 Hyperentanglement

We will work with hyperentangled two-photon states of the form $|\Pi\rangle \otimes |\eta\rangle \equiv |\Pi\rangle\,|\eta\rangle$. Here $|\Pi\rangle$ and $|\eta\rangle$ are the four dimensional vectors representing the polarization and momentum degrees of freedom of the two photons, respectively. In the basis defined by linear horizontal (H) and linear vertical (V) polarization, the polarization-entangled

Bell-states are:

$$\left|\Psi^{\pm}\right\rangle = \frac{1}{\sqrt{2}}(\left|H\right\rangle_1 \left|V\right\rangle_2 \pm \left|V\right\rangle_1 \left|H\right\rangle_2), \tag{4.16a}$$

$$\left|\Phi^{\pm}\right\rangle = \frac{1}{\sqrt{2}}(\left|H\right\rangle_1 \left|H\right\rangle_2 \pm \left|V\right\rangle_1 \left|V\right\rangle_2), \tag{4.16b}$$

where $\left|\sigma\right\rangle_j$ stands for the polarization state of the photon j. Likewise, the momentum-entangled Bell-states are:

$$\left|\psi^{\pm}\right\rangle = \frac{1}{\sqrt{2}}(\left|a\right\rangle_1 \left|b\right\rangle_2 \pm \left|b\right\rangle_1 \left|a\right\rangle_2), \tag{4.17a}$$

$$\left|\phi^{\pm}\right\rangle = \frac{1}{\sqrt{2}}(\left|a\right\rangle_1 \left|a\right\rangle_2 \pm \left|b\right\rangle_1 \left|b\right\rangle_2), \tag{4.17b}$$

where $\left|a\right\rangle_j$ and $\left|b\right\rangle_j$ represent different spatial modes of photon j. We note here that polarization states have been denoted with uppercase letters and momentum states with lowercase letters.

For our hyperentangled-Bell-state analysis we will consider states of the form $\left|\Pi\right\rangle \left|\psi^{+}\right\rangle$, where $\left|\Pi\right\rangle$ is one of the polarization Bell states (4.16), though one could use any of the states (4.17) with similar results. Recently, it was shown that this type of hyperentangled two-photon state could be used to violate a generalized form of the Greenberger-Horne-Zeilinger theorem [129], and may be useful in creating decoherence-free subspaces [130]. These states can be generated by means of spontaneous parametric down-conversion (SPDC) in several ways [16, 129, 131]. For example, the type-I two-crystal source [16] emits polarization-entangled photons of the same wavelength around the rim of a cone (figure 4.6) as discussed in section 2.3.3. In this source, crystal 1 emits pairs of (say) H-polarized photons and crystal 2 emits pairs of V-polarized photons in superimposed emission cones. Phase-matching conditions guarantee that photon pairs are emitted on opposite sides of the cone. If the two-crystal interaction region lies entirely within a coherence volume of the pump laser beam, a polarization- and momentum-entangled state of the form $\left|\Pi\right\rangle \left|\eta\right\rangle$ can be selected by the two sets of regions a_1b_2 and a_2b_1. By changing the optical path of –say, a photon in a_1– one can adjust the phase between the two possible coincidence events so that the momentum state is $\left|\psi^{+}\right\rangle$. Half- and quarter-wave plates can be used to switch between the four polarization Bell-states [13]. It should be noted that because there are also vacuum and higher-order terms present with this source, the state $\left|\Pi\right\rangle \left|\psi^{+}\right\rangle$ can be achieved only

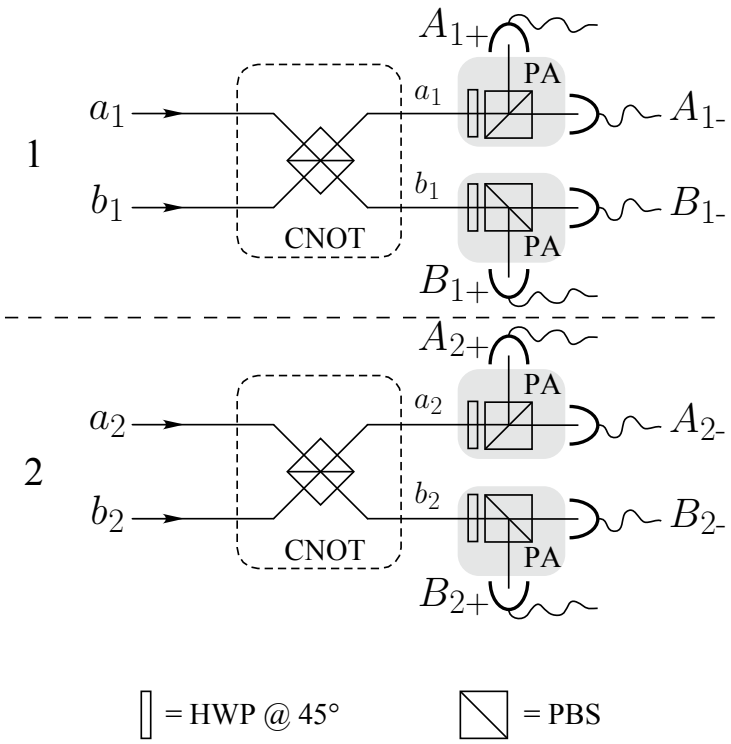

Figure 4.7: *The hyperentangled Bell-state analyzer. Hyperentangled photons, which can be generated by SPDC (see figure 4.6), are input the Bell state analyzer. The PBS are polarizing beam splitters in the $H-V$ basis. HWP are half-wave plates. The* CNOT *operation uses the polarization as the control and momentum as the target. The PA are polarization analyzers in the $\pm 45°$ basis (denoted as $\pm$) consisting of a HWP and a PBS.*

by post-selection: considering only those events which give two-photon coincidence detections. Very recently, hyperentangled states were produced using this source by F. De Martini's group [132].

4.4.3 Bell-state analysis

The hyperentangled-Bell-state analyzer is shown in figure 4.7. The hyperentangled state $|\Pi\rangle\,|\psi^+\rangle$ is first incident on a set of polarizing-beam splitters (PBS), which reflect H-polarized photons and transmit V-polarized photons. The PBS perform a controlled-not (CNOT) logic operation between the polarization (control) and spatial (target) degrees of freedom [30, 133]. If the polarization is V then the photon is transmitted, and switches modes. If the polarization is H, then the photon is reflected, and remains

in the same mode[1]. The complete PBS operation on the polarization and spatial mode of photon j is

$$\begin{aligned}
|H\rangle_j |a\rangle_j &\longrightarrow |H\rangle_j |a\rangle_j \\
|H\rangle_j |b\rangle_j &\longrightarrow |H\rangle_j |b\rangle_j \\
|V\rangle_j |a\rangle_j &\longrightarrow |V\rangle_j |b\rangle_j \\
|V\rangle_j |b\rangle_j &\longrightarrow |V\rangle_j |a\rangle_j
\end{aligned} \tag{4.18}$$

It is straightforward to show that the four states $|\Pi\rangle\,|\psi^+\rangle$ transform as

$$\begin{aligned}
\left|\Psi^\pm\right\rangle \left|\psi^+\right\rangle &\longrightarrow \left|\Psi^\pm\right\rangle \left|\phi^+\right\rangle \\
\left|\Phi^\pm\right\rangle \left|\psi^+\right\rangle &\longrightarrow \left|\Phi^\pm\right\rangle \left|\psi^+\right\rangle
\end{aligned} \tag{4.19}$$

A quick look at (4.19) shows that the PBS's mark the momentum state by performing a polarization-controlled logic operation. The momentum state can then be used to discriminate between the $|\Psi^\pm\rangle$ and $|\Phi^\pm\rangle$ polarization states: coincidence detections in modes a_1a_2 or b_1b_2 imply states $|\Psi^\pm\rangle$ while coincidences in a_1b_2 or b_1a_2 imply states $|\Phi^\pm\rangle$. Using additional polarization analyzers (PA in figure 4.7) oriented at 45°, we can discriminate between the respective $\pm$ states. Specifically, $|\Psi^+\rangle$ and $|\Phi^+\rangle$ give coincidence counts at the $+45, +45$ or $-45, -45$ output ports while $|\Psi^-\rangle$ and $|\Phi^-\rangle$ give coincidence counts at the $-45, +45$ or $+45, -45$ output ports. A summary of the detector signatures for the polarization Bell states are shown in table 4.2.

We note that all four Bell-states are recognized in the coincidence basis, with no need for detectors that are sensitive to photon number, and without the use of two-photon interference effects. Furthermore, the BSM can be performed non-locally at the cost of 2 bits of classical communication, since the physicist measuring system 1 needs to communicate one of four possible outcomes to system 2 (or vice versa).

The hyperentangled Bell-state analyzer is well within the scope of present technology, necessitating only wave plates, polarizing beam splitters and single photon detectors.

[1]This convention has been chosen for the sake of simplicity. Conventional PBS's generally operate in the opposite way, H-polarized fields are transmitted and V-polarized fields are reflected. Using additional HWP's to rotate polarzation at the input and output ports of a conventional PBS, the CNOT operation as described above can be achieved.

state	detector signature
$\|\Psi^+\rangle$	$A_{1+}A_{2+}$ or $B_{1+}B_{2+}$ or $A_{1-}A_{2-}$ or $B_{1-}B_{2-}$
$\|\Psi^-\rangle$	$A_{1+}A_{2-}$ or $B_{1+}B_{2-}$ or $A_{1-}A_{2+}$ or $B_{1-}B_{2+}$
$\|\Phi^+\rangle$	$A_{1+}B_{2+}$ or $B_{1+}A_{2+}$ or $A_{1-}B_{2-}$ or $B_{1-}A_{2-}$
$\|\Phi^-\rangle$	$A_{1+}B_{2-}$ or $B_{1+}A_{2-}$ or $A_{1-}B_{2+}$ or $B_{1-}A_{2+}$

Table 4.2: *Detector signatures for polarization Bell-states using the momentum state* $|\psi^+\rangle$ *as an ancilla. "+"* $\equiv +45°$ *and "−"*$\equiv -45°$.

A short analysis of the stability of the scheme proposed here may be in order. In addition to mode overlap at the polarizing beam splitters, the use of the ancillary momentum state $|\psi^+\rangle$ requires phase stability between the modes. A phase error α of the form

$$\begin{aligned}\left|\psi^+\right\rangle \longrightarrow & \frac{1}{\sqrt{2}}(\left|a\right\rangle_1 \left|b\right\rangle_2 + e^{i\alpha}\left|b\right\rangle_1 \left|a\right\rangle_2) \\ = & \frac{1}{2}(1+e^{i\alpha})\left|\psi^+\right\rangle + \frac{1}{2}(1-e^{i\alpha})\left|\psi^-\right\rangle \end{aligned} \tag{4.20}$$

introduces an error in the BSM, since the CNOT operations with the ancillary momentum state $|\psi^-\rangle$ are:

$$\begin{aligned}\left|\Psi^\pm\right\rangle\left|\psi^-\right\rangle &\longrightarrow \left|\Psi^\mp\right\rangle\left|\phi^-\right\rangle, \\ \left|\Phi^\pm\right\rangle\left|\psi^-\right\rangle &\longrightarrow \left|\Phi^\mp\right\rangle\left|\psi^-\right\rangle. \end{aligned} \tag{4.21}$$

The momentum states continue to show the same type of correlation, (the polarization states $|\Psi^\pm\rangle$ at a_1a_2 or b_1b_2, etc.). However, the polarization states have been switched. From (4.20), the probability to obtain the correct Bell state is thus $|1+\exp(i\alpha)|^2/2$. To avoid bilateral phase errors, we could use the momentum state $|\psi^-\rangle$ instead of the $|\psi^+\rangle$ as an ancilla. It has been shown that $|\psi^-\rangle$ is insensitive to collective decoherence [130].

It is also possible to use the polarization degrees of freedom as the ancilla and encode information in the momentum Bell-states. A hyperentangled Bell-state analyzer for such an implementation is shown in figure 4.8. The CNOT operation is performed by half-wave plates (HWP) aligned at 45° in modes b_1 and b_2. The beam splitters (BS) and polarizing beam splitters (PBS) separate the 4 hyperentangled states. The beam splitters transform the input modes as $a \longrightarrow (a+b)/\sqrt{2}$ and $b \longrightarrow (a-b)/\sqrt{2}$, which

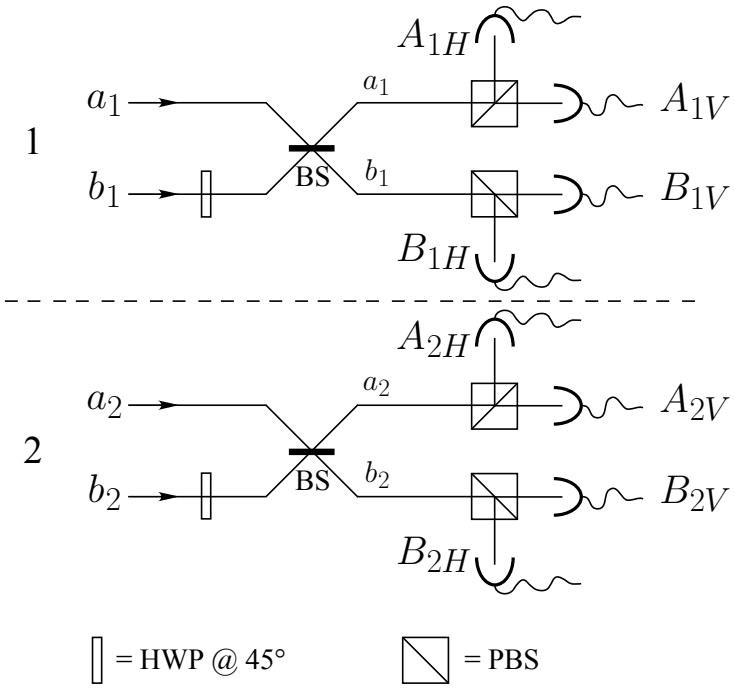

Figure 4.8: *The hyperentangled Bell-state analyzer for momentum Bell-states, using the polarization state as an ancilla. Hyperentangled states created by the source shown in figure 4.6 are input into the analyzer. The* CNOT *operation is now performed by the half-wave plates (HWP). The BS are non-polarizing beam splitters. The PBS are polarizing beam splitters in the* $H - V$ *basis.*

state	detector signature
$\|\psi^+\rangle$	$A_{1H}A_{2H}$ or $B_{1H}B_{2H}$ or $A_{1V}A_{2V}$ or $B_{1V}B_{2V}$
$\|\psi^-\rangle$	$A_{1H}B_{2H}$ or $B_{1H}A_{2H}$ or $A_{1V}B_{2V}$ or $B_{1V}A_{2V}$
$\|\phi^+\rangle$	$A_{1H}A_{2V}$ or $B_{1H}B_{2V}$ or $A_{1V}A_{2H}$ or $B_{1V}B_{2H}$
$\|\phi^-\rangle$	$A_{1H}B_{2V}$ or $B_{1H}A_{2V}$ or $A_{1V}B_{2H}$ or $B_{1V}A_{2H}$

Table 4.3: *Detector signatures for momentum Bell-states using the polarization state* $|\Psi^+\rangle$ *as an ancilla.*

gives different correlations for the $\pm$ states. The polarizing beam splitters separate the polarization ancilla states $|\Phi^+\rangle$ and $|\Psi^+\rangle$ after the CNOT operation. The detector signatures are shown in table 4.3.

4.4.4 Applications

We now discuss the possible application of hyperentangled Bell-state analysis to dense coding and quantum teleportation.

Dense Coding

The quantum dense coding protocol [95] allows for the transmission of two bits of information in one quantum bit. Two parties, Alice and Bob, each possess one photon of an entangled Bell-state ($|\Phi^+\rangle$, for example). Since the reduced density matrix for Bob's photon is $\mathbf{I}/2$, where $\mathbf{I}$ is the 2×2 identity matrix, there is no information present in Bob's photon alone. Some time later, Alice wishes to send a 2 bit message to Bob. She switches among the four Bell-states using local operations, and then sends her photon to Bob, who performs a Bell-state measurement on the photon pair, and retrieves Alice's message. Since there was no information present in Bob's photon, then the 2 bits of information present was sent in Alice's photon. However, the reduced density matrix of Alice's photon is also $\mathbf{I}/2$, so an eavesdropper could not extract any information from Alice's photon alone.

An appealing feature of the hyperentangled product states $|\Pi\rangle\,|\eta\rangle$ is that the two degrees of freedom can be manipulated independently. For example, one can switch among the polarization Bell states using local operations (quarter- and half-wave plates in modes a_j and b_j) on the polarization state, while leaving the momentum state untouched. One could then implement a dense-coding scheme in which information is encoded in the polarization state, while the momentum state remains as an ancilla to assist in the complete Bell-state measurement. We note that this implementation requires 4 qubits (encoded in 2 photons) to transmit 2 classical bits of information and thus it may be debatable as to whether this is actually "dense" coding. However, since the density matrix of (say) photon 2 is

$$\hat{\rho}_2 = \mathrm{trace}_1(\hat{\rho}_{12}) = \frac{1}{4}\mathbf{I}_4, \tag{4.22}$$

where $\hat{\rho}_{12}$ is the total 16×16 density matrix of photons 1 and 2 and $\mathbf{I}_4$ is the 4×4 identity matrix, we can still send 2 classical bits of information in one photon (containing 2 qubits) in such a way that an eavesdropper with access to only this photon cannot extract any information.

Teleportation

Another use of a Bell-state measurement is in the quantum teleportation protocol [94], which can be used to swap entanglement [59, 94, 120] and perform quantum logic operations for quantum computation [97]. Unfortunately, Bell-state measurement of hyperentangled states offers no gain in the quantum teleportation protocol. Here various aspects are discussed.

In quantum teleportation, two spatially separate parties Alice and Bob each are in possession of one photon of an entangled pair, prepared in a Bell-state. One of them, say Alice, wants to teleport the quantum state of a third photon to Bob. Of course, Alice does not know what state she is teleporting, or else she could simply call Bob on the telephone and tell him to prepare that state. Instead, Alice performs a Bell-state measurement on her two photons. She then communicates classically to Bob, telling him the results of her BSM, at which point Bob, performs a local operation and recovers the state of the third photon, now encoded in his photon. In this way Alice can teleport a quantum state to Bob without actually knowing what state she is sending.

To date, quantum teleportation implementations using 3 photons [56] can be performed with a Bell-state measurement that is 50% efficient using only two-photon interference, polarization analysis and single photon detectors[2]. Given an unknown quantum state, Alice, who shares a pair of maximally entangled photons with Bob, can teleport this state to him with 50% efficiency. Suppose Alice and Bob share a pair of polarization-entangled photons in the Bell-state $|\Phi^+\rangle_{12}$ and Alice would like to teleport the unknown polarization state $|u\rangle_3$ of photon 3. To take advantage of hyperentangled Bell-state analysis, Alice would need to entangle the momentum degree of freedom of photon 2 with that of photon 3. To do so requires a controlled logic operation between the two photons, such as a CNOT gate. But if she could perform an efficient two-photon CNOT operation then she might as well use it to perform her BSM, which can be done with the same efficiency using a CNOT gate and a single photon Hadamard rotation [30].

One might think that Alice could first entangle the momentum degrees of freedom of photons 2 and 3 using an inefficient CNOT gate, and discard the cases where the gate

[2]Other implementations using non-linear processes can distinguish between all 4 Bell-states [57]. However, the efficiency is very low.

did not give the desired output (which is usually checked by measuring the ancillary modes). She could then pass photon 3 on to a friend who performs some sort of complex quantum computation using the polarization as a qubit, and then passes it back to Alice for teleportation. The complex quantum computation, which we assume to be much more difficult and time consuming than the teleportation protocol, need be performed only once, since the Bell-state measurement on photons 2 and 3 is now 100% efficient. However, since photon 3 is part of an entangled momentum state, it is now defined by 2 spatial modes. So Alice's friend is required to run the computation on both spatial modes, which in principle is the same as running the computation twice, as is required on average in the 50% efficient teleportation scheme. Thus, a teleportation protocol using Bell-state measurement of hyperentangled states of this form does not present any gain over previous methods.

4.5 Conclusion

It has been shown that Hong-Ou-Mandel interference at a beam splitter can be controlled to facilitate Bell-state analysis. Creating polarization-entangled photons with spontaneous parametric down-conversion using an antisymmetric Hermite-Gaussian pump beam, we invert the usual interference behavior of the Bell states. We have shown how that this simplifies the standard methods for incomplete Bell-state analysis of down-converted photon pairs, removing the necessity for detectors sensitive to photon number. We have shown that we can use the transverse symmetry of the biphoton to improve on a previous scheme for complete Bell-state analysis of down-converted photon pairs [124], enabling complete Bell-state analysis in the coincidence basis. These results illustrate the use of additional degrees of freedom of the two-photon state as a control parameter in quantum state engineering.

In addition, a simple method for complete Bell-state analysis using hyperentangled photons was presented. This scheme requires only linear optics and single photon detectors, can be implemented non-locally with 2 bits of classical communication, and is well within the bounds of current technology. Since the hyperentangled states required in our scheme can be generated using spontaneous parametric down-conversion and post-selection, implementation of a complete Bell-state measurement using our technique is experimentally feasible.

The application of these results to the quantum teleportation protocol has been

discussed. Given that our scheme requires photons entangled in multiple degrees of freedom, it does not provide any increase in efficiency to Bell-state measurements for quantum teleportation. However, our method can be applied directly to implementations of quantum dense coding, resulting in the secure transmission of 2 bits of classical information in one photon (containing 2 qubits).

It is important to note that all of the above results are applicable for down-converted pairs only, and thus are not entirely helpful for BSM's in quantum teleportation [56] or entanglement swapping [59, 120] protocol which use photon pairs which are not created simultaneously from a common source. However, it should be emphasized that these results are directly applicable to quantum dense coding schemes [28, 52].

5

Conservation *and* Entanglement *of* Orbital Angular Momentum *in* SPDC

It is shown that the transfer of the plane wave spectrum of the pump beam to the fourth-order transverse spatial correlation function of the two-photon field generated by spontaneous parametric down-conversion leads to the conservation and entanglement of orbital angular momentum of light. By means of a simple experimental setup based on fourth-order (or two-photon) interferometry, we show that our theoretical model provides a good description for down-converted fields carrying orbital angular momentum. These results have been reported in Physical Review A **69**, 023811 (2004).

5.1 Introduction

For over a decade it has been known that any electromagnetic paraxial beam with an azimuthal phase dependence of the form $e^{il\phi}$ carries an orbital angular momentum $l\hbar$

per photon [113]. The Laguerre-Gaussian (LG) beams presented in section 2.4.3 are the most known and studied examples of beams carrying orbital angular momentum. In addition to interesting implications in classical and quantum optics, this fact also raises possibilities for technical applications. For example, the orbital angular momentum of single photons in LG modes provides a possible qudit encoding scheme [106]. The quantum number l can be coherently raised or lowered using holographic masks [134]. Devices that discriminate the orbital angular momentum of Laguerre-Gaussian beams have been reported [135] and experimentally tested [118, 136]. In principle, these devices should operate at the single photon level.

A fruitful potential application of light beams carrying orbital angular momentum is the generation of photon pairs with discrete multidimensional entanglement [46], which can be obtained by spontaneous parametric down-conversion (SPDC) with a LG pump beam. Let $|m\rangle$ denote a single photon state carrying an orbital angular momentum $m\hbar$ and l be the azimuthal index of the the LG pump beam, the two-photon state generated by SPDC can be written as

$$|\psi\rangle = \sum_{m=-\infty}^{+\infty} C_m \, |l-m\rangle \, |m\rangle \, . \tag{5.1}$$

This expression is based on the hypothesis that orbital angular momentum is conserved in SPDC. Some authors have studied this issue [82, 106, 107, 108, 137], and experimental results [19, 46] suggest that orbital angular momentum is in fact conserved. One has to consider, however, that although the process of down-conversion itself may conserve angular momentum, in most cases, the pump beam propagates in a birefringent nonlinear crystal as an extraordinary beam. The anisotropy of the medium causes a small astigmatism in the LG beam as it propagates, breaking its circular symmetry in the transverse plane. This symmetry breaking is equivalent to an exchange of angular momentum between the medium and the pump beam, so that the conservation holds only on average. This effect depends on both the angular momentum of the pump beam and on the crystal length, being negligible for thin crystals and low values of l. The propagation of LG beams in uniaxial birefringent media has been studied by Costa Moura and Monken [138].

As discussed in section 2.2.4, Monken, Souto Ribeiro and Pádua [77] have previously shown that the phase matching conditions in SPDC are responsible for a transfer of the angular spectrum of the pump beam (amplitude and phase characteristics) to

the fourth-order spatial correlation properties of the two-photon field. In this chapter, we will demonstrate theoretically and experimentally that the conservation of orbital angular momentum as well as the multi-dimensional entanglement in the SPDC process in the thin crystal paraxial approximation is a direct consequence of the transfer of the plane wave spectrum from the pump beam to the two-photon state. By means of a simple experimental setup based on fourth-order multimode Hong-Ou-Mandel interferometry, it will be shown that our theoretical model provides a good description for down-converted fields carrying orbital angular momentum.

5.2 Theory

5.2.1 The state generated by SPDC

In section 2.2.4 we arrived at an expression for the two-photon state. For simplicity, we will assume that the biphoton polarization state is a product state of the down-converted fields. As before, we will work in the monochromatic and paraxial approximations, in which the two-photon component of the quantum state generated by non-collinear SPDC is given by Eq. (2.25):

$$|\psi\rangle = \iint_D d\mathbf{q}_s d\mathbf{q}_i \; \Phi(\mathbf{q}_s, \mathbf{q}_i) \, |\mathbf{q}_s, \sigma_s\rangle_s \, |\mathbf{q}_i, \sigma_i\rangle_i \, . \tag{5.2}$$

The function $\Phi(\mathbf{q}_s, \mathbf{q}_i)$ is given by Eq. (2.26)

$$\Phi(\mathbf{q}_s, \mathbf{q}_i) = \frac{1}{\pi}\sqrt{\frac{2L}{K}} \; v(\mathbf{q}_s + \mathbf{q}_i) \; \mathrm{sinc}\left(\frac{L|\mathbf{q}_s - \mathbf{q}_i|^2}{4K}\right), \tag{5.3}$$

Here $v(\mathbf{q})$ is the normalized angular spectrum of the pump beam, L is the length of the nonlinear crystal in the propagation (z) direction, and K is the magnitude of the pump field wave vector. The two-photon detection amplitude is given by Eq. (2.28)

$$\mathbf{\Psi}(\mathbf{r}_s, \mathbf{r}_i) = \langle \mathrm{vac} | \, \mathbf{E}_i^{(+)}(\mathbf{r}_i) \mathbf{E}_s^{(+)}(\mathbf{r}_s) \, |\psi\rangle \, , \tag{5.4}$$

where $\mathbf{E}_j^{(+)}(\mathbf{r})$ is the field operator for the plane wave mode j in the paraxial approximation given by Eq. (2.29). In this analysis we do not consider polarization, so $\mathbf{\Psi}(\mathbf{r}_s, \mathbf{r}_i)$ will be treated as a scalar function. In addition, we will work in the far field and make the following simplifications: $z_s = z_i = Z$, $k_s = k_i = \frac{1}{2}K$. As shown in section 2.2.5, it is known that if the paraxial approximation is valid, the two-photon wave function

can be put in the form

$$\Psi(\boldsymbol{\rho}_s, \boldsymbol{\rho}_i, z_s, z_i) = \mathcal{W}\left(\frac{\boldsymbol{\rho}_s + \boldsymbol{\rho}_i}{2}, Z\right)\ \mathcal{F}\left(\frac{\boldsymbol{\rho}_s - \boldsymbol{\rho}_i}{\sqrt{2}}, Z\right), \tag{5.5}$$

where $\mathcal{W}(\boldsymbol{\rho}, z)$ is the normalized electric field amplitude of the pump beam and

$$\mathcal{F}(\boldsymbol{\rho}, z) = \frac{\sqrt{KL}}{2\pi z}\ \mathrm{sinc}\left(\frac{KL}{8z^2}\rho^2\right). \tag{5.6}$$

In order to clean-up the notation, we will omit the dependence on the z coordinate hereafter. We see that the two-photon wave function Ψ carries the same functional form as the pump beam amplitude, calculated in the coordinate $\boldsymbol{\rho} = \frac{1}{2}\boldsymbol{\rho}_s + \frac{1}{2}\boldsymbol{\rho}_i$. The pump beam field $\mathcal{W}(\boldsymbol{\rho})$ is characterized by its wavelength λ_p and its waist w_p. To be more precise, we will write $\mathcal{W}$ as $\mathcal{W}(\boldsymbol{\rho}; \lambda_p, w_p)$. Since we are working with down-converted fields satisfying $\lambda_s = \lambda_i = 2\lambda_p$, it is convenient to write Ψ in terms of a beam with the same angular spectrum of the pump field, as required by Eq. (5.5), but with a wavelength $\lambda_c = 2\lambda_p$, and a waist $w_c = \sqrt{2}\, w_p$. From the general form of gaussian beams, apart from a phase factor and normalization constants, it is evident that

$$\mathcal{W}(\boldsymbol{\rho}; \lambda_o, w_o) = \mathcal{W}(\sqrt{2}\,\boldsymbol{\rho}; 2\lambda_o, \sqrt{2}\, w_o) \equiv \mathcal{U}(\sqrt{2}\,\boldsymbol{\rho}). \tag{5.7}$$

So, Ψ can be put in the more convenient form

$$\Psi(\boldsymbol{\rho}_s, \boldsymbol{\rho}_i) = \mathcal{U}\left(\frac{\boldsymbol{\rho}_s + \boldsymbol{\rho}_i}{\sqrt{2}}\right)\ \mathcal{F}\left(\frac{\boldsymbol{\rho}_s - \boldsymbol{\rho}_i}{\sqrt{2}}\right) \tag{5.8}$$

Let us now suppose that the down-converter is pumped by a LG beam whose orbital angular momentum is $l\,\hbar$ per photon, described by the amplitude $\mathcal{W}_p^l(\boldsymbol{\rho}; \lambda_p, w_p)$. Here, p is the radial index. In order to study the conservation of angular momentum in SPDC, we will expand the two-photon wave function $\Psi(\boldsymbol{\rho}_s, \boldsymbol{\rho}_i)$ in terms of the LG basis functions $\mathcal{U}_{p_s}^{l_s}(\boldsymbol{\rho}_s)\,\mathcal{U}_{p_i}^{l_i}(\boldsymbol{\rho}_i)$. That is,

$$\Psi(\boldsymbol{\rho}_s, \boldsymbol{\rho}_i) = \sum_{l_s, p_s}\sum_{l_i, p_i} C_{p_s p_i}^{l_s l_i}\, \mathcal{U}_{p_s}^{l_s}(\boldsymbol{\rho}_s)\, \mathcal{U}_{p_i}^{l_i}(\boldsymbol{\rho}_i) \tag{5.9}$$

From the orthogonality of the LG basis, $C_{p_s p_i}^{l_s l_i}$ is given by

$$C_{p_s p_i}^{l_s l_i} = \iint d\boldsymbol{\rho}_s d\boldsymbol{\rho}_i\ \mathcal{U}_p^l\left(\frac{\boldsymbol{\rho}_s + \boldsymbol{\rho}_i}{\sqrt{2}}\right)\ \mathcal{F}\left(\frac{\boldsymbol{\rho}_s - \boldsymbol{\rho}_i}{2}\right) \mathcal{U}_{p_s}^{*l_s}(\boldsymbol{\rho}_s)\, \mathcal{U}_{p_i}^{*l_i}(\boldsymbol{\rho}_i). \tag{5.10}$$

Let us make the following coordinate transformation in Eq. (5.10): $\mathbf{R} = \boldsymbol{\rho}_s + \boldsymbol{\rho}_i$ and $\mathbf{S} = \frac{1}{2}(\boldsymbol{\rho}_s - \boldsymbol{\rho}_i)$. So,

$$C_{p_s p_i}^{l_s l_i} = \iint d\mathbf{R}\, d\mathbf{S}\, \mathcal{U}_p^l\left(\frac{\mathbf{R}}{\sqrt{2}}\right) \mathcal{F}(\sqrt{2}\,\mathbf{S}) \mathcal{U}_{p_s}^{*l_s}\left(\frac{\mathbf{R}}{2} + \mathbf{S}\right) \mathcal{U}_{p_i}^{*l_i}\left(\frac{\mathbf{R}}{2} - \mathbf{S}\right). \tag{5.11}$$

When L is small enough (the thin crystal approximation), $\mathcal{F}$ can be approximated by 1 in Eq. (5.11), provided the order of the LG modes ($N = 2p + |l|$) is not too large. In this case, the integral in $\mathbf{S}$ is proportional to the convolution $\mathcal{U}_{p_s}^{*l_s}(\mathbf{R}) * \mathcal{U}_{p_i}^{*l_i}(\mathbf{R})$ [139]. Numerical calculations show that in the worst case, that is, $p_s = p_i$, $|l_s| = |l_i|$ and $R = 0$, for a 1 mm-thick crystal, pumped by a laser with $\lambda_p = 351$ nm and a waist of $w_p = 1$ mm, the mean square error is less than 1% for $N = 100$. Since we are neglecting the effects due to the anisotropy of the crystal, as discussed before, there is no point in seeking exact solutions for large values of N.

Under the thin crystal approximation, equation (5.11) is more conveniently written in terms of Fourier transforms, as

$$\begin{aligned} C_{p_s p_i}^{l_s l_i} &\propto \iiint d\mathbf{R}\, d\mathbf{q}\, d\mathbf{q}'\ \mathcal{V}_p^l(\sqrt{2}\,\mathbf{q}') \mathcal{V}_{p_s}^{*l_s}(\mathbf{q})\, \mathcal{V}_{p_i}^{*l_i}(\mathbf{q})\ e^{i\mathbf{R}\cdot(\mathbf{q}'-\mathbf{q})} \\ &\propto \int d\mathbf{q}\ \mathcal{V}_p^l(\sqrt{2}\,\mathbf{q})\, \mathcal{V}_{p_s}^{*l_s}(\mathbf{q})\, \mathcal{V}_{p_i}^{*l_i}(\mathbf{q}), \end{aligned} \tag{5.12}$$

where $\mathcal{V}_\mu^\nu(\mathbf{q})$ is the Fourier transform of $\mathcal{U}_\mu^\nu(\mathbf{R})$. Writing equation (5.12) in cylindrical coordinates $\mathbf{q} \to (q, \phi)$, the LG profiles are $\mathcal{V}_\mu^\nu(\mathbf{q}) = v_\mu^\nu(q)\, e^{i\nu\phi}$. Then, we have

$$\begin{aligned} C_{p_s p_i}^{l_s l_i} &\propto \iint q\, dq\, d\phi\ v_p^l(\sqrt{2}\,q)\, v_{p_s}^{*l_s}(q)\, v_{p_i}^{*l_i}(q)\ e^{i(l-l_s-l_i)\phi} \\ &\propto \delta_{l_s+l_i,l} \int q\, dq\ v_p^l(\sqrt{2}\,q)\, v_{p_s}^{*l_s}(q)\, v_{p_i}^{*l_i}(q). \end{aligned} \tag{5.13}$$

The delta function $\delta_{l_s+l_i,l}$ guarantees that orbital angular momentum is conserved in the SPDC process. In principle, this conservation could be satisfied by fields exhibiting either a classical or quantum correlation (entanglement) of orbital angular momentum. We will now show that the conservation leads to entanglement of orbital angular momentum of the down-converted fields.

From (5.8) it is evident that, when $\mathcal{F} = 1$, the biphoton wave function reproduces the pump beam transverse profile. Let us assume that (5.8) (with $\mathcal{F} = 1$) accurately describes the two-photon state from SPDC and that the pump beam is a LG mode

with $l \neq 0$. Then, the biphoton wave function is

$$\Psi(\boldsymbol{\rho}_s, \boldsymbol{\rho}_i) = \mathcal{U}_p^l \left(\frac{\boldsymbol{\rho}_s + \boldsymbol{\rho}_i}{\sqrt{2}} \right), \tag{5.14}$$

from which, it is evident that $\Psi(\boldsymbol{\rho}_s + \boldsymbol{\Delta}, \boldsymbol{\rho}_i - \boldsymbol{\Delta}) = \Psi(\boldsymbol{\rho}_s, \boldsymbol{\rho}_i)$. Due to the phase structure of $\mathcal{U}_p^l$, for $l \neq 0$ there exist transverse spatial positions $\boldsymbol{\rho}_{s0}$ and $\boldsymbol{\rho}_{i0}$ such that $\mathcal{U}_p^l(\boldsymbol{\rho}_{s0} + \boldsymbol{\rho}_{i0}) = 0$. Then, clearly

$$\Psi(\boldsymbol{\rho}_{s0} + \boldsymbol{\Delta}, \boldsymbol{\rho}_{i0} - \boldsymbol{\Delta}) = \Psi(\boldsymbol{\rho}_{s0}, \boldsymbol{\rho}_{i0}) = 0, \tag{5.15}$$

and the coincidence detection probability $\mathcal{P}(\boldsymbol{\rho}_s, \boldsymbol{\rho}_i) = |\Psi(\boldsymbol{\rho}_s, \boldsymbol{\rho}_i)|^2$ satisfies

$$\mathcal{P}(\boldsymbol{\rho}_{s0} + \boldsymbol{\Delta}, \boldsymbol{\rho}_{i0} - \boldsymbol{\Delta}) = \mathcal{P}(\boldsymbol{\rho}_{s0}, \boldsymbol{\rho}_{i0}) = 0. \tag{5.16}$$

Now suppose that the down-converted fields exhibit a classical correlation that conserves orbital angular momentum. The detection probability $\mathcal{P}_{\text{cc}}$ for such a correlation can be written as

$$\mathcal{P}_{\text{cc}}(\boldsymbol{\rho}_s, \boldsymbol{\rho}_i) = \sum_{l_i=-\infty}^{\infty} P_{l_i} |F_{l-l_i}(\boldsymbol{\rho}_s)|^2 |G_{l_i}(\boldsymbol{\rho}_i)|^2, \tag{5.17}$$

where $F_{l_s}(\boldsymbol{\rho}_s)$ and $G_{l_i}(\boldsymbol{\rho}_i)$ represent down-converted signal and idler fields with orbital angular momentum $l_s\hbar$ and $l_i\hbar$ per photon, respectively. Here the coefficients P_{l_i} satisfy $\sum_{l_i=-\infty}^{\infty} P_{l_i} = 1$ and $P_{l_i} \geq 0$. Now, if the classical probability (5.17) accurately describes the two-photon state, then it must also satisfy the equivalent of condition (5.16):

$$\mathcal{P}_{\text{cc}}(\boldsymbol{\rho}_{s0} + \boldsymbol{\Delta}, \boldsymbol{\rho}_{i0} - \boldsymbol{\Delta}) = \mathcal{P}_{\text{cc}}(\boldsymbol{\rho}_{s0}, \boldsymbol{\rho}_{i0}) = 0,$$

which gives

$$\sum_{l_i=-\infty}^{\infty} P_{l_i} |F_{l-l_i}(\boldsymbol{\rho}_{s0} + \boldsymbol{\Delta})|^2 |G_{l_i}(\boldsymbol{\rho}_{i0} - \boldsymbol{\Delta})|^2 = 0. \tag{5.18}$$

Since $P_{l_i} \geq 0$, a non-trivial solution to (5.18) exists (for the cases where at least one $P_{l_i} \neq 0$) only if $|F_{l-l_i}(\boldsymbol{\rho}_{s0} + \boldsymbol{\Delta})|^2 = 0$ or $|G_{l_i}(\boldsymbol{\rho}_{i0} - \boldsymbol{\Delta})|^2 = 0$ for all $\boldsymbol{\Delta}$, which implies that $F_{l-l_i} \equiv 0$ or $G_{l_i} \equiv 0$. Thus, a classical correlation of orbital angular momentum states cannot reproduce the two photon wave function (5.8).

With the reasoning above, we have shown that, assuming Eq. (5.8) accurately describes the biphoton wave function from SPDC, the conservation of orbital angular momentum in SPDC is not satisfied by a classical correlation of the down-converted fields. This implies that the fields are entangled in orbital angular momentum.

5.2.2 Biphoton phase measurements

Having demonstrated that the two-photon wave function (5.5) leads to conservation and entanglement of orbital angular momentum, the next step is to prove that it describes accurately the state generated by SPDC within the assumed approximations. Although direct coincidence detection provides information about the modulus of $\Psi(\boldsymbol{\rho}_s, \boldsymbol{\rho}_i)$, its phase structure can only be revealed by some sort of interference measurement. We do this with the help of the Hong-Ou-Mandel (HOM) interferometer [64], represented in Fig. 3.1 and described in chapter 3. Coincidence measurements are taken from the two output ports of the beam splitter.

If $\mathbf{r}_1$ and $\mathbf{r}_2$ are the positions of detectors D_1 and D_2, each located at one output of the beam splitter, the coincidence detection amplitude is given by

$$\Psi_c = \Psi_{tt}(\mathbf{r}_1, \mathbf{r}_2) + \Psi_{rr}(\mathbf{r}_1, \mathbf{r}_2), \tag{5.19}$$

where the indices tt and rr refer to the cases when both photons are transmitted or reflected by the beam splitter, respectively. Using the amplitude (5.8) with the two-port coincidence amplitude (3.14), it is straightforward to show that, for $t = r = 1/\sqrt{2}$, apart from a common factor,

$$\Psi_c(\boldsymbol{\rho}_1, \boldsymbol{\rho}_2) \propto \frac{1}{2}\left[\mathcal{U}\left(\frac{x_1+x_2}{\sqrt{2}}, \frac{y_1+y_2}{\sqrt{2}}\right) - \mathcal{U}\left(\frac{x_1+x_2}{\sqrt{2}}, \frac{-y_1-y_2}{\sqrt{2}}\right)\right]. \tag{5.20}$$

Since the pump beam is a LG beam, $\mathcal{U}$ has the form

$$\mathcal{U}(\boldsymbol{\rho}) = u_p^l(\rho)e^{il\phi}. \tag{5.21}$$

Then, according to Eq. (5.20), the corresponding coincidence detection amplitude is

$$\begin{aligned}\Psi_c(\boldsymbol{\rho}_1, \boldsymbol{\rho}_2) =& u_p^l\left(\frac{1}{\sqrt{2}}\sqrt{|x_1+x_2|^2 + |y_1+y_2|^2}\right) \times \\ & \left\{\exp\left(il\arctan\frac{y_1+y_2}{x_1+x_2}\right) - \exp\left(-il\arctan\frac{y_1+y_2}{x_1+x_2}\right)\right\}\end{aligned} \tag{5.22}$$

which can be put in the form

$$\Psi_c(\boldsymbol{\rho}_1, \boldsymbol{\rho}_2) = \Psi_c(R, \theta) \propto u_p^l(R)\sin l\theta, \tag{5.23}$$

where $R = \frac{1}{\sqrt{2}}|\boldsymbol{\rho}_1 + \boldsymbol{\rho}_2|$ and θ is defined by the relations

$$\sin\theta = \frac{\rho_1\sin\phi_1 + \rho_2\sin\phi_2}{R} \tag{5.24}$$

$$\cos\theta = \frac{\rho_1\cos\phi_1 + \rho_2\cos\phi_2}{R}. \tag{5.25}$$

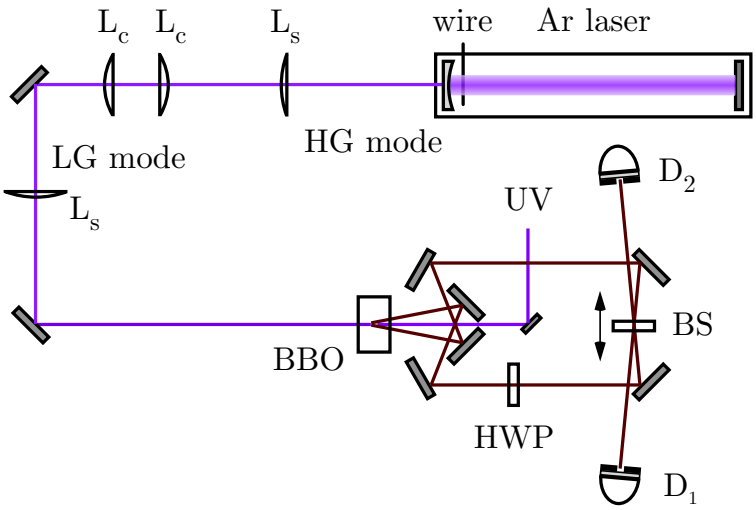

Figure 5.1: *Experimental setup to show conservation of orbital angular momentum. A wire is inserted into the laser cavity in order to generate a HG mode. A mode converter consisting of two identical spherical (L_s) and cylindrical (L_c) lenses converts the HG mode to a LG mode of the same order. The LG mode is then used to pump the BBO crystal, generating entangled photons incident on a HOM interferometer. The beam splitter BS is mounted on a motorized stage. Coincidence counts are recorded at detectors D_1 and D_2.*

The coincidence detection probability, which is proportional to $|\Psi_c(R,\theta)|^2$, is

$$P_{12}(\boldsymbol{\rho}_1, \boldsymbol{\rho}_2) \propto |u_p^l(R)|^2 \sin^2 l\theta. \tag{5.26}$$

5.3 Experiment and results

The experimental setup, shown in Fig. 5.1, consists of two basic parts. The first part is the generation of a Laguerre-Gaussian (LG) mode using a mode converter, which transforms a Hermite-Gaussian (HG) mode into a LG mode, as discussed in section 2.4.4. A detailed account of mode conversion can be found in refs. [111, 112]. To create the HG-mode, we insert a 25 μm $\varnothing$ wire into the cavity of an Argon laser, operating at ~ 30 mW with wavelength 351.1 nm. The wire breaks the circular symmetry of the laser cavity. It is aligned in the horizontal or vertical and mounted on an xy-translation stage. By adjusting the position and orientation of the wire, we can generate the modes HG_{01}, HG_{10}, HG_{02}, and HG_{20}. The beam then passes through a mode converter consisting of two spherical lenses (L_s) with focal length $f_s = 500$ mm and two cylindrical lenses (L_c)

with focal length $fc = 50.2\,\text{mm}$. The first spherical lens is used for mode-matching and is located $\approx 1.88\,\text{m}$ from the beam center of curvature. The second spherical lens is placed confocal with the first, and is used to "collimate" the beam. The cylindrical lenses are placed ($d = f_c/\sqrt{2} \approx 35\,\text{mm}$) on either side of the focal point of lens L_s and aligned at 45°. The cylindrical lenses transform the HG mode into a LG mode of the same order by introducing a relative $\pi/2$ phase between successive HG components (in the $\pm 45°$ basis, due to the orientation of the cylindrical lenses) of the input beam [111, 112]. The quality of the output mode was checked by visual examination of the intensity profile [115] as well as by interference techniques: using additional beam splitters and mirrors (not shown), the interference of the LG pump beam with a plane wave resulted in the usual spiral interference pattern [112].

The second part of the setup is a typical HOM interferometer [64]. The Argon laser is used to pump a 7 mm long BBO (β-BaB_2O_4) crystal cut for type II phase matching, generating non-collinear entangled photons by SPDC. The down-converted photons are reflected through a system of mirrors and incident on a beam splitter with measured transmittance $|t| \approx 0.67$ and reflectance $|r|^2 \approx 0.33$. These values were used for technical reasons. Ideally, the beam splitter should have $t = r = 1/\sqrt{2}$. Since the down-converted photons are orthogonally polarized, a half-wave plate (HWP) is used to rotate the polarization of one of the photons ($V \to H$). A computer-controlled stepper motor is used to adjust the position of the beam splitter. The detectors are EG & G SPCM 200 photodetectors, mounted on precision translation stages. D_2 remained fixed while computer-controlled stepper motors were used to scan detector D_1 in the transverse plane. Coincidence and single counts were registered using a personal computer. Interference filters (1 nm FWHM centered at 702 nm) and 2 mm ⌀ circular apertures where used to align the HOM interferometer. The transverse intensity profiles were measured with the interference filters removed and circular apertures with 0.5 mm ⌀ and 1 mm ⌀ on D_1 and D_2, respectively.

The results are shown in Figs. 5.2 to 5.4. The left sides of the figures show the expected coincidence patterns, obtained from the squared modulus of Eq. (5.8) in the non-interfering regime (interferometer unbalanced), and from (5.26) in the fourth-order interference regime (interferometer balanced). The right sides of the figures show the measured coincidences.

In Fig. 5.2, the nonlinear crystal was pumped by a LG_0^1 ($l = 1$) beam. Its

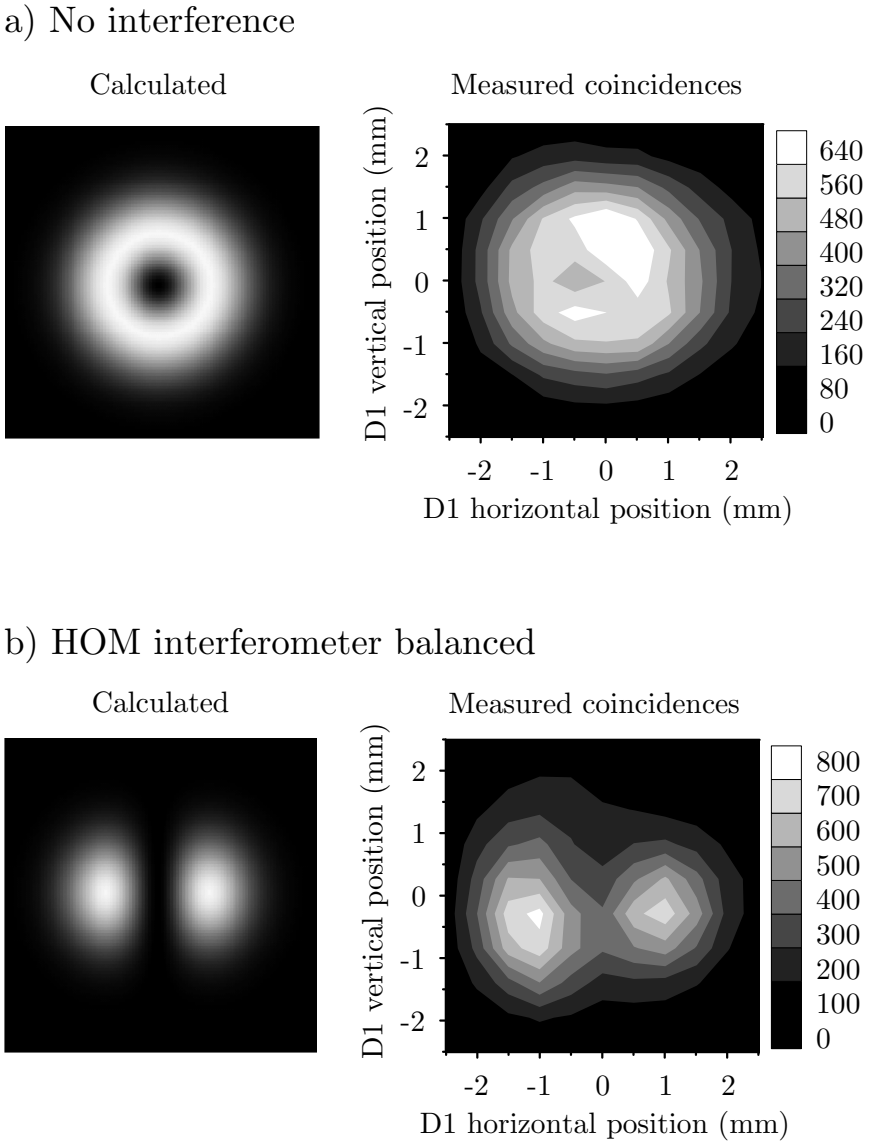

Figure 5.2: *Coincidence profiles predicted (left) and measured (right) when the crystal is pumped by a LG_0^1 beam. a) No-interference regime (Hong-Ou-Mandel interferometer unbalanced). b) Fourth-order interference regime (interferometer balanced).*

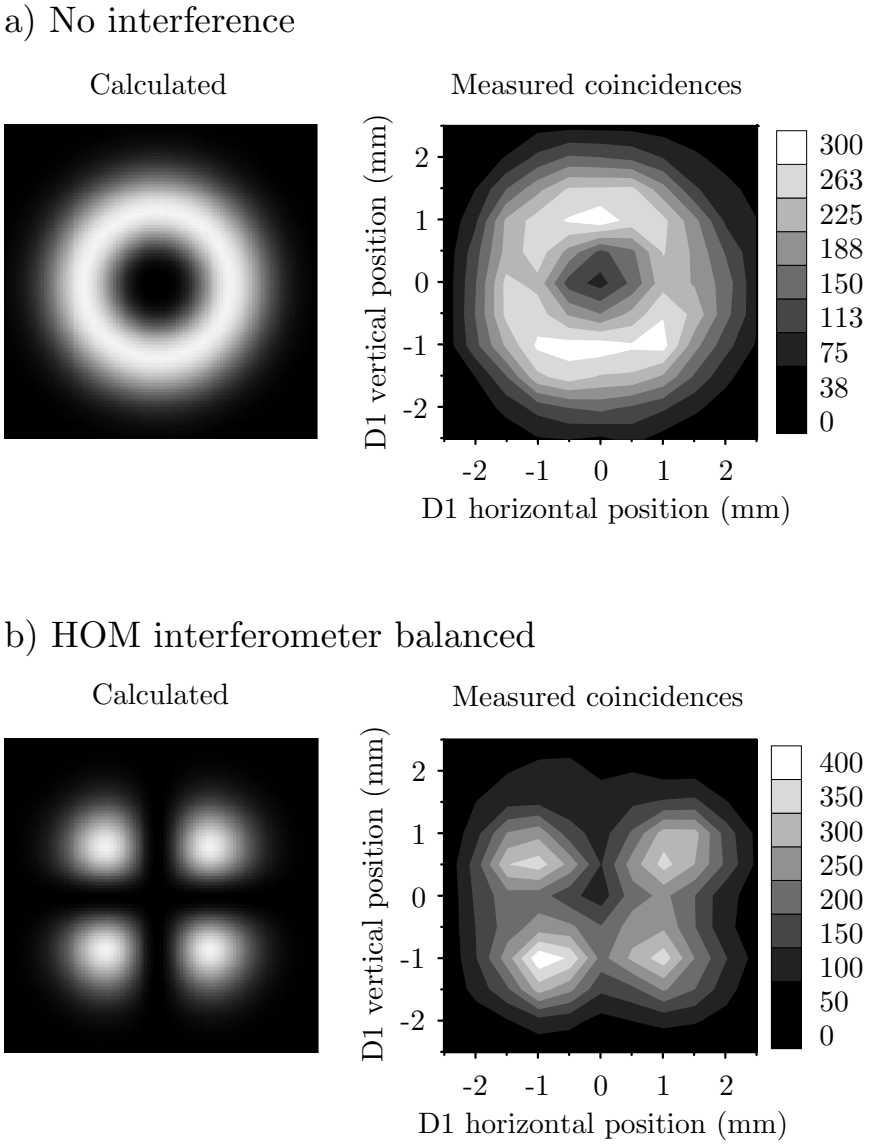

Figure 5.3: *Coincidence profiles predicted (left) and measured (right) when the crystal is pumped by a LG_0^2 beam. a) No-interference regime (Hong-Ou-Mandel interferometer unbalanced). b) Fourth-order interference regime (interferometer balanced).*

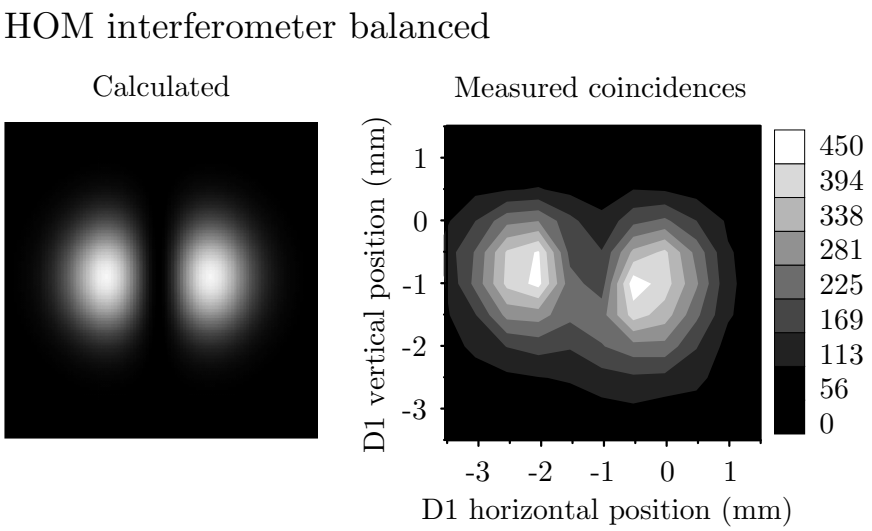

Figure 5.4: *Coincidence profile predicted (left) and measured (right) when the crystal is pumped by a LG_0^1 beam, in the fourth-order interference regime (Hong-Ou-Mandel interferometer balanced). Detector D_2 was displaced by $\Delta x = \Delta y = 1$ mm.*

intensity profile is shown in Fig. 5.2a, in agreement with Eq. (5.8). In the interference regime, shown in Fig. 5.2 b), the two interference peaks predicted by Eq. (5.26) are easily seen. In Fig. 5.3, the nonlinear crystal was pumped by a LG_0^2 ($l = 2$) beam. Now, the interference pattern shows four peaks, in agreement with Eq. (5.26).

In order to test the the translational invariance of $\Psi(\boldsymbol{\rho}_1, \boldsymbol{\rho}_2)$, which leads to the conclusion that the two-photon state is entangled in orbital angular momentum, we repeated the measurement of Fig. 5.2b, with detector D_2 displaced by $\Delta x = \Delta y = 1$ mm. The interference pattern obtained is shown in Fig. 5.4. The coincidence pattern measured by scanning D_1 is now dislocated by $\Delta x = \Delta y = -1$ mm, still in agreement with Eq. (5.26).

5.4 Conclusion

It has been shown that the transfer of the plane wave spectrum of the pump beam to the fourth-order transverse spatial correlation function of the two-photon field generated by SPDC leads to the conservation and entanglement of the orbital angular momentum of the down-converted fields. Information about the modulus and phase structure of the fourth-order correlation function were obtained by direct coincidence detection

and coincidence detection of fourth-order HOM interference effects, respectively. The expermental results confirm that our theoretical description of the two-photon wave function is accurate.

Since the completion of this work, Law and Eberly [140] have calculated the Schmidt decomposition [4, 30, 141] in transverse spatial degrees of freedom for the two-photon state (2.25) for a gaussian pump beam. They have shown that this state always displays some amount of entanglement, depending upon the phase matching and other parameters in the SPDC process. The Schmidt basis vectors are linear combinations of the Laguerre-Gaussian modes. The authors show that the Schmidt number, which is a measure of the entanglement present, is strictly greater than one, which implies that the state (2.25) (with a gaussian pump beam) is indeed entangled. A similar decomposition for any Laguerre-Gaussian pump beam should be straightforward.

It should be stressed that the conservation and entanglement of OAM is restricted to the context of two approximations. The first is the paraxial approximation, in which our model for the transfer of plane wave spectrum in SPDC is based. However, the paraxial approximation is also the context in which the angular momentum carried by electromagnetic beams can be separated into an intrinsic part, associated to polarization, and an orbital part, associated to the transverse phase structure of the beam [113]. The second approximation is the so-called thin crystal approximation. It is possible to show that this approximation would not be necessary if the non-linear medium were isotropic. The birefringence of the crystals used for SPDC causes non-conservations of the orbital angular momentum that are proportional to the crystal length [138]. Rigorously speaking, orbital angular momentum would never be conserved in SPDC due to this effect. In thin crystals (few millimeters in length) however, it can be neglected. The arguments and the experiment reported here provide additional evidence of conservation and entanglement of the orbital angular momentum of light in SPDC, as well as the limits within which they should be understood.

6

Conservation *and* Entanglement *of* Hermite-Gaussian Modes *in* SPDC

It is shown that the angular spectrum transfer in spontaneous parametric down-conversion enables the generation of entangled Hermite-Gaussian modes. Analytical expression for the two-photon state in terms of Hermite-Gaussian modes is derived which shows that there are restrictions on both the parity and order of the down-converted Hermite-Gaussian fields. The general form of the two-photon state indicates that it is indeed entangled in Hermite-Gaussian modes. The generation of maximally-entangled Bell states and non-maximally entangled pure states of first order Hermite-Gaussian modes is discussed. These results will be reported in Physical Review A (accepted 2005).

6.1 Introduction

As mentioned in section 2.3.4, the Hermite Gaussian (HG) modes (2.34) may be of use in quantum information schemes. In particular, the first-order HG and Laguerre-Gaussian (LG) modes can be described and manipulated in a way that is analogous to linear and circular polarization of the electromagnetic field [142]. Devices that act on the first-order transverse mode in a manner equivalent to polarizing beam splitters, half-wave plates and quarter-wave plates can be constructed using asymmetric interferometers [135, 143], Dove prisms [142] and mode converters [111]. The first-order modes can thus be used to define qubits and the above devices implement single qubit rotations. Recently, Langford *et al.* have produced photons entangled in first-order HG mode using SPDC and performed quantum state tomography using holographic masks and single mode fibers [110].

Here a theoretical description of the generation of entangled HG modes for arbitrary HG pump beams is provided. It is shown that there are restrictions on the parity and order of the down-converted Hermite-Gaussian fields. The basic building blocks are already in place: the HG modes have been previously defined in section 2.4.1, the relationship between the HG modes and the diagonal Hermite-Gaussian (DHG) modes was provided in section 2.4.4 and the two-photon state generated by SPDC was developed in section 2.2. In section 6.2, the main results concerning the generation of correlated HG modes using SPDC are derived. In section 6.3 it is shown that the down-converted HG modes are indeed entangled. The experimental generation of maximally- and non-maximally entangled bipartite pure states is discussed in section 6.3.4 .

6.2 Conservation of Hermite-Gaussian modes with SPDC

In the following we will denote $v_{nm}(\mathbf{q})$ as the normalized angular spectrum of the HG mode, which can be calculated by taking the two-dimensional Fourier transform of (2.34). Explicitly,

$$v_{nm}(q_x, q_y) = \frac{1}{2\pi} \int \mathrm{HG}_{nm}(x, y, z) e^{-iq_x x} e^{-iq_y y} dx dy. \tag{6.1}$$

Using the identity [1]

$$\int dy H_n(y) e^{-y^2/2} e^{ity} = \sqrt{2\pi} i^n e^{-t^2/2} H_n(t), \tag{6.2}$$

[1] See ref. [144], eq. (4.12.3).

and $\text{HG}_{nm}(x, y, 0)$ given by equation (2.34), it is a simple matter to show that

$$\begin{aligned} v_{nm}(q_x, q_y) =& wD_{nm}H_n\left(\frac{wq_x}{\sqrt{2}}\right)H_m\left(\frac{wq_y}{\sqrt{2}}\right)\times \\ & \exp\left(-\frac{w^2(q_x^2+q_y^2)}{4}\right)\times \\ & \exp\left\{-i(n+m+1)\varepsilon(z)\right\}, \end{aligned} \tag{6.3}$$

where $w \equiv w(z)$ and

$$D_{nm} = \frac{(-i)^{(n+m)}}{2}C_{nm}. \tag{6.4}$$

We can check that $v_{nm}(q_x, q_y)$ is properly normalized [2]:

$$\begin{aligned} |v_{nm}(q_x, q_y)|^2 =& w^2|D_{nm}|^2\int dq_x H_n^2\left(\frac{wq_x}{\sqrt{2}}\right)e^{-w^2q_x^2/2}\times \\ & \int dq_y H_m^2\left(\frac{wq_x}{\sqrt{2}}\right)e^{-w^2q_y^2/2} \\ =& w^2|D_{nm}|^2\left(\frac{\sqrt{2\pi}}{w}2^n n!\right)\left(\frac{\sqrt{2\pi}}{w}2^m m!\right) \\ =& 1 \qquad \surd \end{aligned} \tag{6.5}$$

The basic situation that we are considering is illustrated in figure 6.1. We suppose that the non-linear crystal is pumped with a Hermite-Gaussian beam HG_{nm}, generating a two-photon state $|\psi\rangle_{nm}$. We wish to calculate the possible down-converted HG modes v_{jk} and v_{ut} generated in the SPDC process.

In our developement of the biphoton state given by equations (2.24), (2.25) and (2.26), we have considered the degenerate case of SPDC, that is, the down-converted fields have a wavelength $\lambda_c = 2\lambda_p$, where λ_p is the wavelength of the pump field. To account for the different wavelengths of the pump and down-converted fields, we will write the angular spectrum of the HG pump beam as $\mathcal{V}_{nm}$, which is equivalent to expression (6.3) but characterized by wavelength λ_p and beam radius w_{0p}. The angular spectrum of the down-converted fields $v_{\alpha\beta}$ is characterized by wavelength λ_c and beam radius w_{0c}.

Since the HG beams form a complete basis, we can expand the two-photon state

[2] See ref. [144] eq. (4.13.4)

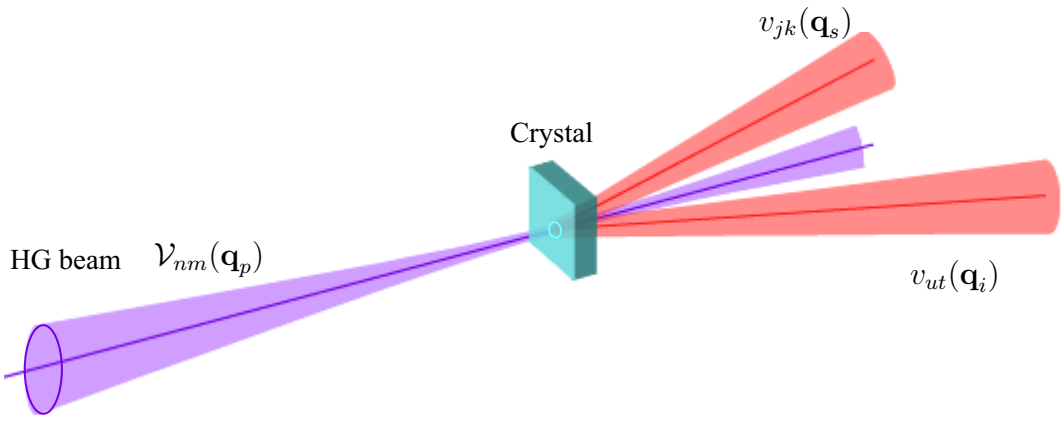

Figure 6.1: *The angular spectrum of the pump beam $\mathcal{V}_{nm}(\mathbf{q}_p)$, characterized by the wavelength λ_p and beam width the w_{0p}, creates down-converted fields with angular spectra $v_{jk}(\mathbf{q}_s)$ and $v_{ut}(\mathbf{q}_i)$, characterized by the wavelength $\lambda_c = 2\lambda_p$ and the beam width $w_{0c} = \sqrt{2}w_{0p}$.*

(2.25) as

$$|\psi_{nm}\rangle = \sum_{j,k,u,t=0}^{\infty} \{{}_i\langle v_{ut}|\,{}_s\langle v_{jk}|\psi\rangle\}\,|v_{jk}\rangle_s\,|v_{ut}\rangle_i\,, \tag{6.6}$$

where we have introduced the shorthand notation

$$|v_{\alpha\beta}\rangle = \int d\mathbf{q} v_{\alpha\beta}(\mathbf{q})\,|\mathbf{q}\rangle\,. \tag{6.7}$$

We note here that j (k) and u (t) are the x (y) indices of the signal and idler fields, repsectively. To facilitate the calculations, we will assume that $z_s = z_i = 0$ at the crystal face. Defining the coefficient

$$C^{nm}_{jkut} = {}_i\langle v_{ut}|\,{}_s\langle v_{jk}|\psi\rangle\,, \tag{6.8}$$

we have

$$|\psi_{nm}\rangle = \sum_{j,k,u,t=0}^{\infty} C^{nm}_{jkut}\,|v_{jk}\rangle_s\,|v_{ut}\rangle_i \tag{6.9}$$

Our objective is to calculate the coefficients C^{nm}_{jkut}.

For simplicity, we assume that the the down-converted fields are not entangled in polarization. We will then drop the polarization dependence of the two-photon state (2.25). Depending on the type of phase matching, the pump and down-converted fields

may suffer a small astigmatism when propagating through the birefringent non-linear crystal [145]. This astigmatism, depends on the order of the modes as well as the length L of the non-linear crystal, being negligible for thin crystals and/or low-order modes. Here we will assume that the crystal is cut for type-I phase matching such that the pump beam is polarized in the extraordinary direction and suffers an astigmatism, while the ordinarily polarized down-converted fields do not suffer any deformation. We will also assume that the pump beam is of low order $\mathcal{N} = n+m \leq 2$ and consider that the crystal length is on the order of a few millimeters. Under these conditions, we can ignore the birefringence and astigmatism effects. Then, using equations (2.25), (2.26) and (6.7) in equation (6.8), we have

$$C^{nm}_{jkut} = \frac{1}{\pi}\sqrt{\frac{2L}{K}} \iint d\mathbf{q}_s\, d\mathbf{q}_i v^*_{jk}(\mathbf{q}_s) v^*_{ut}(\mathbf{q}_i) \mathcal{V}_{nm}(\mathbf{q}_s + \mathbf{q}_i)\, \mathrm{sinc}\left(\frac{L}{4K}|\mathbf{q}_s - \mathbf{q}_i|^2\right). \quad (6.10)$$

In appendix A, it is shown that

$$\begin{aligned} C^{nm}_{jkut} =& \frac{4A}{\pi}\sqrt{\frac{(N-n)!(M-m)!}{\pi}} i^{N-n+M-m} \times \\ & b(j,u,N-n) b(k,t,M-m) (1+A)^{-\frac{N-n+M-m}{4}} \times \\ & \sum_{\alpha=0}^{\frac{N-n}{2}} \sum_{\beta=0}^{\frac{M-m}{2}} \mathrm{sinc}\left[\left(\frac{N-n}{2} - \alpha + \frac{M-m}{2} - \beta\right) A\right] \times \\ & \frac{1}{\alpha!\beta!(\frac{N-n}{2}-\alpha)!(\frac{M-m}{2}-\beta)!} \left(-\frac{1}{2}\sqrt{1+A^2}\right)^{\alpha+\beta} \end{aligned} \quad (6.11)$$

if $j+u \geq n$ and $k+t \geq m$ or else $C^{nm}_{jkut} = 0$. Here we have defined $A = L/Kw_p^2$.

For thin non-linear crystals ($L \sim 1$ mm), it is shown in appendix A that equation (6.11) can be approximated by a simpler expression:

$$\begin{aligned} C^{nm}_{jkut} \to \tilde{C}^{nm}_{jkut} =& \frac{4}{w}\sqrt{\frac{L}{\pi K}} b(j,u,N-n) b(k,t,M-m) \times \\ & \frac{H_{N-n}(0) H_{M-m}(0)}{\sqrt{(N-n)!(M-m)!2^{N-n+M-m}}}. \end{aligned} \quad (6.12)$$

if $j+u \geq n$ and $k+t \geq m$ and $C^{nm}_{jkut} = 0$ otherwise. $H_\gamma(0)$ is the Hermite polynomial $H_\gamma(x)$ evaluated at $x = 0$. When γ is odd, $H_\gamma(0) = 0$, which gives another conservation condition: $N-n$ and $M-m$ must be even. In other words, the sum of the x (y) indices

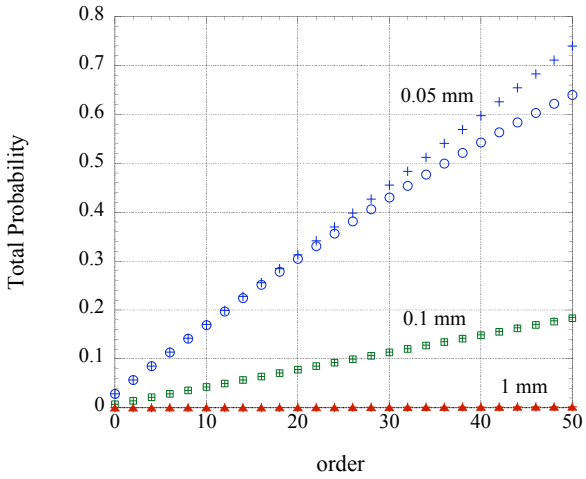

Figure 6.2: *Total probability of HG mode generation as a function of the order $j+k+u+t$ for gaussian pump beams with beam waist 1 mm, 0.1 mm and 0.05 mm. Actual values up to second order are shown in table 4.2.*

of the down converted fields $N = j + u$ ($M = k + t$) must have the same parity as the x (y) index of the pump field n (m). In summary, the conservation conditions are

$$j + u \geq n \text{ and } \text{parity}(j + u) = \text{parity}(n) \tag{6.13a}$$

$$k + t \geq m \text{ and } \text{parity}(k + t) = \text{parity}(m). \tag{6.13b}$$

By expanding the two-photon quantum state in terms of the angular spectrum $|v_{jk}(\mathbf{q}_s)\rangle$ and $|v_{ut}(\mathbf{q}_i)\rangle$ of the signal and idler fields, we have arrived at the coefficient (6.12) and conservation relations (6.13) above involving the x and y indices of the down-converted fields. We note here that the conditions above restrict (for example) the sum $j+u$ and not j and s individually. Thus there is indeed a correlation between the parity of the x and y indices of the signal and idler fields. In section 6.3 we will show that the signal and idler fields are entangled. We will now look at some situations for different HG pump beams.

A Maple program that calculates values of the coefficients C^{nm}_{jkut} up to a given order for any n, m is included in section B.1 of the appendix. Figure 6.2 shows the total probabilities obtained by summing all the exact $|C^{00}_{jkut}|^2$ or approximate $|\tilde{C}^{00}_{jkut}|^2$ (crosses) probabilities up to a given order $\mathcal{O} = j + k + u + t$. The pump beam is a Gaussian ($n = m = 0$) with $\lambda_p = 351\,\text{nm}$ and the crystal length L is 1 mm. Results

$\mathcal{O}$	jk	ut	C^{00}_{jkut}	$\lvert C^{00}_{jkut}\rvert^2$	$\tilde{C}^{00}_{jkut}$	$\lvert \tilde{C}^{00}_{jkut}\rvert^2$
0	00	00	0.008434	0.000071	0.008434	0.000071
2	00	02	-0.002982	0.000009	-0.002982	0.000009
2	00	20	-0.002982	0.000009	-0.002982	0.000009
2	01	01	0.004217	0.000018	0.004217	0.000018
2	10	10	0.004217	0.000018	0.004217	0.000018
2	02	00	-0.002982	0.000009	-0.002982	0.000009
2	20	00	-0.002982	0.000009	-0.002982	0.000009
0	00	00	0.016868	0.000285	0.016868	0.000285
2	00	02	-0.005964	0.000036	-0.005964	0.000036
2	00	20	-0.005964	0.000036	-0.005964	0.000036
2	01	01	0.008434	0.000071	0.008434	0.000071
2	10	10	0.008434	0.000071	0.008434	0.000071
2	02	00	-0.005964	0.000036	-0.005964	0.000036
2	20	00	-0.005964	0.000036	-0.005964	0.000036
0	00	00	0.084338	0.007113	0.084339	0.007113
2	00	02	-0.029817	0.000889	-0.029818	0.000889
2	00	20	-0.029817	0.000889	-0.029818	0.000889
2	01	01	0.042167	0.001778	0.042170	0.001778
2	10	10	0.042167	0.001778	0.042170	0.001778
2	02	00	-0.029817	0.000889	-0.029818	0.000889
2	20	00	-0.029817	0.000889	-0.029818	0.000889

Table 6.1: *Amplitudes C^{00}_{jkut}, $\tilde{C}^{00}_{jkut}$ and probabilities $|C^{00}_{jkut}|^2$, $|\tilde{C}^{00}_{jkut}|^2$ for a Gaussian pump beam ($n = m = 0$) up to second order for pump beam waist $w_p = 1\,mm$ (top), $w_p = 0.5\,mm$ (middle) and $w_p = 0.1\,mm$ (bottom). The order is defined as $\mathcal{O} = j + k + u + t$.*

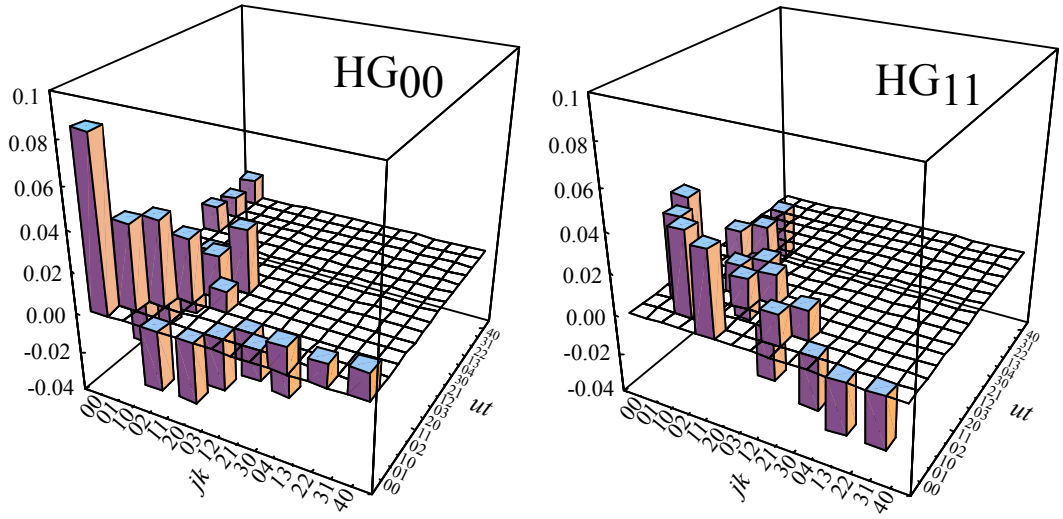

Figure 6.3: *Coefficients C^{nm}_{jkut} for a* HG_{00} *and* HG_{11} *pump beam with width $w_p = 0.1\,mm$ up to order $\mathcal{O} = 4$. For visual clarity, only nonzero terms are shown.*

are shown for pump beam waist $w_p = 1\,\mathrm{mm}$, $0.5\,\mathrm{mm}$ and $0.1\,\mathrm{mm}$. The total probability $|C^{00}_{jkut}|^2$ approaches unity faster for narrow waist pump beams. This indicates that experimentally one can increase the generation efficiency of lower order modes by focusing the pump beam at the plane of the nonlinear crystal. Looking at equations (6.11) and (6.12), we see that using slightly longer crystal will also increase efficiency.

Table 6.1 contains the amplitudes C^{00}_{jkut}, $\tilde{C}^{00}_{jkut}$ and probabilities $|C^{00}_{jkut}|^2$, $|\tilde{C}^{00}_{jkut}|^2$ for a Gaussian HG_{00} pump beam with waist $w_p = 1\,\mathrm{mm}$, $w_p = 0.5\,\mathrm{mm}$ and $w_p = 0.1\,\mathrm{mm}$ up to second order for a crystal length $L = 1\,\mathrm{mm}$, where the order is defined as $\mathcal{O}$. The coefficients C^{00}_{jkut} are also shown in figure 6.3 for a pump beam with width $w_p = 0.1\,\mathrm{mm}$. We note that the crystal length and pump beam waist appear only as multiplicative factors in (6.11) and (6.12). Thus the ratio between the probabilities for any two pairs of HG modes does not depend on the crystal length or waist of the pump beam. For example, $C^{00}_{0002}/C^{00}_{0000}$ is the same for all w_p. For smaller w_p, the approximate solution fails for higher orders. The approximate solution (6.12) is linear in the order $\mathcal{O}$, and thus is not normalized.

To show that the coefficients (6.11) are properly normalized, we calculate the total probability up to 50^{th} order for a $1\,\mathrm{cm}$ crystal and pump beam waist $w_p = 0.05\,\mathrm{mm}$. Results for a HG_{00} and HG_{01} are shown in figure 6.4. The coefficients (6.11)

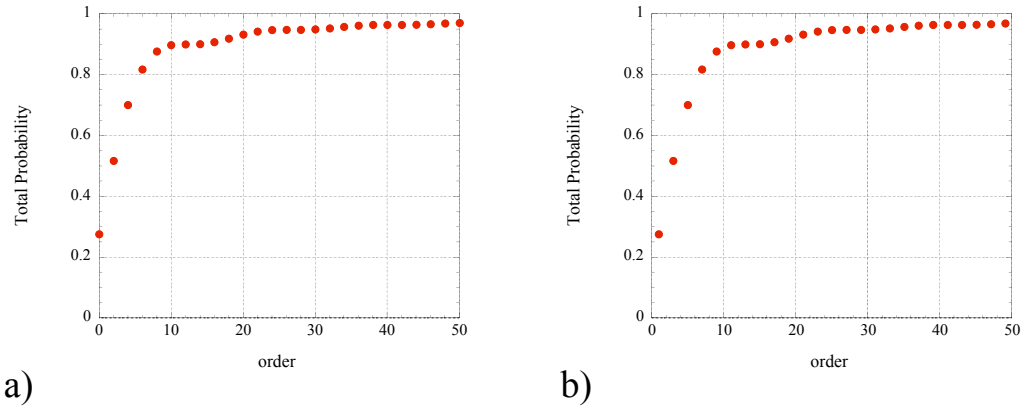

Figure 6.4: *Total probability of HG mode generation as a function of the order $j+k+u+t$ for a)* HG_{00} *and b)* HG_{01} *beams. Using crystal length* 1 *cm and pump beam waist* $w_p = 0.05$ *mm, shows that the sum of the coefficients* $|C^{nm}_{jkut}|^2$ *approaches 1.*

may not be accurate under these conditions, due to the increased astigmatism in the longer non-linear crystal. However, we include these results here to show that the total probability approaches unity. For an even more unrealistic experimental situation (not shown) using 1 m non-linear crystal, the total probability clearly approaches unity asymptotically.

As another example, table 6.2 shows the probabilities and amplitudes for generation of down converted HG modes with a HG_{11} pump beam. The coefficients C^{11}_{jkut} are also shown in figure 6.3 for a pump beam with width $w_p = 0.1$ mm. For clarity, only nonzero terms are shown.

6.3 Entanglement of Hermite-Gaussian modes

Generally, there are several methods that one can use to show that a bipartite pure state is entangled, as well as several metrics available to quantify entanglement (Schmidt number, von Neumann entropy,... [30, 146]). Many of these entanglement measures require the diagonalization of the reduced density operator ρ of (in this case) either the signal or idler photon. However, since we are working with a Hilbert space of infinite, or at least arbitrarily large dimension, these methods are analytically impractical. Here we provide a proof that, in general, the two-photon state (6.9) is indeed entangled in transverse spatial modes. We will first consider the finite dimensional

$\mathcal{O}$	jk	ut	C^{11}_{jkut}	$\lvert C^{11}_{jkut}\rvert^2$	$\tilde{C}^{11}_{jkut}$	$\lvert \tilde{C}^{11}_{jkut}\rvert^2$
2	00	11	0.042169	0.001778	0.042170	0.001778
2	01	10	0.042169	0.001778	0.042170	0.001778
2	10	01	0.042169	0.001778	0.042170	0.001778
2	11	00	0.042169	0.001778	0.042170	0.001778
4	00	13	-0.025822	0.000667	-0.025823	0.000667
4	00	31	-0.025822	0.000667	-0.025823	0.000667
4	01	12	0.014908	0.000222	0.014909	0.000222
4	01	30	-0.025822	0.000667	-0.025823	0.000667
4	10	03	-0.025822	0.000667	-0.025823	0.000667
4	10	21	0.014908	0.000222	0.014909	0.000222
4	02	11	0.014908	0.000222	0.014909	0.000222
4	11	02	0.014908	0.000222	0.014909	0.000222
4	11	20	0.014908	0.000222	0.014909	0.000222
4	20	11	0.014908	0.000222	0.014909	0.000222
4	03	10	-0.025822	0.000667	-0.025823	0.000667
4	12	01	0.014908	0.000222	0.014909	0.000222
4	21	10	0.014908	0.000222	0.014909	0.000222
4	30	01	-0.025822	0.000667	-0.025823	0.000667
4	13	00	-0.025822	0.000667	-0.025823	0.000667
4	31	00	-0.025822	0.000667	-0.025823	0.000667

Table 6.2: *Amplitudes C^{11}_{jkut}, $\tilde{C}^{11}_{jkut}$ and probabilities $|C^{11}_{jkut}|^2$, $|\tilde{C}^{11}_{jkut}|^2$ for a Hermite-Gaussian pump beam* HG_{11} *up to fourth order for crystal length $L = 1\,mm$ and pump beam waist $w_p = 0.1\,mm$. The order is defined as $\mathcal{O} = j + k + u + t$.*

case. Generalization to infinite dimension will be straightforward.

6.3.1 Finite dimension

Let us assume that the dimensionality of the Hilbert space associated to the signal and idler photons is arbtrarily large but finite. Since the coefficients C^{nm}_{jkut} are properly normalized, this is not an unreasonable restriction, since for higher orders (large j, k, s, t) the probabilities $|C^{nm}_{jkut}|^2$ approach zero, as can been seen in figure 6.4. We will then truncate the infinite series in the state (6.9):

$$|\psi_{nm}\rangle = \sum_{j,k,u,t=0}^{\mathcal{N}} C^{nm}_{jkut} \, |v_{jk}\rangle_s \, |v_{ut}\rangle_i \,, \tag{6.14}$$

where we assume that the coefficients C^{nm}_{jkut} have been adjusted so that $|\psi_{nm}\rangle$ is normalized. The reduced density matrix for - say - the signal photon of the two-photon state (6.14) is given by

$$\begin{aligned} \rho &= \mathrm{tr}_i \, \rho_\psi \\ \rho &= \mathrm{tr}_i(|\psi_{nm}\rangle \, \langle\psi_{nm}|) \\ &= \sum_{jkdf}^{\mathcal{N}} F_{jkdf} \, |v_{jk}\rangle_s \, {}_s\langle v_{df}| \,, \end{aligned} \tag{6.15}$$

where

$$F_{jkdf} \equiv \sum_{ut}^{\mathcal{N}} C^{nm}_{jkut} C^{nm}_{dfut}. \tag{6.16}$$

Above we have used the fact that the coefficients C^{nm}_{jkut} are real, which can be seen in equations (6.11) or (6.12). We note here that ρ_ψ is the density matrix of the two-photon state, while ρ is the reduced density matrix of the signal photon. From here on we will drop the s subscript on the kets for notational convenience. Since ρ is a density matrix, the following properties apply [30]:

$$\mathrm{tr}\rho = 1, \tag{6.17a}$$

$$\rho \text{ is a positive operator,} \tag{6.17b}$$

and

$$\mathrm{tr}\rho^2 \leq 1. \tag{6.17c}$$

We note the following properties of F_{jkdf}:

$$\sum_{jk}^{\mathcal{N}} F_{jkjk} = 1 \qquad \text{[from (6.17a)]}, \tag{6.18a}$$

$$F_{jkjk} \geq 0 \qquad \text{[from (6.16)]}, \tag{6.18b}$$

$$F_{jkdf} = F_{dfjk} \qquad \text{[from (6.16)]}, \tag{6.18c}$$

and

$$F_{jkdf} = 0 \text{ if parity } j \neq \text{parity } d \text{ or parity } k \neq \text{parity } f. \tag{6.18d}$$

Equation (6.18d) can be verified by applying the conservation conditions (6.13) to the definition (6.16). For a given u and n in the sum in (6.16), the conditions (6.13) require that j and d must have the same parity. The same is true for k and f for a given t and m.

Equality of the trace condition (6.17c) implies that the reduced density matrix ρ is a pure state, while if $\mathrm{tr}\rho^2 < 1$, then ρ represents a mixed state [30]. Since we assume that the two-photon state $|\psi_{nm}\rangle$ is pure, $\mathrm{tr}\rho^2 = 1$ indicates $|\psi_{nm}\rangle$ is a product state [147] of the form $|\phi\rangle_s \otimes |\varphi\rangle_i$. Similarly, if ρ is a mixed state, then $|\psi_{nm}\rangle$ is entangled.

We begin by calculating the trace (6.17c):

$$\begin{aligned}
\mathrm{tr}\rho^2 &\leq 1 \\
\mathrm{tr}\left(\sum_{jkdf}^{\mathcal{N}}\sum_{\alpha\beta\gamma\delta}^{\mathcal{N}} F_{jkdf}F_{\alpha\beta\gamma\delta}\,|v_j k\rangle\langle v_{df}|v_{\alpha\beta}\rangle\langle v_{\gamma\delta}|\right) &\leq 1 \\
\mathrm{tr}\left(\sum_{jkdf}^{\mathcal{N}}\sum_{\gamma\delta}^{\mathcal{N}} F_{jkdf}F_{df\gamma\delta}\,|v_j k\rangle\langle v_{\gamma\delta}|\right) &\leq 1 \\
\sum_{jkdf}^{\mathcal{N}} F_{jkdf}F_{dfjk} &\leq 1 \\
\sum_{jkdf}^{\mathcal{N}} (F_{jkdf})^2 &\leq 1,
\end{aligned} \tag{6.19}$$

where we used the orthogonality of the HG modes and the symmetry property (6.18c). Using property (6.18a), we can write

$$\sum_{jkdf}^{\mathcal{N}} (F_{jkdf})^2 - \sum_{jk}^{\mathcal{N}} F_{jkjk}\sum_{df}^{\mathcal{N}} F_{dfdf} \leq 1 - \sum_{jk}^{\mathcal{N}} F_{jkjk}\sum_{df}^{\mathcal{N}} F_{dfdf}.$$

Using property (6.18a) and rearranging gives

$$\sum_{jkdf}^{\mathcal{N}} (F_{jkdf})^2 - \sum_{jkdf}^{\mathcal{N}} F_{jkjk}F_{dfdf} \leq 0,$$
$$\sum_{jkdf}^{\mathcal{N}} \left[(F_{jkdf})^2 - F_{jkjk}F_{dfdf}\right] \leq 0. \tag{6.20}$$

Since ρ is a positive operator, its elements obey the generalized Cauchy-Schwartz-Buniakowski inequality: [3]

$$(F_{jkdf})^2 \leq F_{jkjk}F_{dfdf} \tag{6.21}$$

for any j, k, d and f, which means that all the terms in the summation in equation (6.20) are either zero or negative. Then, if at least one $\{(F_{jkdf})^2 - F_{jkjk}F_{dfdf}\}$ is nonzero, the equality in (6.20) cannot be true, which indicates that ρ represents a mixed state and consequently $|\psi_{nm}\rangle$ is entangled.

We will now show that under most experimental situations $|\psi_{nm}\rangle$ is indeed entangled. $(F_{jkdf})^2 - F_{jkjk}F_{dfdf} < 0$ requires that $F_{jkjk} > 0$ and $F_{dfdf} > 0$, that is, there must exist at least two nonzero diagonal terms in ρ. Suppose that there exist two nonzero terms F_{jkjk} and F_{dfdf} such that parity $j \neq$ parity d or parity $k \neq$ parity f. Then using properties (6.18d) and (6.18b) we see that in this case $(F_{jkdf})^2 - F_{jkjk}F_{dfdf} = -F_{jkjk}F_{dfdf} < 0$, and thus the state is entangled. This gives us an obvious condition on the order $\mathcal{N}$, namely $\mathcal{N} > 0$, since it can also be seen from the order restriction in (6.13) that for $\mathcal{N} = 0$ a two-photon term exists only if $n = m = 0$. However, this term is $|v_{00}\rangle\,|v_{00}\rangle$, which is a product state.

Obviously, $\mathcal{N}$ must be large enough to allow for the detection of two photons in coincidence. How large must $\mathcal{N}$ be in order for the state $|\psi_{nm}\rangle$ to be entangled? For the moment, let us ignore the m index (marked by the bullet $\bullet$) and suppose that the n index is even. Referring back to the parity and order conditions, this implies that in order to detect an entangled state, $\mathcal{N}$ must at least be large enough for the two-photon state to have terms such as:

$$\left|v_{n/2,\bullet}\right\rangle \left|v_{n/2,\bullet}\right\rangle \text{ and } \left|v_{(n\pm1)/2,\bullet}\right\rangle \left|v_{(n\mp1)/2,\bullet}\right\rangle. \tag{6.22}$$

[3] See [148], section V.6. Noting that $F_{jkdf} = \langle v_{jk}|\,\rho\,|v_{df}\rangle$, replacing ρ with the identity operator gives the usual Cauchy-Schwartz inequality: $|\langle v_{jk}|v_{ut}\rangle|^2 \leq \langle v_{jk}|v_{jk}\rangle\langle v_{ut}|v_{ut}\rangle$. We note that equation (6.21) holds for infinite dimension as well.

If n is odd, $\mathcal{N}$ must allow for the state to have components such as:

$$\left|v_{(n+1)/2,\bullet}\right\rangle \left|v_{(n-1)/2,\bullet}\right\rangle \text{ and } \left|v_{(n-1)/2,\bullet}\right\rangle \left|v_{(n+1)/2,\bullet}\right\rangle . \tag{6.23}$$

Of course the same restrictions apply for even and odd m. We can sum all of this up into the following:

$$\mathcal{N} > \max(f(n), f(m)) \geq 0, \tag{6.24}$$

where

$$f(n) = \begin{cases} \frac{n}{2} \text{ if } n \text{ even} \\ \frac{n+1}{2} \text{ if } n \text{ odd.} \end{cases} \tag{6.25}$$

As $\mathcal{N}$ increases, so does the number of elements of ρ that satisfy the above conditions. However, it is not clear that the left-hand side of (6.20) necessarily gets smaller as $\mathcal{N}$ grows. It is true that for any $\mathcal{N}$ that satisfies the conditions (6.24), all elements of ρ obey equation (6.21), which indicates that the two-photon state is entangled for arbitrarily large (or infinite) $\mathcal{N}$.

One would expect that the amount of entanglement present in the two-photon state would increase with $\mathcal{N}$. For example, consider the reduced density operator $\rho_{\mathcal{D}}$ of a maximally-entangled pair of $\mathcal{D}$-dimensional qudits. $\rho_{\mathcal{D}}$ is a maximally-mixed state $\rho_{\mathcal{D}} = \mathbf{I}/\mathcal{D}$, where $\mathbf{I}$ is the $\mathcal{D}$-dimension identity operator. It has been shown by Bennett *et al.* that the von Neumann entropy $\mathcal{S}(\rho)$ of the reduced density matrices is an accurate measure of the entanglement of a pure bipartite quantum system [149]. In this case, $\mathcal{S}(\rho_{\mathcal{D}}) = -\text{tr}(\rho_{\mathcal{D}} \log_2 \rho_{\mathcal{D}}) = \log_2 \mathcal{D}$, which is to say that the bipartite state has $\log_2 \mathcal{D}$ "ebits" of entanglement [149]. Since $\log_2 \mathcal{D}$ increases with $\mathcal{D}$, this implies that an entangled pair of higher-dimensional systems has more entanglement, in the sense that entanglement is a physical resource that can be used to teleport an unknown quantum state [94].

For the maximally mixed state $\text{tr}\rho_{\mathcal{D}}^2 = 1/\mathcal{D} \to 0$ as $\mathcal{D} \to \infty$, which shows that any density operator ρ satisfies $0 < \rho^2 \leq 1$. Even in the case of a bipartite pure state, $\text{tr}\rho^2$ is not a proper measure of entanglement [146], but it can tell us something about the two-photon state. Namely, we can compare $\text{tr}\rho^2$ given by equation (6.19) for given $\mathcal{N}$ with that of a maximally-mixed density operator of equal dimension. $\text{tr}\rho^2$ will then tell us if the two-photon state is pure, non-maximally entangled or maximally entangled.

Figure 6.5 shows values of $\mathrm{tr}\rho^2$ (dark red bars) for several HG pump beams for $\mathcal{N}$ from 0 to 5.[4] For $\mathcal{N} = 0$, there is no two-photon component for the HG_{01}, HG_{11} and HG_{02} pump beams. For comparison, the light grey bars correspond to $\mathrm{tr}\rho_{\mathcal{D}}^2 = 1/\mathcal{D} = 1/(\mathcal{N}+1)^2$ of a maximally entangled state. It is interesting to note that for $\mathcal{N} = 1$, a HG_{11} pump beam produces a maximally entangled state of qudits with $\mathcal{D} = 4$. In almost all cases, the reduced density operator is less mixed than $\rho_{\mathcal{D}}$, which indicates that the two-photon state is non-maximally entangled.

In the proof above we have truncated the state (6.9) in the form (6.14) for notational convenience. Perhaps a more experimentally reasonable restraint would be the order $j+k$, $u+t$ of the down-converted photons, so that the state is of the form

$$|\psi_{nm}\rangle = \sum_{r_u=0}^{\mathcal{R}_u} \sum_{r_j=0}^{\mathcal{R}_j} \sum_{j=0}^{r_j} \sum_{u=0}^{r_u} C_{jkut}^{nm} \, |v_{jk}\rangle_s \, |v_{ut}\rangle_i \,, \tag{6.26}$$

where $k = r_j - j$ and $t = r_u - u$. The same properties (6.3.1) exist for the reduced density matrix of the state (6.26), so the proof can be performed in the same way, with the same conclusions. We note that it is not necessary that $\mathcal{R}_j = \mathcal{R}_u$ [4].

We have also calculated $\mathrm{tr}\rho^2$ for small values of $\mathcal{R}_j = \mathcal{R}_u \equiv \mathcal{R}$ for several HG pump beams (dark red bars, figure 6.6), as well as $\mathrm{tr}\rho_{\mathcal{D}}^2 = 1/\mathcal{D}$ (light grey bars) of a maximally entangled pair of qudits of dimension $\mathcal{D} = \sum_{r=0}^{R}(r+1)$.[5] In all cases of $\mathcal{R} > 0$ where some entanglement is present, the two-photon state is non-maximally entangled.

It could also be interesting to consider stricter experimental post-selection, in which only a few HG modes are considered. Due to the reduced complexity of the system, one can write the reduced density matrix using the coefficients (6.16) and calculate the entanglement present. In section 6.3.3 we outline several methods of creating useful entangled states.

6.3.2 Infinite dimension

We have shown at the end of section 6.2 that the two-photon state (6.9) is normalized, so all the steps taken in the above proof are true for an infinite dimensional space. We can set $\mathcal{N} \longrightarrow \infty$ and conclude that the two-photon state given by (6.9) is indeed

[4] The Maple program used to calculate (6.19) for given $\mathcal{N}$ is included section B.2.
[5] The Maple program used to calculate (6.19) for given $\mathcal{R}$ is included section B.3.

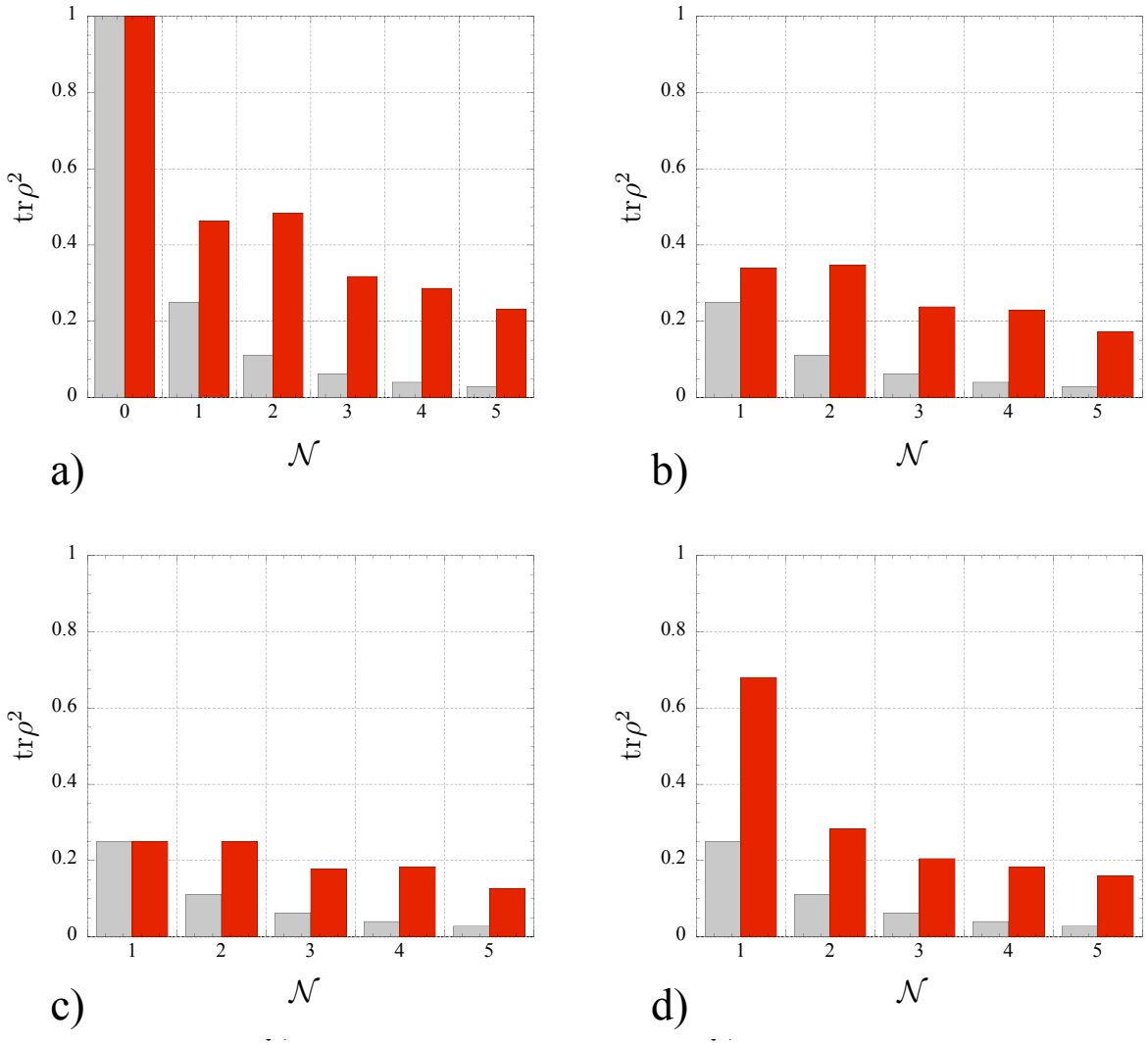

Figure 6.5: $\mathrm{tr}\rho^2$ *for* $0 \leq \mathcal{N} \leq 5$ *for a)* HG_{00}*, b)* HG_{01}*, c)* HG_{11} *and d)* HG_{02} *pump beams. The light bars show* $\mathrm{tr}\rho_{\mathcal{D}}^2$ *of a maximally mixed* $\mathcal{D}$*-dimensional density operator (see text).*

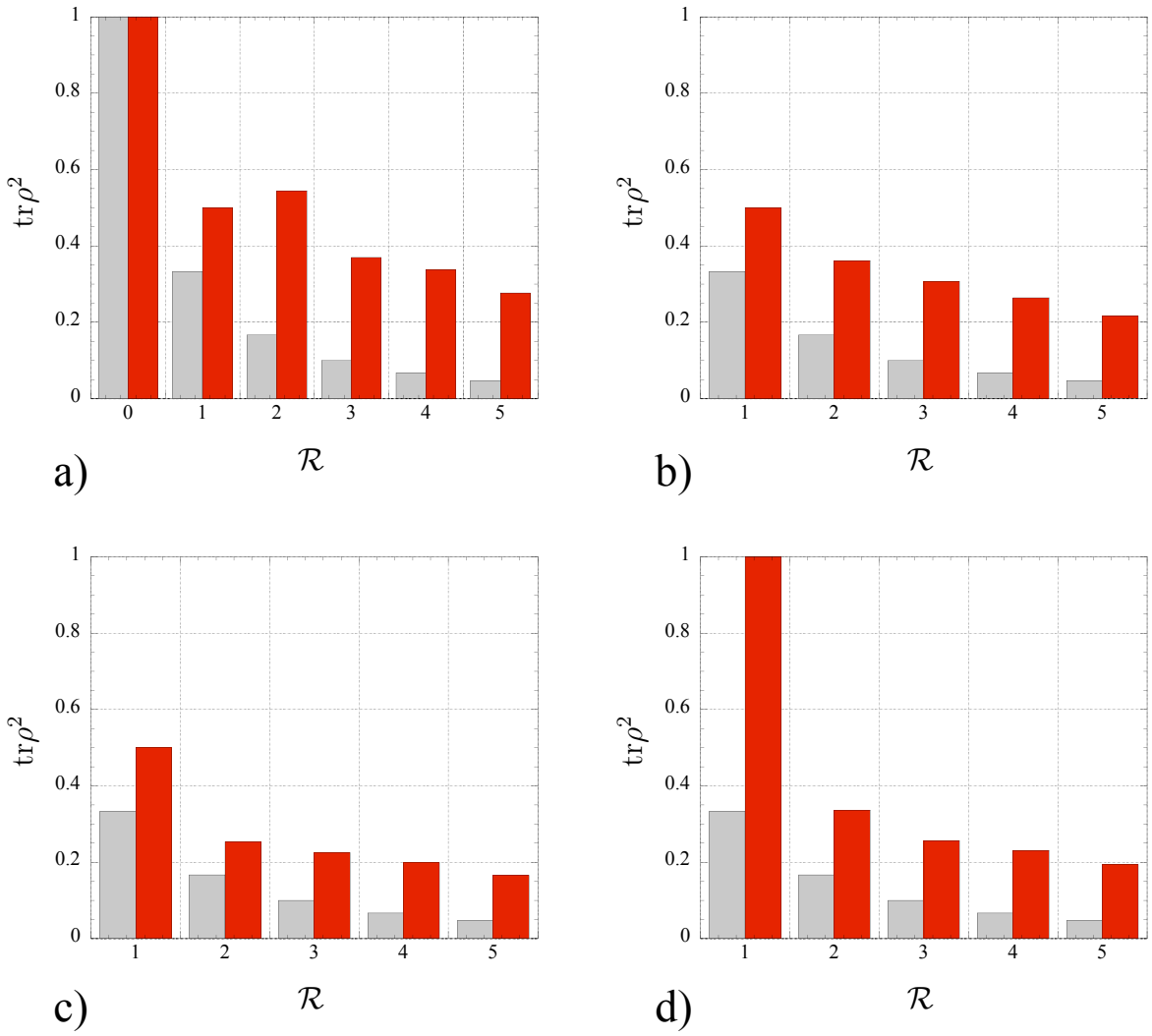

Figure 6.6: $\mathrm{tr}\rho^2$ *for* $0 \leq \mathcal{R} \leq 5$ *for a)* HG_{00}*, b)* HG_{01}*, c)* HG_{11} *and d)* HG_{02} *pump beams. The light bars show* $\mathrm{tr}\rho_{\mathcal{D}}^2$ *of a maximally mixed* $\mathcal{D}$*-dimensional density operator (see text).*

entangled in HG modes. Since all orders are included in the summation in (6.9), $|\psi_{nm}\rangle$ is always entangled.

6.3.3 Generating Bell states

Through post-selection, it is possible to obtain finite-dimensional entangled states of higher-order Gaussian modes. Experimentally, post-selection is performed by coupling the down-converted fields into optical fibers [46, 19, 150, 110], which filter out unwanted modes. Similarly, entanglement concentration of LG modes was achieved by properly coupling these modes into optical fibers [150].

Referring to table 6.1 for the HG_{00} pump beam, if one considers only first-order down-converted fields ($j+k=1$, $u+t=1$), the resulting quantum state is maximally entangled, resembling the ϕ^+ Bell state, as was observed in [110]. It is then fairly straightforward to experimentally generate all four Bell states using first-order HG modes. Using a Dove prism (aligned at 45°) to rotate $\text{HG}_{01} \longleftrightarrow \text{HG}_{10}$ of either the signal or idler field, one can generate the ψ^+ Bell state. Placing one additional mirror reflection (or a Dove prism aligned at 90°) in either the signal or idler path, such that $\text{HG}_{01} \longrightarrow -\text{HG}_{01}$ and $\text{HG}_{10} \longrightarrow \text{HG}_{10}$, one can then generate the maximally entangled ϕ^- and ψ^- states.

Another method of generating Bell-states of first-order HG modes is with the second-order pump beam HG_{11}. Isolating only first-order modes, the output state resembles the maximally-entangled ψ^+ state, as seen in table 6.2. This method may be advantageous since the high-probability zero-order HG_{00}-HG_{00} term is not present.

6.3.4 Generating non-maximally entangled states

Table 6.3 shows results up to second-order for HG_{02} and HG_{20} beams. Looking at first order terms only (HG_{01} and HG_{10}), the HG_{02} pump beam creates an $\text{HG}_{01} - \text{HG}_{01}$ term, while a HG_{20} pump generates the $\text{HG}_{10} - \text{HG}_{10}$ term. Creating a pump beam that is an arbitrary coherent superposition of these two beams, we can generate arbitrary bipartite pure states of the form given in equation (2.32). FIG. 6.7 shows a possible experimental setup. The input pump beam is a horizontally polarized HG_{02} beam. A half- (HWP1) and quarter-wave plate (QWP1) are used to adjust the pump polarization. Rotating HWP1, one can change the pump polarization as $|H\rangle \longrightarrow \cos\theta\,|H\rangle + \sin\theta\,|V\rangle$, where H and V stand for horizontal and vertical polarization. By tilting QWP1 one can adjust the relative phase [16]. The pump polarization is then $|H\rangle \longrightarrow \cos\theta\,|H\rangle + e^{i\phi}\sin\theta\,|V\rangle$

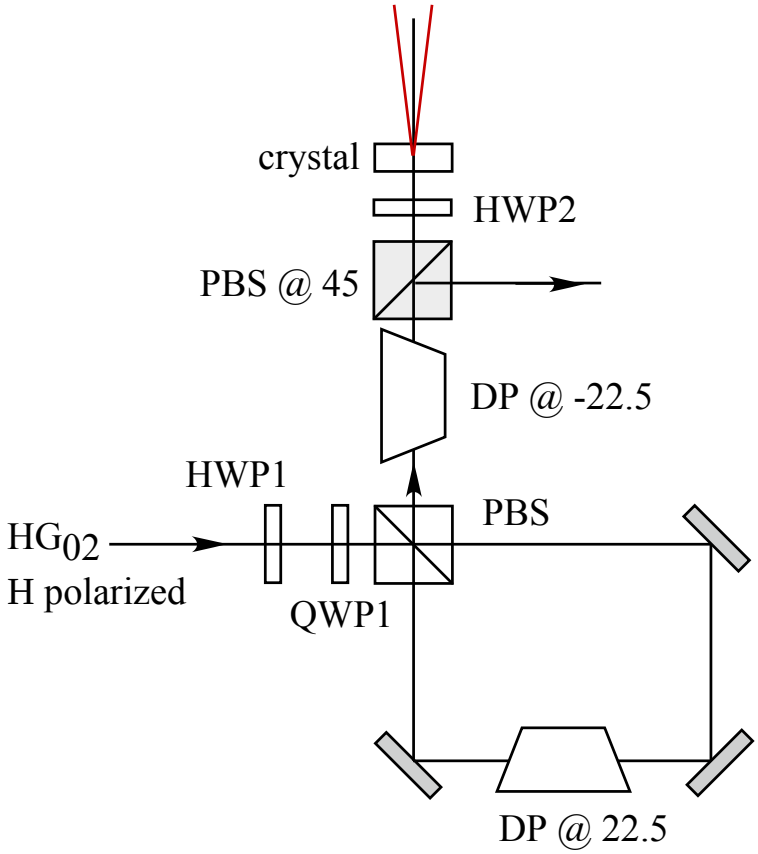

Figure 6.7: *Possible experimental setup to generate non-maximally entangled states of first-order HG modes. The input pump beam is a vertically polarized* HG_{02} *beam. A half- (HWP1) and quarter-wave plate (QWP1) are used to adjust the pump polarization. The pump beam enters a polarization-sensitve Sagnac interferometer with a nested Dove prism (DP) orientated at* $22.5°$*. The PBS are polarizing beam splitters.*

$\mathcal{O}$	jk	ut	C^{02}_{jkut}	$\lvert C^{02}_{jkut}\rvert^2$	$\tilde{C}^{02}_{jkut}$	$\lvert\tilde{C}^{02}_{jkut}\rvert^2$
2	00	02	0.042169	0.001778	0.042170	0.001778
2	01	01	0.059636	0.003556	0.059637	0.003557
2	02	00	0.042169	0.001778	0.042170	0.001778
$\mathcal{O}$	jk	ut	C^{20}_{jkut}	$\lvert C^{20}_{jkut}\rvert^2$	$\tilde{C}^{20}_{jkut}$	$\lvert\tilde{C}^{20}_{jkut}\rvert^2$
2	00	20	0.042169	0.001778	0.042170	0.001778
2	10	10	0.059636	0.003556	0.059637	0.003557
2	20	00	0.042169	0.001778	0.042170	0.001778

Table 6.3: *Amplitudes and probabilities for Hermite-Gaussian pump beams* HG_{02} *(top) and* HG_{20} *(bottom) up to second order for crystal length* $L = 1\,mm$ *and beam waist* $w_p = 0.1\,mm$*. The order is defined as* $\mathcal{O} = j + k + u + t$*.*

up to a global phase. The pump beam then enters a polarization-dependent Sagnac interferometer with a nested Dove prism (DP) orientated at 22.5°. This type of Sagnac interferometer is experimentally advantageous since it is insensitive to phase fluctuations, and has been used to construct an optical single-photon CNOT gate [42] and to measure the spatial Wigner function of single-photon field [151]. It is well known that a Dove prism orientated at an azimuthal angle φ rotates an image by an angle φ in the transverse plane. The polarizing beam splitter sends H and V-polarized components into opposite ends of the interferometer, where the Dove prism rotates the image of the H-polarized component by 45°, while the V-polarized component, which is propagating in the opposite direction, is rotated by $-45°$. The second Dove prism (located outside the interferometer) is used to realign the images in the horizontal-vertical coordinate system. A Dove prism will also slightly rotate the polarization direction. However, since in all cases the Dove prisms are followed by PBS's which project onto the desired polarization direction, this will result in only a slight reduction in beam intensity. After the second Dove prism, the pump beam is in a superposition: $\cos\theta\,|H\rangle\,\mathcal{V}_{02}+e^{i\phi}\sin\theta\,|V\rangle\,\mathcal{V}_{20}$. Using a polarizing beam splitter (PBS) aligned in the $\pm45°$ basis, we can project onto the 45°-polarization component, after which the pump beam is in the superposition: $|45\rangle\,(\cos\theta\mathcal{V}_{02} + e^{i\phi}\sin\theta\mathcal{V}_{20})$. The last half-wave plate (HWP2) is used to realign the polarization before entering the non-linear crystal, where the HG components generate the terms in table 6.3. Post-selecting the first-order terms ($j + k = 1, u + t = 1$), the

two photon state is

$$|\psi\rangle = \cos\theta\,|v_{01}\rangle_s\,|v_{01}\rangle_i + e^{i\phi}\sin\theta\,|v_{10}\rangle_s\,|v_{10}\rangle_i \tag{6.27}$$

The weights and relative phase of the two-photon state (6.27) can be adjusted by rotating HWP1 and tilting QWP1, allowing for the creation of any pure state.

6.3.5 Hyperentangled states

Another interesting possibility is the creation of hyperentangled states [131]. It has been shown that such states may be useful in quantum dense coding and quantum cryptography [152]. Using one of the experimental situations described above and replacing the single type-I crystal we have considered with either the type-II "crossed cone" source [13] discussed in section 2.3.1 or the two-crystal type-I source [16] of polarization-entangled photons, it should be possible to generate a two-photon state entangled in HG-mode and polarization. These sources generally require that the crystals are thin (on the order of a few millimeters), so the possible astigmatism effects discussed in section 6.2 should be minimal, even for the type-II source. Moreover, the experimental setups described above require only lower order HG modes.

6.4 Conclusion

We have shown that it is possible to generate entangled Hermite-Gaussian modes through spontaneous parametric down-conversion and have derived exact and approximate analytical expressions for the probability amplitudes C^{nm}_{jkut}. The entanglement of Hermite-Gaussian modes is guaranteed by the transfer of the angular spectrum of the pump beam to the two-photon quantum state [77]. We have provided a proof that, under most experimental conditions, the two-photon state is entangled.

We note here that recently Law and Eberly [140] have shown the two-photon state (2.25) with a Gaussian pump beam is always entangled in transverse modes, as was discussed briefly at the end of chapter 5. Since a Gaussian beam is the same in both HG and LG bases, their conclusions hold for the two-photon state $|\psi\rangle_{00}$ given by (6.9).

We have discussed the generation of maximally entangled Bell-states and non-maximally entangled pure states of first-order Hermite-Gaussian modes. These results promise to be useful in quantum information schemes.

7

Conclusion

7.1 Conclusion

The quantum optics laboratory at the Federal University of Minas Gerais (UFMG) has produced several theses studying the spatial characteristics of photons created with spontaneous parametric down-conversion (SPDC) [1]. This thesis is a further study of the spatial characteristics of down-converted photons, with an emphasis placed on the recent field of quantum information. Three main topics are covered: multimode interference, optical Bell-state analysis and generation of entangled states of transverse modes. The central theme which links these slightly different topics into a somewhat coherent study is the multimode treatment of SPDC, in particular the use of the theory of angular spectrum transfer developed by Monken *et al.* [77].

In chapter 3, multimode Hong-Ou-Mandel interference was studied both theoretically and experimentally. It was shown that the transverse spatial characteristics of biphoton pair influence the fourth-order interference behavior. Due to the transfer of the angular spectrum from the pump beam to the down-converted photon pair in SPDC, the transverse spatial characteristics of the biphoton are directly related to the pump beam. We showed that, by manipulating the parity of the pump beam, one can control the fourth-order interference behavior. A multimode version of the Hong-Ou-Mandel interference experiment was performed to confirm our theoretical predictions. Using a first order Hermite-Gaussian beam to create photons in symmetric and anti-symmetric polarization states using SPDC, we were able to send the photons into either

[1] Several theses are available online: http://www.fisica.ufmg.br/opticaq.

the same output or different outputs of the beam splitter by changing the parity of the pump beam. We used multimode interference to create a two-photon singlet beam, which exhibits non-classical antibunching behavior[2] [70]. Future work in multimode interference might include multimode interference of more than 2 photons, as well as the implementation of linear optical quantum logic gates using multimode interference.

The theme of chapter 4 is Bell-state measurement: the discrimination of the four Bell states given in equation (2.31). Bell-state measurement is required in several quantum information tasks including quantum teleportation and quantum dense coding. Previous methods of Bell-state anlalysis of polarization-entangled photon pairs utilize two-photon interference at a 50:50 beam splitter. One drawback to this method is that it requires detectors that are sensitive to photon number. At present, reliable and efficient detectors that can distinguish between one and two photons are not yet available. Using multimode interference, this requirement on the detectors can be eliminated. An experiment was performed in which 3 classes of Bell states were discriminated by detecting in the coincidence basis with single photon detectors.

In addition, multimode interference allows for the improvement of a previous Bell-state measurement scheme of Kwiat and Weinfurter [124]. Their scheme uses hyperentangled photons, which are entangled in more than one degree of freedom, and again requires detectors sensitive to photon number. In section 4.3 we showed that a multimode version of their proposal allows for discrimination of all four Bell-states in the coincidence basis with single photon detectors.

In section 4.4.3 we propose a new Bell-state measurement scheme using hyperentangled photons entangled in momentum and polarization. Very recently, these hyperentangled two-photon states were produced by F. De Martini's group using the source described in section 4.4.2. We show theoretically that all four Bell-states can be identified in the coincidence basis. The proposed experiment is realizable with current technology, as it requires only polarizing beam splitters, wave plates and single photon detectors. At the cost of an additional two bits of classical communication, our Bell-state measurement scheme can be implemented non-locally.

Unfortunately, all the Bell-state measurement schemes mentioned above cannot be used to perform quantum teleportation, as discussed at the end of chapter 4. However, all the methods mentioned above can be used for quantum dense coding and

[2]This experiment is part of W. A. T. Nogueira's doctoral research (in progress).

may be useful in quantum cryptography. It has been shown that an entangled pair of photons can be used as an ancilla in a type of quantum teleportation experiment to implement difficult quantum logic operations [97]. It might be fruitful to investigate the use of hyperentangled states in such a protocol. An implementation using hyperentangled states might reduce the resources required for the realization of quantum logic operations.

The second half of this thesis deals with the generation of photons entangled in transverse spatial degrees of freedom. In both classical and quantum optics, there has been a lot of recent interest in the Laguerre-Gaussian and Hermite-Guassian modes of the electromagnetic field. The first order Laguerre-Gaussian and Hermite-Gaussian modes form bases that are analogous to circular and linear polarization (respectively), and consequently could be used to represent a qubit. Since both sets of modes form orthonormal bases, they could be used to construct higher order $\mathcal{D}$-dimensional alphabets, or qudits.

Chapter 5 deals with the generation of down-converted photons entangled in orbital angular momentum. Using the Laguerre-Gaussian beams, which are known to carry orbital angular momentum in the form of an azimuthal phase dependence [113], we show that a down-converter pumped with a Laguerre-Gaussian beam generates photons entangled in orbital angular momentum. We conducted a fourth-order multimode interference experiment to measure the amplitude and phase of the biphoton, which allowed us to confirm the theoretical predictions.

In the same spirit, we investigated the generation of photons entangled in Hermite-Gaussian mode (chapter 6). We calculated the probability amplitude to generate photons entangled in any combination of Hermite-Guassian modes for an arbitrary Hermite-Guassian pump beam. We encountered several conservation conditions: (i) the sum of the x (y) Hermite-Guassian indices of the down-converted photons preserves the parity of the pump beam and (ii) the sum of the x (y) indices of the down-converted modes is greater than the x (y) index of the pump beam. We also show that the down-converted photons are indeed entangled. We propose an experimental setup that could be used to generate pure bipartite states with any degree of entanglement.

The calculations included in this chapter may be used to engineer pump beams that generate a desired state of photons in Hermite-Guassian modes. By properly engineering the pump beam or crystal source, it may be possible to create entangled

states without using post-selection. Another interesting path could be the creation of a post-selection free product state of transverse modes. It would then be possible to create triggered single photon states in a given transverse mode without post-selection. By eliminating transverse spatial entanglement, we can further isolate other degrees of freedom such as polarization, creating higher quality polarization entangled photons.

In chapters 5 and 6 we emphasize that the conservation and entanglement of transverse modes is valid in the paraxial approximation, and for thin non-linear crystals. The study of the deformation of transverse modes propagating in birrefringent media and consequently the non-conservation of orbital angular momentum and in SPDC is currently being studied in the quantum optics group at UFMG [3].

For the past two decades, SPDC has provided the physics community with an accessible testing ground for the fundamental ideas of quantum optics, quantum mechanics and quantum information. Due to the conservation of momentum conditions, multimode spatial correlations are an intrinsic property of SPDC. Many experiments, particularly in quantum information, have eliminated the multimode nature of these sources by post-selection. Here we have chosen a different route by attempting to use the multimode character of SPDC to our advantage. Though, as technology progresses, SPDC sources may be replaced by better single-photon or entangled photon sources, experiments performed with SPDC will continue to teach us much about the generation and manipulation of quantum states.

[3] A. G. da Costa Moura, Master's thesis (2003) [138] and Doctoral Research (in progress).

A

Derivation *of the* Coefficients C_{jkut}^{nm}

A.1 Derivation of the coefficients C_{jkut}^{nm}

In this appendix we provide a detailed derivation of the coefficients C_{jkut}^{nm} for the generation of entangled Hermite-Gaussian (HG) modes as discussed in chapter 6.

In section 6.2 it is shown that the coefficient C_{jkut}^{nm} is given by

$$C_{jkut}^{nm} = \frac{1}{\pi}\sqrt{\frac{2L}{K}} \iint d\mathbf{q}_s \, d\mathbf{q}_i v_{jk}^*(\mathbf{q}_s) v_{ut}^*(\mathbf{q}_i) \mathcal{V}_{nm}(\mathbf{q}_s + \mathbf{q}_i) \operatorname{sinc}\left(\frac{L}{4K}|\mathbf{q}_s - \mathbf{q}_i|^2\right). \quad \text{(A.1)}$$

Changing coordinates to

$$\begin{aligned} \mathbf{Q} =& \mathbf{q}_s + \mathbf{q}_i \\ \mathbf{P} =& \mathbf{q}_s - \mathbf{q}_i, \end{aligned} \quad \text{(A.2)}$$

such that $d\mathbf{q}_s \, d\mathbf{q}_i = d\mathbf{Q} \, d\mathbf{P}/2$, we have

$$C_{jkut}^{nm} = \frac{1}{\pi}\sqrt{\frac{L}{2K}} \iint d\mathbf{Q} d\mathbf{P} v_{jk}^*\left(\frac{\mathbf{Q}+\mathbf{P}}{2}\right) v_{ut}^*\left(\frac{\mathbf{Q}-\mathbf{P}}{2}\right) \mathcal{V}_{nm}(\mathbf{Q}) \operatorname{sinc}\left(\frac{L}{4K}P^2\right). \quad \text{(A.3)}$$

Now consider a down-converted HG mode v_{nm} with wavelength λ_c and beam radius w_{0c}. To be more precise, let us temporarily write $v_{nm}(\mathbf{q}, \lambda_c, w_{0c})$. Since we are working with down-converted fields satisfying $\lambda_c = 2\lambda_p$, it is easy to show from the general form of HG modes that $v_{nm}(\mathbf{q}/\sqrt{2}, \lambda_c, \sqrt{2}w_{0p}) = \mathcal{V}_{nm}(\mathbf{q}, \lambda_p, w_{0p})$. That is, the down-converted HG modes with $w_{0c} = \sqrt{2}w_{0p}$ will have the same Rayleigh range z_R, Gouy phase $\varepsilon(z)$ and radius of curvature $R(z)$ as the pump field.

Looking at the form of equation (6.3), it is easy to see that $v_{jk}^*((\mathbf{Q}+\mathbf{P})/2)$ and $v_{ut}^*((\mathbf{Q}-\mathbf{P})/2)$ are separable in x and y terms. Then, using definitions (2.35) and (6.4) to show that $D_{jk}^* D_{ut}^* = D_{ju}^* D_{kt}^*$, we can regroup the x and y terms, which gives

$$v_{jk}^*\left(\frac{\mathbf{Q}+\mathbf{P}}{2}\right) v_{ut}^*\left(\frac{\mathbf{Q}-\mathbf{P}}{2}\right) = 2\mathcal{V}_{ju}^*\left(\frac{Q_x+P_x}{\sqrt{2}}, \frac{Q_x-P_x}{\sqrt{2}}\right) \times \mathcal{V}_{kt}^*\left(\frac{Q_y+P_y}{\sqrt{2}}, \frac{Q_y-P_y}{\sqrt{2}}\right). \tag{A.4}$$

We note here that relation (A.4) is valid for all $z_s = z_i$. Then, using the definition of DHG modes (2.42), Eq. (A.4) can be expressed as

$$v_{jk}^*\left(\frac{\mathbf{Q}+\mathbf{P}}{2}\right) v_{ut}^*\left(\frac{\mathbf{Q}-\mathbf{P}}{2}\right) = 2\sum_{\alpha=0}^{N} b(j,u,\alpha)\mathcal{V}_{N-\alpha,\alpha}^*(Q_x,P_x) \times \sum_{\beta=0}^{M} b(k,t,\beta)\mathcal{V}_{M-\beta,\beta}^*(Q_y,P_y), \tag{A.5}$$

where $N = j+u$ and $M = k+t$. Noting that $D_{N-\alpha,\alpha}^* D_{M-\beta,\beta}^* = D_{N-\alpha,M-\beta}^* D_{\alpha,\beta}^*$ and again using the separability of the x and y components of the HG modes, it is straightforward to show that the product of angular spectra on the right-hand side of equation (A.5) can be rewritten as

$$\mathcal{V}_{N-\alpha,\alpha}^*(Q_x,P_x)\,\mathcal{V}_{M-\beta,\beta}^*(Q_y,P_y) = \mathcal{V}_{N-\alpha,M-\beta}^*(\mathbf{Q})\mathcal{V}_{\alpha,\beta}^*(\mathbf{P}). \tag{A.6}$$

Putting these results back into Eq. (A.3), the coefficent C_{jkut}^{nm} becomes

$$C_{jkut}^{nm} = \frac{1}{\pi}\sqrt{\frac{2L}{K}}\sum_{\alpha=0}^{N}\sum_{\beta=0}^{M} b(j,u,\alpha)b(k,t,\beta)\int d\mathbf{Q}\,\mathcal{V}_{N-\alpha,M-\beta}^*(\mathbf{Q})\mathcal{V}_{nm}(\mathbf{Q}) \times \int d\mathbf{P}\,\mathcal{V}_{\alpha,\beta}^*(\mathbf{P})\,\mathrm{sinc}\left(\frac{L}{4K}P^2\right). \tag{A.7}$$

The HG modes are orthonormal, so

$$\int d\mathbf{Q}\, \mathcal{V}^*_{N-\alpha,M-\beta}(\mathbf{Q})\mathcal{V}_{nm}(\mathbf{Q}) = \delta_{N-\alpha,n}\delta_{M-\beta,m}, \tag{A.8}$$

which gives

$$C_{jkut}^{nm} = \frac{1}{\pi}\sqrt{\frac{2L}{K}}b(j,u,N-n)b(k,t,M-m)\int d\mathbf{P}\, \mathcal{V}^*_{N-n,M-m}(\mathbf{P})\,\mathrm{sinc}\left(\frac{L}{4K}P^2\right) \tag{A.9}$$

if $j+u \geq n$ and $k+t \geq m$ or else $C_{jkut}^{nm} = 0$.

Using the following expression for the Hermite polynomials [144]:

$$H_n(\xi) = \sum_{j=0}^{n/2}\frac{(-1)^j n!}{j!(n-2j)!}(2\xi)^{n-2j}, \tag{A.10}$$

the $d\mathbf{P}$ integral in (A.9) becomes

$$\begin{aligned} wD_{N-n,M-m}\int d\mathbf{P} \sum_{\alpha=0}^{(N-n)/2}\frac{(-1)^\alpha(N-n)!}{\alpha!(N-n-2\alpha)!}\left(\frac{2wP_x}{\sqrt{2}}\right)^{N-n-2\alpha} e^{-w^2P_x^2/4}\times \\ \sum_{\beta=0}^{(M-m)/2}\frac{(-1)^\beta(M-m)!}{\beta!(M-m-2\beta)!}\left(\frac{2wP_y}{\sqrt{2}}\right)^{M-m-2\beta} e^{-w^2P_y^2/4}\times \\ \mathrm{sinc}\left[\frac{L}{4K}(P_x^2+P_y^2)\right]. \end{aligned} \tag{A.11}$$

Switching to polar coordinates, so that $P_x \longrightarrow P\cos\phi$ and $P_y \longrightarrow P\sin\phi$, we have

$$\begin{aligned} wD_{N-n,M-m} \sum_{\alpha=0}^{(N-n)/2}\frac{(-1)^\alpha(N-n)!}{\alpha!(N-n-2\alpha)!}\sum_{\beta=0}^{(M-m)/2}\frac{(-1)^\beta(M-m)!}{\beta!(M-m-2\beta)!}\times \\ \int PdP(\sqrt{2}wP)^{N-n-2\alpha}(\sqrt{2}wP)^{M-m-2\beta}e^{-w^2P^2/4}\mathrm{sinc}\left[\frac{L}{4K}P^2\right]\times \\ \int_0^{2\pi} d\phi(\cos\phi)^{N-n-2\alpha}(\sin\phi)^{M-m-2\beta}. \end{aligned} \tag{A.12}$$

Using Maple to calculate the $d\phi$ integral directly gives:

$$\int_0^{2\pi}\cdots d\phi = \begin{cases} 0 & \text{if } N-n-2\alpha \text{ or } M-m-2\alpha \text{ is odd} \\ \frac{\Gamma((N-n-2\alpha+1)/2)\Gamma((M-m-2\beta)/2)}{\Gamma((N-n-2\alpha+M-m-2\beta)/2)} & \text{otherwise} \end{cases}, \tag{A.13}$$

where $\Gamma(x)$ is the usual gamma function. Calculating the dP integeral is slightly more laborious but straightforward. Noticing that the integral can be put in the form (on the left-hand side)

$$\int dx x^{d-1} e^{-x/2} \sin(cx) = \Gamma(d) \frac{\sin(d \arctan(2c))}{(\frac{1}{4} + c^2)^{d/2}}, \tag{A.14}$$

Maple can be used to arrive at the right-hand side.

Putting it all together, after some algebraic manipulation, we are left with

$$\begin{aligned} C^{nm}_{jkut} =& \frac{4A}{\pi} \sqrt{\frac{(N-n)!(M-m)!}{\pi}} i^{N-n+M-m} \times \\ & b(j,u,N-n) b(k,t,M-m) (1+A)^{-\frac{N-n+M-m}{4}} \times \\ & \sum_{\alpha=0}^{\frac{N-n}{2}} \sum_{\beta=0}^{\frac{M-m}{2}} \operatorname{sinc}\left[\left(\frac{N-n}{2} - \alpha + \frac{M-m}{2} - \beta \right) A \right] \times \\ & \frac{1}{\alpha! \beta! (\frac{N-n}{2} - \alpha)! (\frac{M-m}{2} - \beta)!} \left(-\frac{1}{2} \sqrt{1+A^2} \right)^{\alpha+\beta} \end{aligned} \tag{A.15}$$

if $j + u \geq n$ and $k + t \geq m$ or else $C^{nm}_{jkut} = 0$. Here we have defined $A = L/Kw_p^2$.

For thin non-linear crystals, it is possible to arrive at a more revealing solution. If the nonlinear crystal is thin ($L \sim 1$ mm), we can approximate $\operatorname{sinc}(L/4KP^2) \approx 1$ in equation (A.9), giving $\int d\mathbf{P} \mathcal{V}^*_{\alpha,\beta}(\mathbf{P}) \operatorname{sinc}(L/4KP^2) \approx \int d\mathbf{P} \mathcal{V}^*_{\alpha,\beta}(\mathbf{P})$. Numerical integration shows that errors due to this approximation are less than 3% for modes as high as $\alpha = \beta = 10$. Then, integration in $\mathbf{P}$ gives

$$\begin{aligned} C^{nm}_{jkut} \to \tilde{C}^{nm}_{jkut} =& \frac{4}{w} \sqrt{\frac{L}{\pi K}} b(j,u,N-n) b(k,t,M-m) \times \\ & \frac{H_{N-n}(0) H_{M-m}(0)}{\sqrt{(N-n)!(M-m)! 2^{N-n+M-m}}}. \end{aligned} \tag{A.16}$$

if $j + u \geq n$ and $k + t \geq m$ and $C^{nm}_{jkut} = 0$ otherwise. $H_\gamma(0)$ is the Hermite polynomial $H_\gamma(x)$ evaluated at $x = 0$.

B

Maple Programs

B.1 Maple program to calculate coefficients C_{jkut}^{nm}

The Maple program used to calculate the coefficients C_{jkut}^{nm} from section 6.2:

```
> ########coefHG_m9.mws - calculate C_jkst^nm coefficients
> # of HG mode expansion of SPDC state
> # last update 07 April 2004
> # S.P. Walborn and C.H. Monken
> restart:
> with(orthopoly):

> Digits:=20:

> b:=proc(a1,a2,a3)
> local y,g,as:
> as:=a1+a2:
> if a3 = 0 then sqrt((as)!/(a1!*a2!*2^as))
> elif a3 > as then 0
> else
> g:=diff((1-y)^a1*(1+y)^a2,y$a3);
> coeff(g,y,0)*sqrt((as-a3)!/(a1!*a2!*a3!*2^as))
> end if:
> end:

> evalf(b(1,1,0));  # check b coefficients
                        0.70710678118654752440
> sinc:=proc(x)
> local s:
> s:=1:
> if x <> 0 then
> s:=sin(x)/x:
> else
> s:=1:
> end if:
> end:
```

```
> Cn:=proc(n,m,j,k,s,t,C)
> local M,N,c:
> M:=k+t:
> N:=j+s:
> if N < n then 0
> elif M < m then 0
> else
> c:=2*sqrt(C/Pi)*sqrt(1/(2^(M+N-n-m)*(M-m)!*(N-n)!))*H(N-n,0)*H(M-m,0)
> end if
> end:
```

```
> J:=proc(alpha,beta,C)
> local a,b,s,t:
> s:=0:
> t:=0:
> if type(alpha,even) and type(beta,even) then
> for a from 0 to alpha/2  do
> for b from 0 to beta/2  do
> t:=t+(-sqrt(1+C^2)/2)^(a+b)/(a!*b!*(alpha/2-a)!*(beta/2-b)!)
> *sinc(arctan(C)*(alpha/2+beta/2-a-b)):
> od:
> od:
> s:=2*I^(alpha+beta)*sqrt(C*alpha!*beta!/Pi)
> *arctan(C)/(C*(1+C^2)^((alpha+beta)/4))*t:
> end if:
> evalf(s):
> end proc:
```

```
> #######    Define constants    ###############
> n:=0:
> m:=1:
> len:=1:  # mm
> w0:=1:  # mm
> K:=17900:
> rmin:=0:
> rmax:=3:
> file_name:="dat_coef_pump=HG01_w0=1.txt":
> ########################################
> C:=len/(K*w0^2):
> # write print to file labels
> fda:=fopen(file_name, APPEND):
> fprintf(fda,"n=%d m=%d L=%4.1f mm  w0=%4.2f mm
> K=%5.0f C=%5.5f C^2=%5.5f  Digits = %d",n,m,len,w0,K,C,C^2,Digits):
> fprintf(fda,"r jk st parity coe prob coe_approx prob_approx"):
> # write print to screen labels
> printf("r  jk  st par   coeff     prob   tot_prob
> coe_aprx   prob_aprx tot_prob_aprx"):
> fclose(fda):
> ps:=0:ps_approx:=0:
> if type(m+n,odd) then p:=1 else p:=2 end if:
```

```
> ##################Begin Loop###############
> for r from rmin to rmax by 1 do
> if type(p+r,even) then
> for r1 from 0 to r do
> r2:=r-r1:
> for j from 0 to r1 do
> k:=r1-j:
> for s from 0 to r2 do
> t:=r2-s:
> coe:=0:
> prob:=0:
> coe_approx:=0:
> prob_approx:=0:
> alpha:=j+s-n:
> beta:=k+t-m:
> if (alpha>=0) and (beta>=0) then
> coe:=evalf(b(j,s,alpha)*b(k,t,beta)*J(alpha,beta,C)):
> prob:=abs(coe)^2:
> coe_approx:=b(j,s,alpha)*b(k,t,beta)*evalf(Cn(n,m,j,k,s,t,C)):
> prob_approx:=abs(coe_approx)^2:
> end if:
> if type(j+k,even) then par1:=‘e‘ else par1:=‘o‘end if:
> if type(s+t,even) then par2:=‘e‘ else par2:=‘o‘end if:
> if prob > 0 then
> ps:=ps+prob:
> ps_approx:=ps_approx+prob_approx:
> printf("%d  %d%d  %d%d  %s%s %6.4f  %6.6f
> %6.6f  %6.4f   %6.6f    %6.6f  ",r,j,k,s,t,par1,par2,coe,prob,ps,
> coe_approx,prob_approx,ps_approx):
> fda := fopen(file_name, APPEND);
> fprintf(fda,"%d  %d%d  %d%d  %6.6f  %6.6f
> %6.6f  %6.6f",r,j,k,s,t,coe,prob,coe_approx,prob_approx):
> fclose(fda);
> end if:
> od:
> od:
> od:
> end if:
> od:
```

r	jk	st	par	coeff	prob	tot_prob	coe_aprx	prob_aprx	tot_prob_aprx
1	00	01	eo	0.0060	0.000036	0.000036	0.0060	0.000036	0.000036
1	01	00	oe	0.0060	0.000036	0.000071	0.0060	0.000036	0.000071
3	00	03	eo	-0.0037	0.000013	0.000084	-0.0037	0.000013	0.000084
3	00	21	eo	-0.0021	0.000004	0.000089	-0.0021	0.000004	0.000089
3	01	02	oe	0.0021	0.000004	0.000093	0.0021	0.000004	0.000093
3	01	20	oe	-0.0021	0.000004	0.000098	-0.0021	0.000004	0.000098
3	10	11	oe	0.0030	0.000009	0.000107	0.0030	0.000009	0.000107
3	02	01	eo	0.0021	0.000004	0.000111	0.0021	0.000004	0.000111
3	11	10	eo	0.0030	0.000009	0.000120	0.0030	0.000009	0.000120
3	20	01	eo	-0.0021	0.000004	0.000124	-0.0021	0.000004	0.000124
3	03	00	oe	-0.0037	0.000013	0.000138	-0.0037	0.000013	0.000138
3	21	00	oe	-0.0021	0.000004	0.000142	-0.0021	0.000004	0.000142

B.2 Maple program to calculate $\mathrm{tr}\rho^2$ for $0 \leq \mathcal{N} \leq 5$

The Maple program used to calculate equation (6.19) for figure 6.5.

```
> ########coefHG_m9.mws - calculate tr rho^2
> # rho truncated by j,k,d,f <= N
> # last update 26 June 2004
> # S.P. Walborn and C.H. Monken
> restart:
> with(orthopoly):


> Digits:=20:


> b:=proc(a1,a2,a3)
> local y,g,as:
> as:=a1+a2:
> if a3 = 0 then sqrt((as)!/(a1!*a2!*2^as))
> elif a3 > as then 0
> else
> g:=diff((1-y)^a1*(1+y)^a2,y$a3);
> coeff(g,y,0)*sqrt((as-a3)!/(a1!*a2!*a3!*2^as))
> end if:
> end:
> b(1,1,0);  # Check b coeffs
```

$$1/2\,\sqrt{2}$$

```
> sinc:=proc(x)
> local s:
> s:=1:
> if x <> 0 then
> s:=sin(x)/x:
> else
> s:=1:
> end if:
> end:




> Cn:=proc(n,m,j,k,s,t,C)
> local M,N,c:
> M:=k+t:
> N:=j+s:
> if N < n then 0
> elif M < m then 0
> else
> c:=2*sqrt(C/Pi)*sqrt(1/(2^(M+N-n-m)*(M-m)!*(N-n)!))*H(N-n,0)*H(M-m,0)
> end if
> end:
```

```
>  J:=proc(alpha,beta,C)
>  local a,b,s,t:
>  s:=0:
>  t:=0:
>  if type(alpha,even) and type(beta,even) then
>  for a from 0 to alpha/2  do
>  for b from 0 to beta/2  do
>  t:=t+(-sqrt(1+C^2)/2)^(a+b)/(a!*b!*(alpha/2-a)!*(beta/2-b)!)
>  *sinc(arctan(C)*(alpha/2+beta/2-a-b)):
>  od:
>  od:
>  s:=2*I^(alpha+beta)*sqrt(C*alpha!*beta!/Pi)
>  *arctan(C)/(C*(1+C^2)^((alpha+beta)/4))*t:
>  end if:
>  evalf(s):
>  end proc:
>  ##########Define constants   ############
>  n:=0:
>  m:=0:
>  len:=1:  # mm
>  w0:=0.05:  # mm
>  K:=17900:
>  rmin:=0:
>  rmax:=5:
>  file_name:="26-06-04_trrho^2_HG00.txt":
>  ######################
>  C:=len/(K*w0^2):
>  fda:=fopen(file_name, APPEND):
>  fprintf(fda,"n=%d m=%d L=%4.1f mm  w0=%4.2f mm  K=%5.0f C=%5.5f C^2=%5.5f
Digits = %d",n,m,len,w0,K,C,C^2,Digits):
>  fprintf(fda,"N  numstates  1/numstates  tr rho^2  total prob "):
>  fclose(fda):
>  printf("N  numstates  1/numstates  tr rho^2  total prob "):
>  numstates:=0:
>  for r from rmin to rmax by 1 do
>  ps:=0:
>  #calculate total prob for normalization
>  for jp from 0 to r by 1 do
>  for kp from 0 to r by 1 do
>  for sp from 0 to r by 1 do
>  for tp from 0 to r by 1 do
>  coep:=0:
>  prob:=0:
>  alpha:=jp+sp-n:
>  beta:=kp+tp-m:
>  if (alpha>=0) and (beta>=0) then
>  coep:=evalf(b(jp,sp,alpha)*b(kp,tp,beta)*J(alpha,beta,C)):
>  prob:=abs(coep)^2:
>  end if:
>  if prob > 0 then
>  ps:=ps+prob:
>  end if:
>  od:
>  od:
>  od:
>  od:
>  ### end total prob calc#########
```

```
>  #### calculate trace ##########
>  Asum:=0:
>  if ps > 0 then
>  for j from 0 to r by 1 do
>  for k from 0 to r by 1 do
>  for d from 0 to r by 1 do
>  for f from 0 to r by 1 do
>  # s and t loop
>  Fjkdf:=0:
>  for s from 0 to r by 1 do
>  for t from 0 to r by 1 do
>  coe1:=0:
>  coe2:=0:
>  F:=0:
>  if ((j+s-n)>=0) and ((k+t-m)>=0) and ((d+s-n)>=0) and ((f+t-m)>=0) then
>  coe1:=(1/sqrt(ps))*evalf(b(j,s,j+s-n)*b(k,t,k+t-m)*J(j+s-n,k+t-m,C)):
>  coe2:=(1/sqrt(ps))*evalf(b(d,s,d+s-n)*b(f,t,f+t-m)*J(d+s-n,f+t-m,C)):
>  F:=coe1*coe2:
>  else F:=0:
>  end if:
>  Fjkdf:=Fjkdf+F:
>  od:
>  od:
>  Asum:=Asum+Fjkdf^2:
>  od:od:od:od:  #(j k d f loops)
>  numstates:=(r+1)^2:
>  printf("  %d   %d   %6.5f   %6.5f  %6.5f ",r,numstates,1/numstates,Asum,ps):
>  fda := fopen(file_name, APPEND);
>  fprintf(fda,"  %d  %d  %6.5f  %6.5f  %6.5f ",r,numstates,1/numstates,Asum,ps):
>  fclose(fda);
>  end if:
>  od:  # r loop

N        numstates       1/numstates     tr rho^2        total prob
  0              1        1.00000         1.00000        0.02844
  1              4        0.25000         0.46279        0.04442
  2              9        0.11111         0.48386        0.07642
  3             16        0.06250         0.31771        0.10510
  4             25        0.04000         0.28684        0.13607
  5             36        0.02778         0.23197        0.16678
```

B.3 Maple program to calculate $\mathrm{tr}\rho^2$ for $0 \leq \mathcal{R} \leq 5$

The Maple program used to calculate equation (6.19) for figure 6.6.

```
> ########trrho2_order.mws - calculate tr(rho^2) of
> # rho truncated by order (j+k)<= R
> # last update 26 June 2004
> # S.P. Walborn and C.H. Monken
> restart:
> with(orthopoly):


> Digits:=20:


> b:=proc(a1,a2,a3)
> local y,g,as:
> as:=a1+a2:
> if a3 = 0 then sqrt((as)!/(a1!*a2!*2^as))
> elif a3 > as then 0
> else
> g:=diff((1-y)^a1*(1+y)^a2,y$a3);
> coeff(g,y,0)*sqrt((as-a3)!/(a1!*a2!*a3!*2^as))
> end if:
> end:


> sinc:=proc(x)
> local s:
> s:=1:
> if x <> 0 then
> s:=sin(x)/x:
> else
> s:=1:
> end if:
> end:




> Cn:=proc(n,m,j,k,s,t,C)
> local M,N,c:
> M:=k+t:
> N:=j+s:
> if N < n then 0
> elif M < m then 0
> else
> c:=2*sqrt(C/Pi)*sqrt(1/(2^(M+N-n-m)*(M-m)!*(N-n)!))*H(N-n,0)*H(M-m,0)
> end if
> end:
```

```
>  J:=proc(alpha,beta,C)
>  local a,b,s,t:
>  s:=0:
>  t:=0:
>  if type(alpha,even) and type(beta,even) then
>  for a from 0 to alpha/2  do
>  for b from 0 to beta/2  do
>  t:=t+(-sqrt(1+C^2)/2)^(a+b)/(a!*b!*(alpha/2-a)!*(beta/2-b)!)
>  *sinc(arctan(C)*(alpha/2+beta/2-a-b)):
>  od:
>  od:
>  s:=2*I^(alpha+beta)*sqrt(C*alpha!*beta!/Pi)
>  *arctan(C)/(C*(1+C^2)^((alpha+beta)/4))*t:
>  end if:
>  evalf(s):
>  end proc:
>  ######################
>  n:=0:
>  m:=1:
>  len:=1:  # mm
>  w0:=0.05:  # mm
>  K:=17900:
>  rmin:=0:
>  rmax:=5:
>  file_name:="26-06-04_trrho^2_HG01_order.txt":
>  ######################
>  C:=len/(K*w0^2):
>  fda:=fopen(file_name, APPEND):
>  fprintf(fda,"n=%d m=%d L=%4.1f mm  w0=%4.2f mm  K=%5.0f C=%5.5f C^2=%5.5f
Digits = %d",n,m,len,w0,K,C,C^2,Digits):
>  fprintf(fda,"order  numstates  1/r  tr rho^2  total prob "):
>  fclose(fda):
>  printf("order  numstates  1/r  tr rho^2  total prob "):
>  numstates:=0:
>  for r from rmin to rmax by 1 do
>  ps:=0:
>  #calculate total prob for normalization
>  for r1 from 0 to r do
>  for r2 from 0 to r do
>  for jp from 0 to r1 do
>  kp:=r1-jp:
>  for sp from 0 to r2 do
>  tp:=r2-sp:
>  coep:=0:
>  prob:=0:
>  alpha:=jp+sp-n:
>  beta:=kp+tp-m:
>  if (alpha>=0) and (beta>=0) then
>  coep:=evalf(b(jp,sp,alpha)*b(kp,tp,beta)*J(alpha,beta,C)):
>  prob:=abs(coep)^2:
>  end if:
>  if prob > 0 then
>  ps:=ps+prob:
>  end if:
>  od:
>  od:
>  od:
>  od:
>  ######end total prob calc
```

```
>  ######## calculate trace ###########
>  numstates:=r+1+numstates:
>  if ps > 0 then
>  Asum:=0:
>  Fjkdf:=0:
>  for r1 from 0 to r do
>  for r2 from 0 to r do
>  for j from 0 to r1 do
>  k:=r1-j:
>  for d from 0 to r2 do
>  f:=r2-d:
>  # s and t loop
>  Fjkdf:=0:
>  for r3 from 0 to r by 1 do
>  for s from 0 to r3 by 1 do
>  t:=r3-s:
>  coe1:=0:
>  coe2:=0:
>  if (j+s-n>=0) and (k+t-m>=0) and (d+s-n>=0) and (f+t-m>=0) then
>  coe1:=(1/sqrt(ps))*evalf(b(j,s,j+s-n)*b(k,t,k+t-m)*J(j+s-n,k+t-m,C)):
>  coe2:=(1/sqrt(ps))*evalf(b(d,s,d+s-n)*b(f,t,f+t-m)*J(d+s-n,f+t-m,C)):
>  F:=coe1*coe2:
>  else F:=0:
>  end if:
>  Fjkdf:=Fjkdf+F:
>  od:
>  od:
>  Asum:=Asum+Fjkdf^2:
>  od:od:od:od:  #(j k d f loops)
>  printf("  %d  %d  %6.5f  %6.5f  %6.5f ",r,numstates,1/numstates,Asum,ps):
>  fda := fopen(file_name, APPEND);
>  fprintf(fda,"  %d  %d  %6.5f  %6.5f  %6.5f ",r,numstates,1/numstates,Asum,ps):
>  fclose(fda);
>  end if:
>  od:  # r loop

order    numstates       1/r     tr rho^2        total prob
  1      3       0.33333         0.50000         0.02844
  2      6       0.16667         0.36121         0.04265
  3      10      0.10000         0.30701         0.06747
  4      15      0.06667         0.26380         0.08868
  5      21      0.04762         0.21590         0.11225
```

Bibliography

[1] A. Einstein, D. Podolsky, and N. Rosen, Phys. Rev. **47**, 777 (1935). 1.1

[2] E. Schrödinger, Naturwissenschaften **23**, 807 (1935). 1.1

[3] J. A. Wheeler and W. H. Zurek, eds., *Quantum Theory and Measurement* (Princeton University Press, Princeton, NJ, 1983). 1.1

[4] J. Preskill, *Lecture Notes: Caltech Physics 219/Computer Science 219 Quantum Computation* (1998), URL http://www.theory.caltech.edu/people/preskill/ph229. 1.1, 5.4, 6.3.1

[5] J. Clauser, M. Horne, A. Shimony, and R. Holt, Phys. Rev. Lett. **23**, 880 (1969). 1.1

[6] A. Aspect, P. Grangier, and G. Roger, Phys. Rev. Lett. **49**, 91 (1982). 1.1

[7] A. Aspect, J. Dalibard, and G. Roger, Phys. Rev. Lett. **49**, 1804 (1982). 1.1

[8] Z. Y. Ou and L. Mandel, Phys. Rev. Lett. **61**, 50 (1988). 1.1, 1.3.1, 2.3.1

[9] Y. Shih and C. Alley, Phys. Rev. Lett. **61**, 2921 (1988). 1.1, 1.3.1, 2.3.1

[10] J. Rarity and P. Tapster, Phys. Rev. Lett. **64**, 2495 (1990). 1.1, 1.3.1, 2.3, 2.3.3, 4.1

[11] P. Tapster, J. Rarity, and P. Owens, Phys. Rev. Lett. **73**, 1923 (1994). 1.1, 1.3.1, 2.3, 4.1

[12] J. Torgerson, D. Branning, C. Monken, and L. Mandel, Phys. Lett. A **204**, 323 (1995). 1.1, 1.3.1, 3.1

[13] P. G. Kwiat, K. Mattle, H. Weinfurter, A. Zeilinger, A. V. Sergienko, and Y. Shih, Phys. Rev. Lett. **75**, 4337 (1995). 1.1, 1.3.1, 2.3, 2.3.1, 4.1, 4.4.2, 6.3.5

[14] W. Tittel, J. Brendel, T. Herzog, H. Zbinden, and N. Gisin, Phys. Rev. A. **57**, 3229 (1998). 1.1, 1.3.1

[15] G. Weihs, T. Jennewein, C. Simon, H. Weinfurter, and A. Zeilinger, Phys. Rev. Lett. **81**, 5039 (1998). 1.1, 1.3.1

[16] P. G. Kwiat, E. Waks, A. G. White, I. Appelbaum, and P. H. Eberhard, Phys. Rev. A **60**, R773 (1999). 1.1, 1.3.1, 2.3, 2.3.1, 4.1, 4.6, 4.4.2, 6.3.4, 6.3.5

[17] J. Pan, D. Bouwmeester, M. Daniel, H. Weinfurter, and A. Zeilinger, Nature **403**, 515 (2000). 1.1, 1.3.1

[18] C. Kurtsiefer, M. Oberparleiter, and H. Weinfurter, Phys. Rev.A **64**, 023802 (2001). 1.1, 1.3.1

[19] A. Vaziri, G. Weihs, and A. Zeilinger, Phys. Rev. Lett. **89**, 240401 (2002). 1.1, 1.3.1, 1.4, 2.3, 2.3.4, 5.1, 6.3.3

[20] P. Benioff, J. Stat. Phys. **22**, 563 (1980). 1.2

[21] D. Deutsch, Proc. R. Soc. Lond. A **400**, 97 (1985). 1.2

[22] D. Deutsch, Proc. R. Soc. Lond. A **425**, 73 (1989). 1.2

[23] R. P. Feynman, Int. J. Theor. Phys. **21**, 467 (1982). 1.2

[24] R. P. Feynman, Found. Phys. **16**, 507 (1986). 1.2

[25] P. W. Shor, in *Proceedings of the 35th Anual symposium on the Foundations of Computer Science*, edited by S. Goldwasser (IEEE Computer Society, Los Alamitos, CA, 1994), p. 124. 1.2

[26] P. W. Shor, quant-ph/9508027. 1.2

[27] C. H. Bennet and G. Brassard, in *Proceedings of the International Conference on Computer Systems and Signal Processing* (Bangalore, 1984), p. 175. 1.2

[28] C. Bennett, G. Brassard, and A. Ekert, Sci. Am. **267**, 26 (1992). 1.2, 4.5

[29] A. K. Ekert, Phys. Rev. Lett. **67**, 661 (1991). 1.2

[30] M. Nielsen and I. Chuang, *Quantum Computation and Quantum Information* (Cambridge, Cambridge, 2000). 1.2, 1.2.1, 4.4.3, 4.4.4, 5.4, 6.3, 6.3.1, 6.3.1

[31] E. Klarriech, Nature **418**, 270 (2002). 1.3

[32] D. P. DiVincenzo, Phys. Rev. A **51**, 1015 (1995). 1.3

[33] E. Knill, R. Laflamme, and G. J. Milburn, Nature **409**, 46 (2001). 1.3, 2.3.2, 3.4

[34] T. C. Ralph, A. G. White, W. J. Munro, and G. J. Milburn, Phys. Rev. A **65**, 012314 (2001). 1.3

[35] T. C. Ralph, N. K. Langford, T. B. Bell, and A. G. White, Phys. Rev. A **65**, 062324 (2002). 1.3, 3.1, 3.4

[36] T. B. Pittman, B. C. Jacobs, and J. D. Franson, Phys.Rev. Lett. **88**, 257902 (2002). 1.3, 1.3.1, 3.1, 3.4

[37] J. L. O'brien, G. J. Pryde, A. G. White, T. C. Ralph, and D. Branning, Nature **426**, 264 (2003). 1.3, 1.3.1

[38] S. Glancy, J. M. LoSecco, H. M. Vasconcelos, and C. E. Tanner, Phys. Rev. A **65**, 062317 (2002). 1.3

[39] N. J. Cerf, C. Adami, and P. Kwiat, Phys. Rev. A **57**, R1477 (1998). 1.3

[40] A. N. de Oliveira, *Utilização da Polarização e Perfil Espacial de Feixes de Luz como Qubits em Computação Quântica*, Master's thesis, Departamento de Física, Universidade Federal de Minas Gerais (UFMG) (2003). 1.3

[41] A. N. de Oliveira, S. P. Walborn, and C. H. Monken, submitted to Journal of Optics B: Quantum and Semiclassical Optics (2005). 1.3

[42] M. Fiorentino and F. N. C. Wong, Phys. Rev. Lett. **93**, 070502 (2004). 1.3, 6.3.4

[43] D. N. Klyshko, JETP **28**, 522 (1969). 1.3.1, 2.1.1, 2.2

[44] D. Burnham and D. Weinberg, Phys. Rev. Lett. **25**, 84 (1970). 1.3.1, 2.1.1

[45] R. S. Thebaldi, *Estados de Dois Fótons com Momento Angular Orbital*, Master's thesis, Departamento de Física, Universidade Federal de Minas Gerais (UFMG) (2001). 1.3.1, 1.4, 2.2, 2.3

[46] A. Mair, A. Vaziri, G. Weihs, and A. Zeilinger, Nature **412**, 313 (2001). 1.3.1, 1.4, 2.3, 2.3.4, 5.1, 5.1, 6.3.3

[47] P. Kwiat, P. Schwindt, and B. G. Englert, in *Workshop on Mysteries, Puzzles and Paradoxes in Quantum Mechanics*, edited by R. Bonifacio (AIP, Gargnano, Italy, 1998). 1.3.1

[48] Y.-H. Kim, S. Kulik, Y. Shih, and M. Scully, Phys. Rev. Lett. **84**, 1 (2000). 1.3.1

[49] S. P. Walborn, *Um apagador quântico com estados de Bell*, Master's thesis, Departamento de Física, Universidade Federal de Minas Gerais (UFMG) (2000). 1.3.1

[50] S. P. Walborn, M. O. T. Cunha, S. Pádua, and C. H. Monken, Phys. Rev. A **65**, 0338 (2002). 1.3.1

[51] S. P. Walborn, M. O. T. Cunha, S. Pádua, and C. H. Monken, American Scientist **91**, 336 (2003). 1.3.1

[52] K. Mattle, H. Weinfurter, P. Kwiat, and A. Zeilinger, Phys. Rev. Lett. **76**, 4656 (1996). 1.3.1, 2.3.2, 3.1, 4.1, 4.2.1, 4.5

[53] T. Jennewein, C. Simon, G. Weihs, H. Weinfurter, and A. Zeilinger, Phys. Rev. Lett. **84**, 4729 (2000). 1.3.1

[54] D. Naik, C. Peterson, A. White, A. Berlund, and P. Kwiat, Phys. Rev. Lett. **84**, 4733 (2000). 1.3.1

[55] W. Tittel, J. Brendel, H. Zbinden, and N. Gisin, Phys. Rev. Lett. **84**, 4737 (2000). 1.3.1

[56] D. Bouwmeester, J. Pan, K. Mattle, M. Eibl, H. Weinfurter, and A. Zeilinger, Nature **390**, 575 (1997). 1.3.1, 3.1, 4.1, 4.4.4, 4.5

[57] Y.-H. Kim, S. P. Kulik, and Y. H. Shih, Phys. Rev. Lett. **86**, 1370 (2001). 1.3.1, 4.1, 2

[58] J.-W. Pan, M. Daniell, S. Gasparoni, G. Wiehs, and A. Zeilinger, Phys.Rev. Lett. **86**, 4435 (2001). 1.3.1

[59] J.-W. Pan, D. Bouwmeester, H. Weinfurter, and A. Zeilinger, Phys.Rev. Lett. **80**, 3891 (1998). 1.3.1, 4.1, 4.4.4, 4.5

[60] F. D. Martini, D. Pelliccia, and F. Sciarrino, Phys. Rev. Lett. **92**, 067901 (2004). 1.3.1

[61] W. T. M. Irvine, A. L. Linares, M. J. A. de Dood, and D. Bouwmeester, Phys. Rev. Lett. **92**, 047902 (2004). 1.3.1

[62] P. G. Kwiat, S. Barraza-Lopez, A. Stefanov, and N. Gisin, Nature **409**, 1014 (2001). 1.3.1

[63] J.-W. Pan, S. Gasparoni, R. Ursin, G. Wiehs, and A. Zeilinger, Nature **423**, 417 (2003). 1.3.1

[64] C. K. Hong, Z. Y. Ou, and L. Mandel, Phys. Rev. Lett. **59**, 2044 (1987). 1.3.1, 3, 3.1, 3.2.3, 3.3, 4.2.1, 5.2.2, 5.3

[65] E. Fonseca, C. Monken, and S. Pádua, Phys. Rev. Lett. **82**, 2868 (1999). 1.3.1

[66] E. Fonseca, P. S. Ribeiro, S. Pádua, and C. Monken, Phys. Rev. A **60**, 1530 (1999). 1.3.1

[67] E. Fonseca, J. M. da Silva, C. Monken, and S. Pádua, Phys. Rev. A **61**, 023801 (2000). 1.3.1

[68] E. Fonseca, Z. Paulini, P. Nussenzveig, C. Monken, and S. Pádua, Phys. Rev. A **63**, 043819 (2001). 1.3.1

[69] W. A. T. Nogueira, S. P. Walborn, S. Pádua, and C. H. Monken, Phys. Rev. Lett. **86**, 4009 (2001). 1.3.1

[70] W. A. T. Nogueira, S. P. Walborn, S. Pádua, and C. H. Monken, Phys. Rev. Lett. **92**, 043602 (2004). 1.3.1, 3.4, 7.1

[71] P. H. S. Ribeiro, S. Pádua, J. C. M. da Silva, and G. A. Barbosa, Phys. Rev. A **49**, 4176 (1994). 1.3.1

[72] Y. H. Shih, A. V. Sergienko, M. H. Rubin, T. E. Kiess, and C. O. Alley, Phys.Rev. A **50**, 23 (1994). 1.3.1

[73] M. H. Rubin, D. N. Klyshko, Y. H. Shih, and A. V. Sergienko, Phys.Rev. A **50**, 5122 (1994). 1.3.1

[74] L. Mandel and E. Wolf, *Optical Coherence and Quantum Optics* (Cambridge University Press, New York, 1995). 1.3.1, 2.2.5, 3.3

[75] P. H. S. Ribeiro, Phys. Rev. A **56**, 4111 (1996). 1.3.1

[76] T. B. Pittman, D. V. Strekalov, D. N. Klyshko, M. H. Rubin, A. V. Sergienko, and Y. H. Shih, Phys.Rev. A **53**, 2804 (1996). 1.3.1

[77] C. H. Monken, P. S. Ribeiro, and S. Pádua, Phys. Rev. A. **57**, 3123 (1998). 1.3.1, 2.2.1, 2.2.4, 2.2.4, 2.2.4, 3.2.1, 5.1, 6.4, 7.1

[78] E. Fonseca, G. Barbosa, C. Monken, and S. Pádua, Phys. Rev. A **59**, 1608 (1999). 1.3.1

[79] A. F. Abouraddy, B. E. A. Saleh, A. V. Sergienko, and M. C. Teich, Phys. Rev. Lett. **87**, 123602 (2001). 1.3.1

[80] M. Atatüre, G. D. Giuseppe, M. D. Shaw, A. V. Sergienko, B. E. A. Saleh, and M. C. Teich, Phys. Rev. A **66**, 023808 (2002). 1.3.1

[81] M. Atatüre, G. D. Giuseppe, M. D. Shaw, A. V. Sergienko, B. E. A. Saleh, and M. C. Teich, Phys. Rev. A **66**, 023822 (2002). 1.3.1

[82] S. Franke-Arnold, S. M. Barnett, M. J. Padgett, and L. Allen, Phys. Rev. A **65**, 033823 (2002). 1.4, 2.3.4, 5.1

[83] V. Dmitriev, G. Gurzadyan, and D. Nikoyosyan, *Handbook of Nonlinear Optical Crystals (Springer Series in Optical Sciences Vol. 64)* (Springer-Verlag, New York, 1999). 2.1.1

[84] C. K. Hong and L. Mandel, Phys. Rev. A **31**, 2409 (1985). 2.2

[85] L. Wang, *Investigation of Induced Coherence With and Without Induced Emission*, Ph.D. thesis, University of Rochester (1992). 2.2

[86] C. H. Monken, *Geração de luz com estatística de fótons sub-Poissonian a partir da conversão paramétrica descendente*, Ph.D. thesis, Departamento de Física, Universidade Federal de Minas Gerais (UFMG) (1993). 2.2

[87] N. Bloembergen, *Nonlinear Optics* (Pearson Addison Wesley, New York, 1977). 2.2.1

[88] Y. R. Shen, *Principles of Nonlinear Optics* (Wiley-Interscience, New York, 1984). 2.2.1

[89] C. H. Monken, *Transferência de Espectro Angular e Correlações Transversais na Conversão Paramétrica Descendente* (1998-2002), unpublished lecture notes. 2.2.1, 2.2.4

[90] B. E. A. Saleh and M. C. Teich, *Fundamental Photonics* (Wiley, New York, 1991). 2.2.2, 2.4.1

[91] J. W. Goodman, *Introduction to Fourier Optics* (Mc Graw Hill, Boston, 1996). 2.2.2, 2.2.3

[92] H. Bacry and M. Cadihac, Phys. Rev. A **23**, 2533 (1981). 2.2.2

[93] C. H. Monken, *Teoria da difração através da óptica de Fourier* (1998), unpublished lecture notes. 2.2.3

[94] C. H. Bennett, G. Brassard, C. Crépeau, R. Jozsa, A. Peres, and W. K. Wooters, Phys. Rev. Lett. **70**, 1895 (1993). 2.3.2, 4.1, 4.4.4, 6.3.1

[95] C. Bennett and S. Weisner, Phys. Rev. Lett. **69**, 2881 (1992). 2.3.2, 4.1, 4.4.4

[96] H. J. Briegel, W. Dür, J. I. Cirac, and P. Zoller, Phys. Rev. Lett. **81**, 5932 (1998). 2.3.2

[97] D. Gottesman and I. L. Chuang, Nature **402**, 390 (1999). 2.3.2, 4.4.4, 7.1

[98] S. Braunstein and A. Mann, Phys. Rev. A. **51**, R1727 (1995). 2.3.2, 4.1, 4.2.1

[99] A. Zeilinger, H. J. Bernstein, and M. A. Horne, J. Mod. Optics **41**, 2375 (1994). 2.3.2, 4.1, 4.2.1, 4.2.1

[100] L. Vaidman and N. Yoran, Phys. Rev. A **59**, 116 (1999). 2.3.2, 4.1

[101] N. Lütkenhaus, J. Calsamiglia, and K.-A. Suominen, Phys. Rev. A **59**, 3295 (1999). 2.3.2, 4.1

[102] J. Calsamiglia and N. Lütkenhaus, Appl. Phys. B **72**, 67 (2001). 2.3.2, 4.1

[103] S. Ghosh, G. Kar, A. Roy, A. Sen(De), and U. Sen, Phys. Rev. Lett. **87**, 277902 (2001). 2.3.2, 4.1

[104] H. Weinfurter, Europhys. Lett. **25**, 559 (1994). 2.3.3, 4.1

[105] M. Michler, K. Mattle, H. Weinfurter, and A. Zeilinger, Phys. Rev. A. **53**, R1209 (1996). 2.3.3, 4.1, 4.2.1

[106] H. H. Arnaut and G. A. Barbosa, Phys. Rev. Lett. **85**, 286 (2001). 2.3.4, 5.1, 5.1

[107] G. A. Barbosa and H. H. Arnaut, Phys. Rev. A **65**, 053801 (2002). 2.3.4, 5.1

[108] J. P. Torres, Y. Deyanova, L. Torner, and G. Molina-Terriza, Phys. Rev. A. **67**, 052313 (2003). 2.3.4, 5.1

[109] S. P. Walborn, A. N. de Oliveira, R. S. Thebaldi, and C. H. Monken, Phys. Rev. A **69**, 023811 (2004). 2.3.4

[110] N. K. Langford, R. B. Dalton, M. D. Harvey, J. L. O'Brien, G. J. Pryde, A. Gilchrist, S. D. Bartlett, and A. G. White, Phys. Rev. Lett. **93**, 053601 (2004). 2.3.4, 6.1, 6.3.3

[111] M. W. Beijersbergen, L. Allen, H. E. L. O. van der Veen, and J. P. Woerdman, Optics Comm. **96**, 123 (1993). 2.4.2, 2.4.4, 2.4.4, 3.3, 5.3, 6.1

[112] M. Padgett, J. Arlt, N. Simpson, and L. Allen, Am. J. Phys. **64**, 77 (1996). 2.4.2, 2.4.4, 5.3

[113] L. Allen, M. W. Beijersbergen, R. J. C. Spreeuw, and J. P. Woerdman, Phys. Rev. A **45**, 8185 (1992). 2.4.3, 5.1, 5.4, 7.1

[114] S. J. van Enk and G. Nienhuis, Optics Comm. **94**, 147 (1992). 2.4.3

[115] J. Courtial and M. Padgett, Optics Comm. **159**, 13 (1999). 2.4.4, 5.3

[116] C. H. Monken, P. S. Ribeiro, and S. Pádua, Phys. Rev. A. **57**, R2267 (1998). 3.3

[117] S. P. Walborn, A. N. de Oliveira, S. Pádua, and C. H. Monken, Europhys. Lett **62**, 161 (2003). 3.4

[118] J. Leach, M. J. Padgett, S. M. Barnett, S. Franke-Arnold, and J. Courtial, Phys. Rev. Lett. **88**, 257901 (2002). 3.4, 5.1

[119] D. Boschi, S. Branca, F. DeMartini, L. Hardy, and S. Popescu, Phys. Rev. Lett. **80**, 1121 (1998). 4.1

[120] T. Jennewein, G. Weihs, J.-W. Pan, and A. Zeilinger, Phys. Rev. Lett. **88**, 017903 (2002). 4.1, 4.4.4, 4.5

[121] M. G. A. Paris, M. B. Plenio, S. Bose, D. Jonathan, and G. M. D'Ariano, Phys. Lett. A **273**, 153 (2000). 4.1

[122] M. O. Scully, B.-G. Englert, and C. J. Bednar, Phys. Rev. Lett. **83**, 4433 (1999). 4.1

[123] E. DelRe, B. Crosignani, and P. D. Porto, Phys. Rev. Lett. **84**, 2989 (2000). 4.1

[124] P. G. Kwiat and H. Weinfurter, Phys. Rev. A **58**, R2623 (1998). 4.1, 4.5, 4.3, 4.5, 7.1

[125] S. P. Walborn, A. N. de Oliveira, S. Pádua, and C. H. Monken, Phys. Rev. Lett **90**, 143601 (2003). 4.1

[126] P. G. Kwiat, A. Steinberg, and R. Chiao, Phys. Rev. A **47**, R2472 (1993). 4.2.1

[127] J. Kim, S. Takeuchi, Y. Yamamoto, and H. H. Hogue, Appl. Phys. Lett. **74**, 902 (1999). 4.2.1

[128] S. Takeuchi, J. Kim, Y. Yamamoto, and H. H. Hogue, Appl. Phys. Lett. **74**, 1063 (1999). 4.2.1

[129] Z.-B. Chen, J.-W. Pan, Y.-D. Zhang, C. Brukner, and A. Zeilinger, Phys. Rev. Lett. **90**, 160408 (2003). 4.4.2

[130] P. G. Kwiat, A. Berglund, J. Altepeter, and A. White, Science **290**, 498 (2000). 4.4.2, 4.4.3

[131] P. G. Kwiat, J. Mod. Optics **44**, 2173 (1997). 4.4.2, 6.3.5

[132] C. Cinelli, M. Barbieri, F. D. Martini, and P. Mataloni, *Experimental realization of hyper-entangled two-photon states*, quant-ph/0406148. 4.4.2

[133] C. Simon and J.-W. Pan, Phys. Rev. Lett. **89**, 257901 (2002). 4.4.3

[134] N. R. Heckenberg, R. McDuff, C. P. Smith, and A. G. White, Optics Letters **17**, 221 (1992). 5.1

[135] X. Xue, H. Wei, and A. G. Kirk, Optics Letters **26**, 1746 (2001). 5.1, 6.1

[136] H. Wei, X. Xue, J. Leach, M. J. Padgett, S. M. Barnett, S. Franke-Arnold, E. Yao, and J. Courtial, Optics Comm. **223**, 117 (2003). 5.1

[137] J. P. Torres, A. Alexandrescu, and L. Torner, Phys. Rev. A. **68**, 050301 (2003). 5.1

[138] A. G. da Costa Moura, *Propagação de Feixes Eletromagnéticos em Meios Birrefringentes Uniaxiais*, Master's thesis, Departamento de Física, Universidade Federal de Minas Gerais (UFMG) (2003). 5.1, 5.4, 3

[139] M. L. Boas, *Mathematical Methods in the Physical Sciences* (John Wiley & Sons, New York, 1983). 5.2.1

[140] C. K. Law and J. H. Eberly, Phys. Rev. Lett. **92**, 127903 (2004). 5.4, 6.4

[141] A. Peres, *Quantum Theory: Concepts and Methods* (Kluwer, Dordrecht, 1995). 5.4

[142] A. T. O'Neil and J. Courtial, Opt. Comm. **181**, 35 (2000). 6.1

[143] H. Sasada and M. Okamoto, Phys. Rev. A. **68**, 012323 (2003). 6.1

[144] N. N. Lebedev, *Special Functions and Their Applications* (Dover, New York, 1972). 1, 2, A.1

[145] A. G. C. Moura and C. H. Monken, in preparation. 6.2

[146] K. Durstberger, *Something about entanglement* (2004), unpublished. 6.3, 6.3.1

[147] L. Ballentine, *Quantum Mechanics: A Modern Development* (World Scientific, Singapore, 1998). 6.3.1

[148] L. V. Kantorovich and G. P. Akilov, *Functional Analysis* (Pergamon Press, England, 1982). 3

[149] C. H. Bennett, H. J. Bernstein, S. Popescu, and B. Schumacher, Phys. Rev. A **53**, 2046 (1996). 6.3.1

[150] A. Vaziri, J.-W. Pan, T. Jennewein, G. Weihs, and A. Zeilinger, Phys. Rev. Lett. **91**, 227902 (2003). 6.3.3

[151] E. Mukamel, K. Banaszek, I. A. Walmsley, and C. Dorrer, Opt. Lett. **28**, 1317 (2003). 6.3.4

[152] S. P. Walborn, S. Pádua, and C. H. Monken, Phys. Rev. A **68**, 042313 (2003). 6.3.5